Higgs properties: coupling, mass & width at ATLAS and CMS

Moriond 2024: QCD & High Energy interaction conference

Romain Bouquet

on behalf of the ATLAS and CMS collaborations

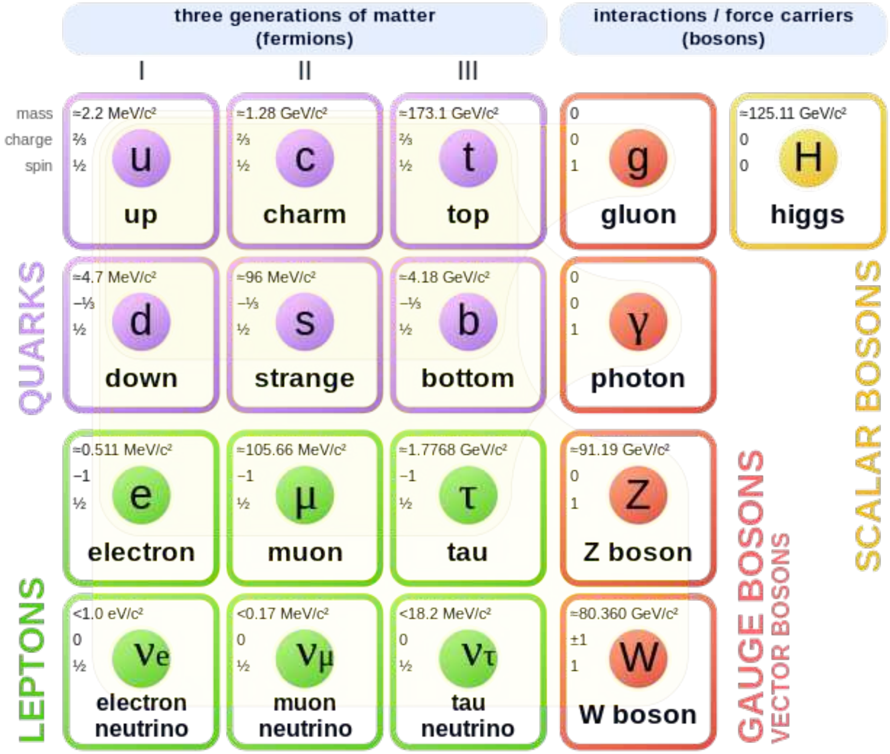

$$\mathcal{L}_{\rm SM} = \mathcal{L}_{\rm EW} + \mathcal{L}_{\rm QCD} + \underbrace{\mathcal{L}_{\rm Higgs} + \mathcal{L}_{\rm Yukawa}}_{\text{Higgs mechanism terms}}$$

The Higgs boson (discovered in 2012 by ATLAS & CMS):

- ***Origin of the mass of elementary particles***
  - *Fermions:* Yukawa couplings
  - *Bosons:* Brout-Englert-Higgs (BEH) mechanism
- ***Electroweak symmetry breaking***
  (BEH mechanism)
- ***Potential portal to new physics***
  e.g. Higgs coupling with dark matter

Higgs coupling to bosons & self coupling $\propto m_V^2$ or m_H^2
(BEH mechanism)

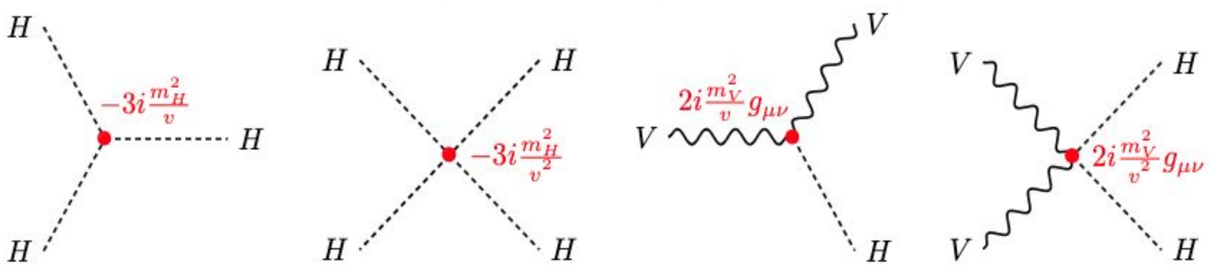

Higgs coupling to fermions $\propto m_f$
(Yukawa)

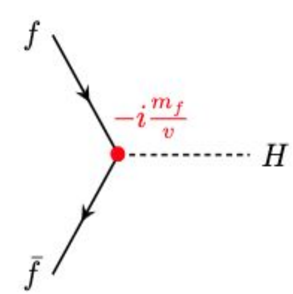

Higgs mass

Higgs mass

- m_H is a **fundamental/free parameter of the SM**
- **Very important to be measured as it determines many properties of the Higgs boson** e.g. cross-section, Higgs decay branching fraction…
- **Two golden channels: *$H\to\gamma\gamma$ & $H\to ZZ^*\to 4l$ for m_H* measurement**
  - Very good mass resolution ~1-2%
  - Efficient identification of final state particles
- **Best fit value for the Run 1 obtained with ATLAS+CMS combination:**
  m_H = 125.09 ± 0.24 (= ± 0.21 (stat) ± 0.11 (syst)) GeV
  → 0.2% precision

LHC Higgs Cross Section Working Group, arXiv:1610.07922

Single Higgs production cross-section w.r.t m_H

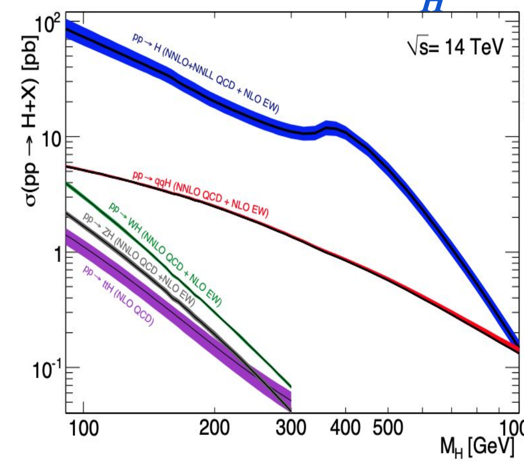

Phys. Rev. Lett. 114, 191803

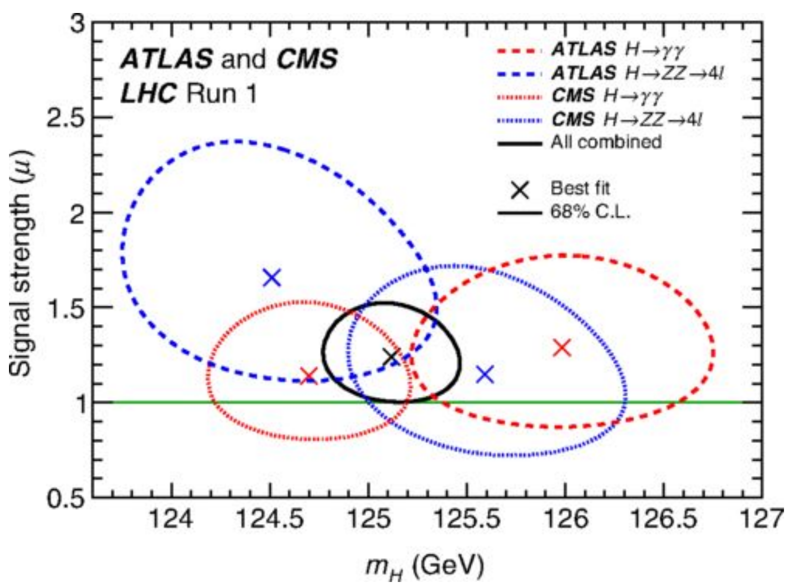

Higgs decay BR w.r.t m_H

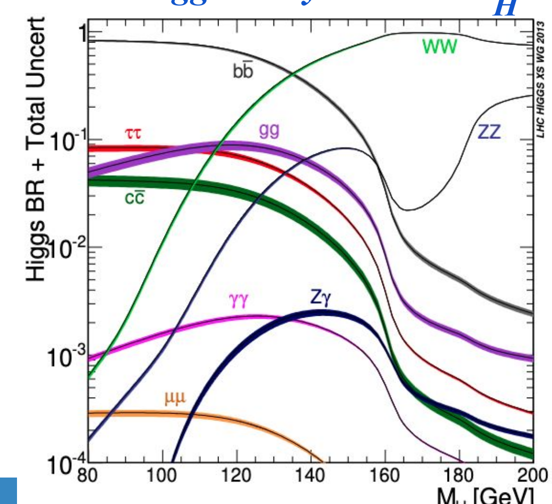

Higgs mass measurement with the $H \to ZZ^* \to 4l$ decay ($l = e,\mu$)

Phys. Lett. B 843 (2023) 137880

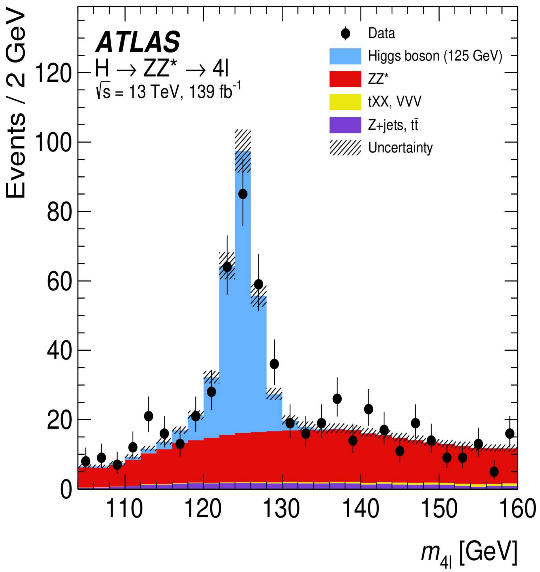

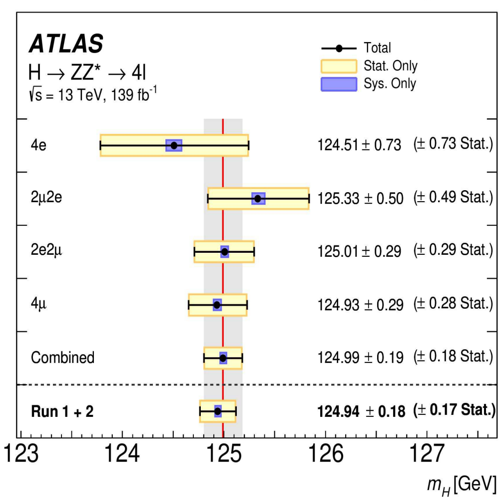

CMS-PAS-HIG-21-019 (2023)

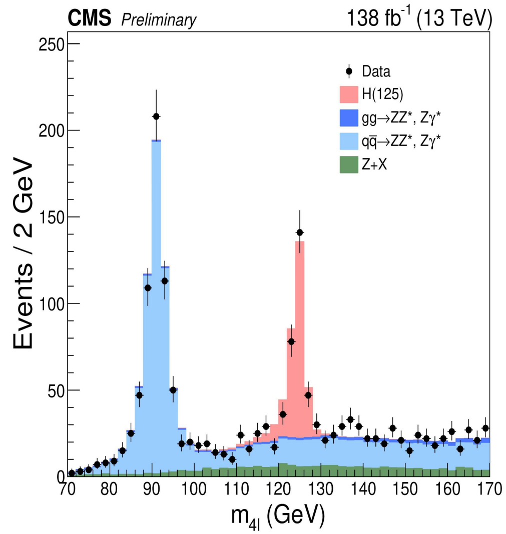

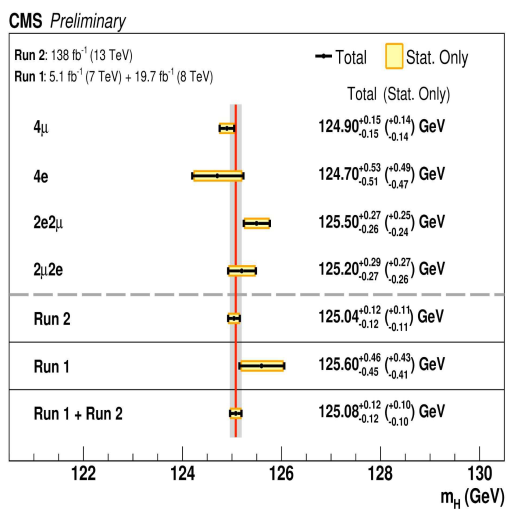

- Low statistic but large S/B & clean final state
- **Main observable m_{4l} (4-lepton mass)**

Run 1+2 result:

ATLAS: $m_H = 124.94 \pm 0.18$ $(= \pm 0.17(stat) \pm 0.03(syst))$ GeV

CMS: $m_H = 125.08 \pm 0.12$ $(= \pm 0.10(stat) \pm 0.07(syst))$ GeV

ATLAS Run 2

- DNN to discriminate signal from background
  → -2% on the m_H uncertainty
- σ_i = per event m_{4l} resolution estimated with a Quantile Regression NN (QRNN) → -1% on the m_H uncertainty
- **Simultaneous fit on data of (m_{4l}, DNN, σ_i)** in 4 categories $4\mu/2e2\mu/2\mu2e/4e$

CMS Run 2

- δ_{4l}/m_{4l} relative per-event m_{4l} uncertainty
  → 9 categories, allows to isolate events with better resolution
- $\mathcal{D}^{\text{kin}}_{\text{bkg}} = \dfrac{\mathcal{P}_{H\to 4l}}{\mathcal{P}_{H\to 4l} + \mathcal{P}_{q\bar{q}\to 4l}}$ kinematic likelihood discriminant,
  P = proba using kinematic information
  → Improvement of 4% on m_H measurement
- **Simultaneous fit on data of (m_{4l}, $D_{kin,\,bkg}$)** for each $\delta_{4l}/m_{4l} \times (4\mu/2e2\mu/2\mu2e/4e) \times$ data period

Phys. Lett. B 847 (2023) 138315

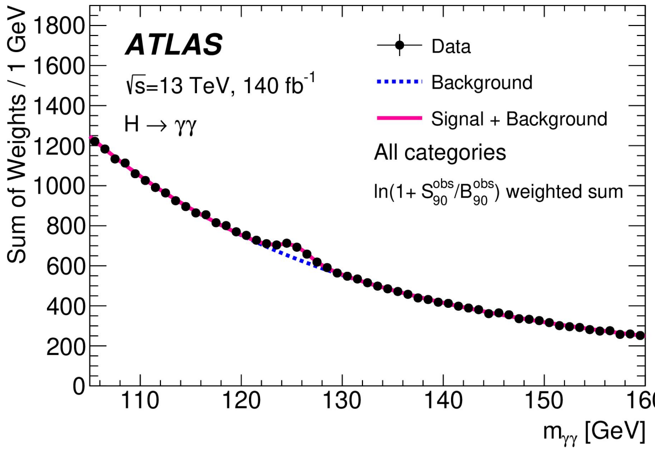

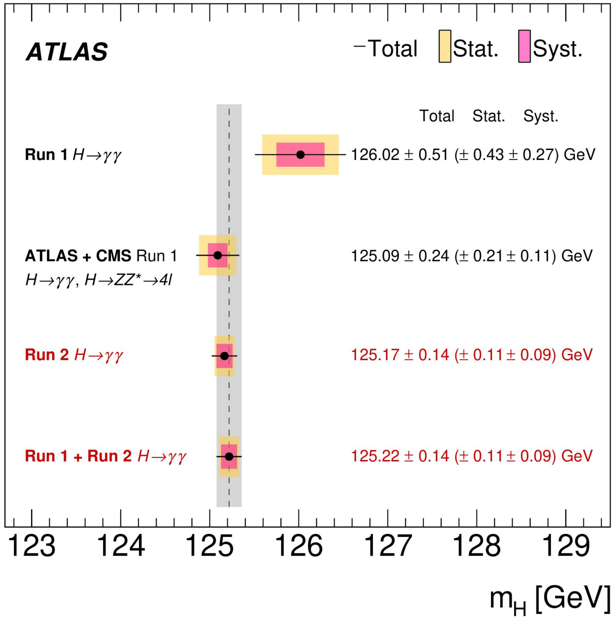

ATLAS Run 1+Run2

$m_H = 125.22 \pm 0.14$ ($= \pm 0.11$(stat) ± 0.09(syst)) GeV

- Small signal yield and S/B ratio, but very good mass resolution
- **Fit on $m_{\gamma\gamma}$:**
  - ***Signal :*** double sided crystal ball (DSCB) function depending on m_H
  - ***Background:*** power law, exponential/exponential of 2nd order polynomial depending on the category
  - ***14 categories depending on:***
    - "U"-event (resp. "C"-event) if no photon conversion (resp. one or two $\gamma \to ee$)
    - Central & outer barrels, and endcaps depending on $|\eta|$ of the calorimeter energy clusters
    - $p_{Tt}(\gamma\gamma)$ related to the di-photon system transverse momentum
- **Largest systematic uncertainties** = photon energy scale (PES)

  → Large improvement of photon energy calibration w.r.t previous iteration

CMS published a partial Run 2 result (see next slide)

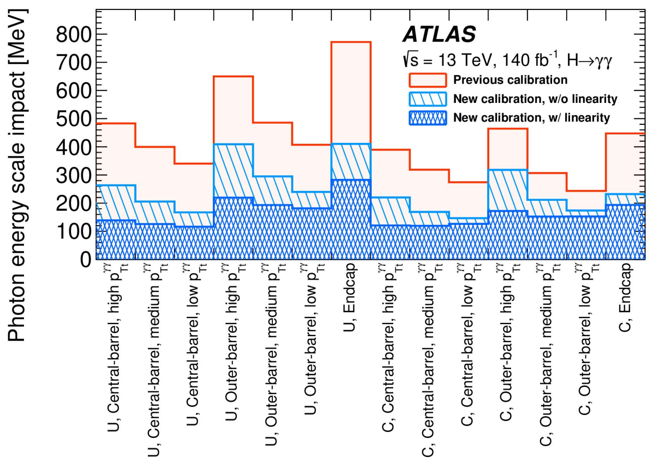

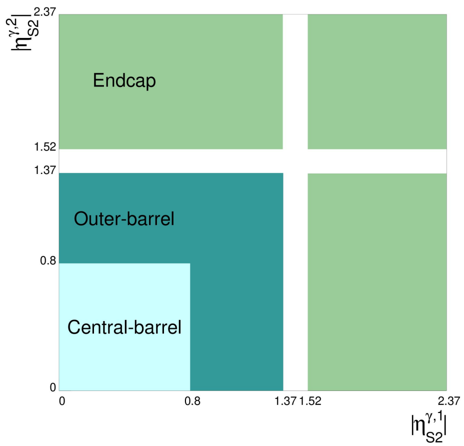

Combination of $H\rightarrow\gamma\gamma$ & $H\rightarrow ZZ^{*}\rightarrow 4l$ for Higgs mass measurement

Phys. Rev. Lett. 131, 251802 (2023)

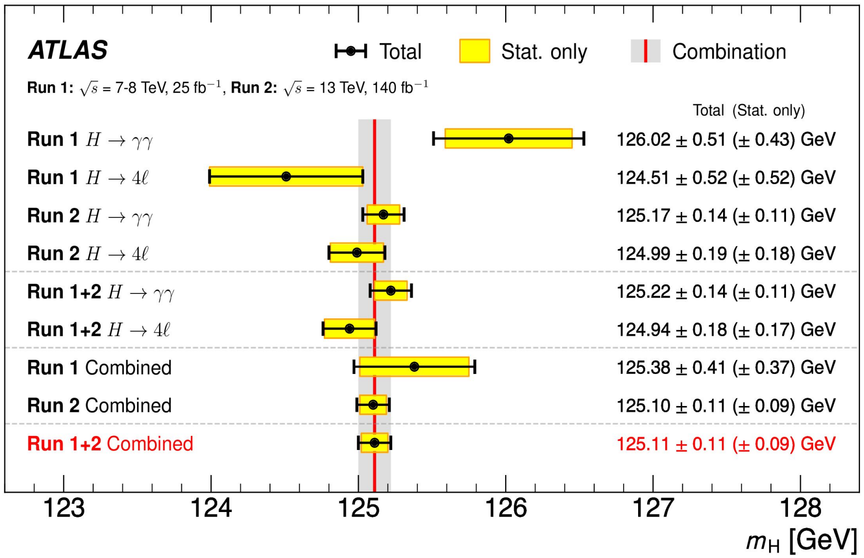

CMS Phys. Lett. B 805 (2020) 135425*

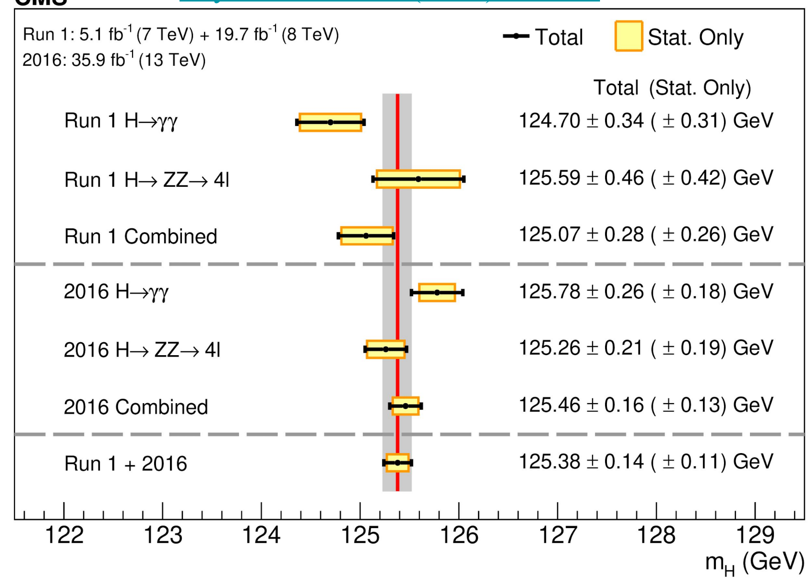

- **ATLAS Run 1+2:** m_H = 125.11 ± 0.11 (= ± 0.09 (stat) ± 0.06 (syst)) GeV
- **CMS Run 1+2016:** m_H = 125.38 ± 0.14 (= ± 0.11 (stat) ± 0.08 (syst)) GeV

→ 0.1% precision achieved with Run 1 + partial or full Run 2 measurement for ATLAS & CMS standalone!

*CMS = partial Run 2

- **ATLAS+CMS Run 1:** m_H = 125.09 ± 0.24 (= ± 0.21 (stat) ± 0.11 (syst)) GeV
  → 0.2% precision

Higgs width

SM Higgs width: Γ_H = 4.1 MeV but could be much larger for BSM theories

→ **In the SM scenario no direct measurement possible due to detector resolution (see previous slides)**

→ **Measure Γ_H in the $H \to ZZ$ channel* comparing on-shell and off-shell production**
→ **Use $H \to ZZ \to 4l$ & $H \to ZZ \to 2l2\nu$ events to enhance sensitivity**

$$\sigma^{\text{on-shell}}_{i \to H^* \to f} \sim \frac{g_i^2 g_f^2}{m_H \Gamma_H}$$ → **depends on Γ_H**

$$\sigma^{\text{off-shell}}_{i \to H^* \to f} \sim \frac{g_i^2 g_f^2}{m_f^2}$$ → **no Γ_H-dependence**

$$\mu_{i \to H^* \to f} = \frac{\sigma_{i \to H^* \to f}}{(\sigma_{i \to H^* \to f})_{\text{SM}}}$$ = **signal strength**

$$\frac{\Gamma_H}{\Gamma_H^{\text{SM}}} = \frac{\mu_{\text{off-shell}}}{\mu_{\text{on-shell}}}$$ → **Measure $\mu_{\text{on-shell}}$ & $\mu_{\text{off-shell}}$** **

About off-shell Higgs boson:

- **ATLAS:** confirmed the evidence of off-shell Higgs boson production from ZZ leptonic decay with an observed (expected) significance of 3.3σ (2.2σ) (Phys. Lett. B 846 (2023) 138223)
- **CMS:** had already observed evidence of such process in a past study (Nature Phys. 18 (2022) 1329)

* The indirect width determination is also possible through $t\bar{t}H$, 4 top & $H \to WW$ measurements
**Assume $g_i \times g_f$ is the same for the on-shell and off-shell ($i \to H \to f$) process

[Phys. Lett. B 846 (2023) 138223](#)

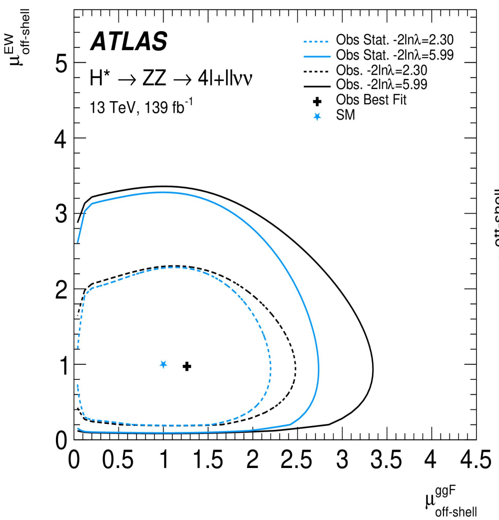

[CMS-PAS-HIG-21-019](#) (2023)

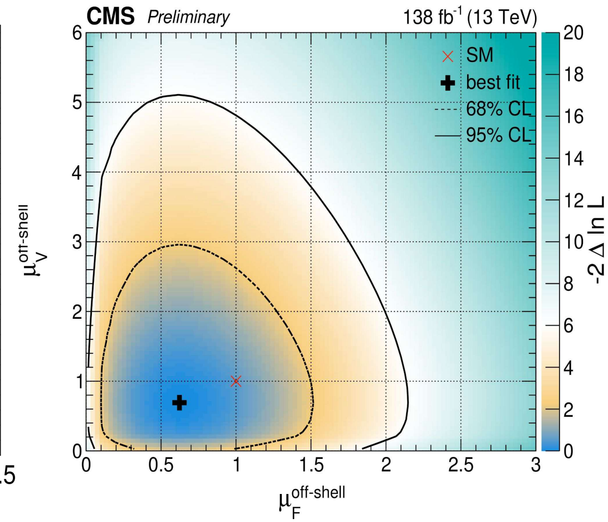

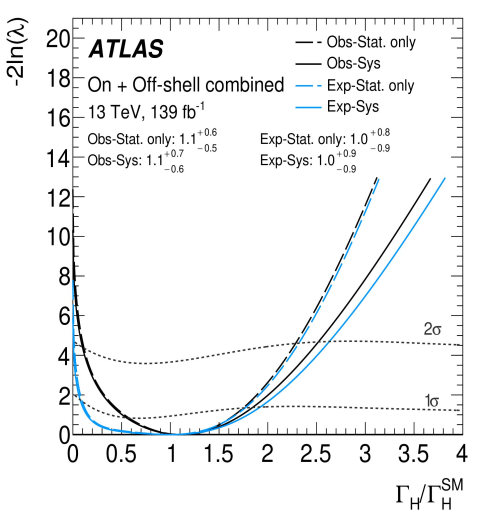

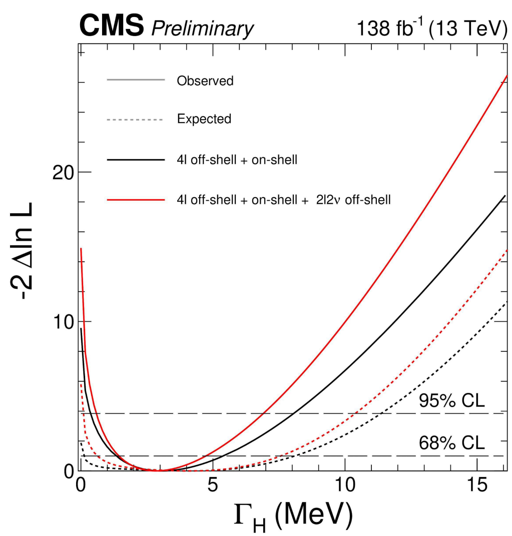

ATLAS

- **Measured value:** $\Gamma_H = 4.5^{+3.3}_{-2.5}$ MeV
- **Observed (expected) upper and lower 95% CL:**
  $0.5 < \Gamma_H < 10.5$ ($0.1 < \Gamma_H < 10.9$) MeV
- The 1σ & 2σ CL intervals are determined with toys because the asymptotic approximation is not valid (Neyman construction)

CMS

- **Measured value:** $\Gamma_H = 2.9^{+1.9}_{-1.4}$ MeV
- **Observed (expected) upper and lower 95% CL:**
  $0.6 < \Gamma_H < 7.0$ ($0.1 < \Gamma_H < 10.5$) MeV
- The 1σ & 2σ CL intervals are determined considering the asymptotic approximation is valid

→ Measured Higgs widths are compatible with the SM predictions

Higgs couplings

SM predictions: single Higgs production modes & Higgs decays

κ = coupling strength modifier = ratio of observed vs SM predicted coupling strengths ⇒ κ =1 ⇔ Higgs coupling compatible with the SM

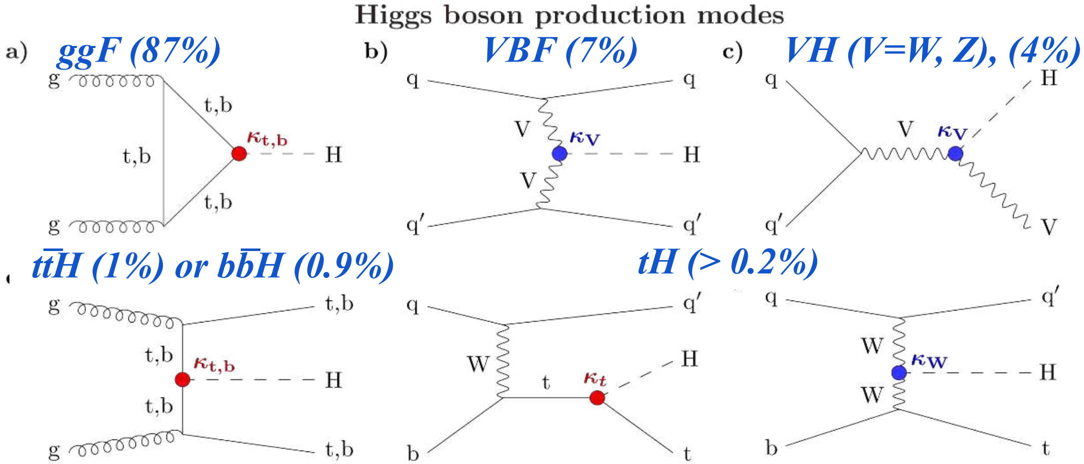

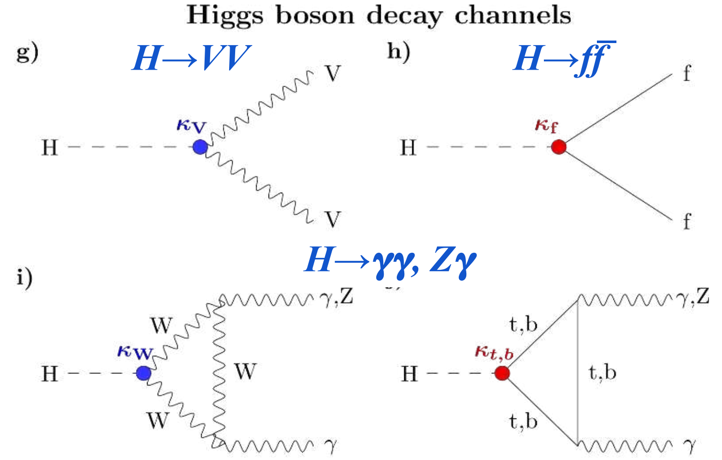

CMS, Nature **607**, 60–68 (2022)

Production mode	Cross section (pb)
ggH	48.31 ± 2.44
VBF	3.771 ± 0.807
WH	1.359 ± 0.028
ZH	0.877 ± 0.036
ttH	0.503 ± 0.035
bbH	0.482 ± 0.097
tH	0.092 ± 0.008

SM predictions for $\sqrt{s}$=13 TeV
m_H = 125 GeV

Decay channel	Branching fraction (%)
bb	57.63 ± 0.70
WW	22.00 ± 0.33
gg	8.15 ± 0.42
ττ	6.21 ± 0.09
cc	2.86 ± 0.09
ZZ	2.71 ± 0.04
γγ	0.227 ± 0.005
Zγ	0.157 ± 0.009
ss	0.025 ± 0.001
μμ	0.0216 ± 0.0004

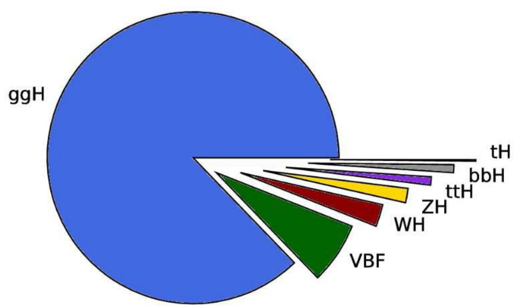

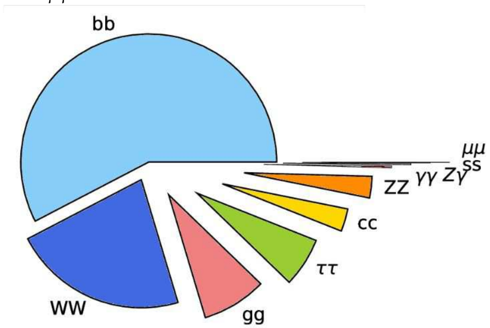

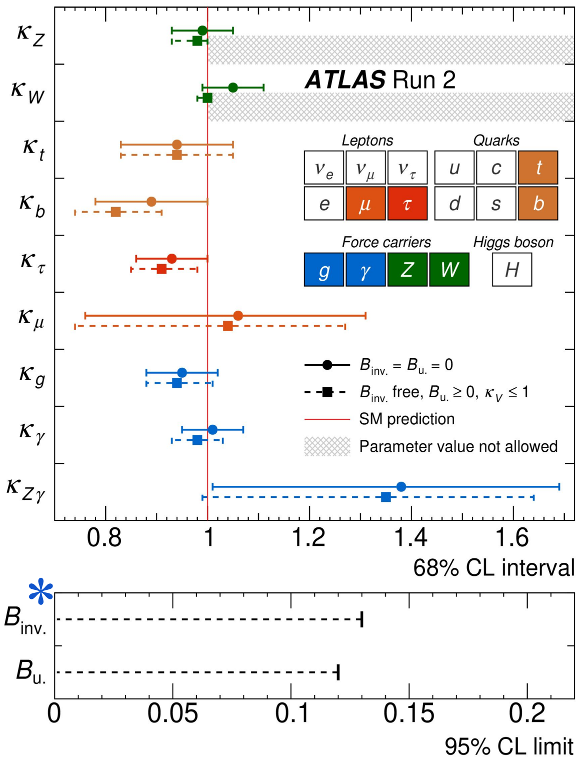

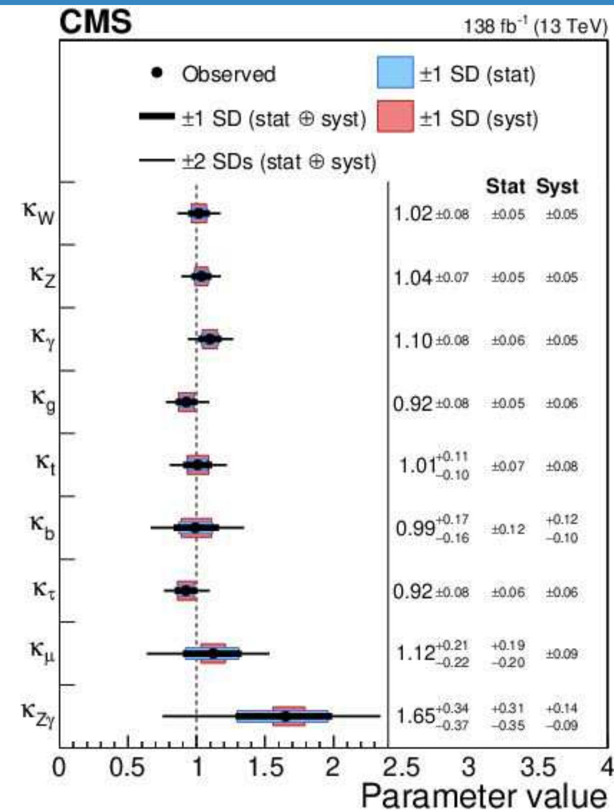

Higgs-to-fermion (κ_f) & Higgs-to-boson couplings (κ_V) simultaneous fit

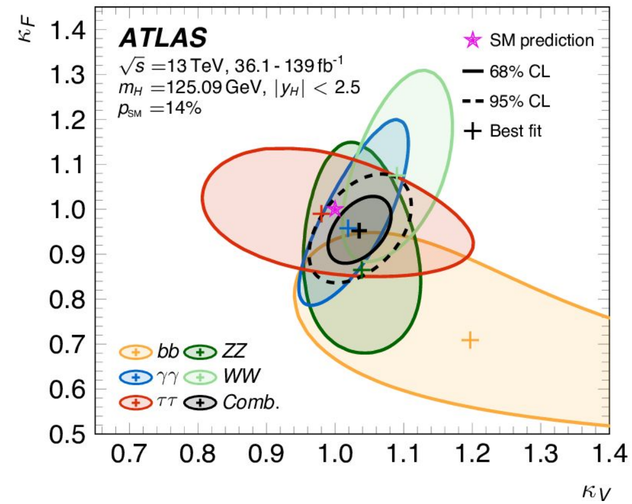

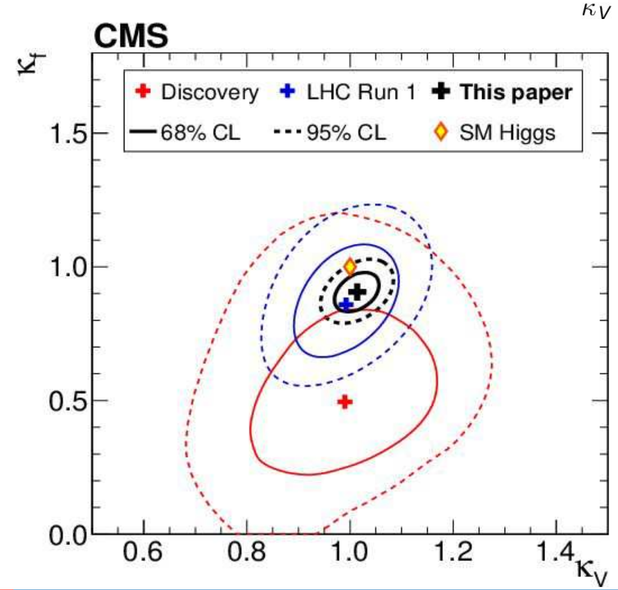

→ Probe the Yukawa & BEH mechanisms

→ Good agreement with the SM predictions

→ Much tighter constraints on Higgs couplings w.r.t Run 1

ATLAS (Nature 607, 52–59 (2022)) & CMS (Nature 607, 60–68 (2022))

Publications for the 10th year of the discovery of the Higgs

* Depending on assumptions (usually $\kappa_V \leq 1$), the determination of B_{inv} (i.e. BR($H\rightarrow$*invisible*)) & B_u (i.e. BR($H\rightarrow$*undetected*)) also provides a limit on Γ_H

Higgs-to-bottom coupling measurement with the $H \to b\bar{b}$ decay

***VH, $H \to b\bar{b}$, $V \to$ leptons* is the most sensitive process**

ATLAS-CONF-2021-051

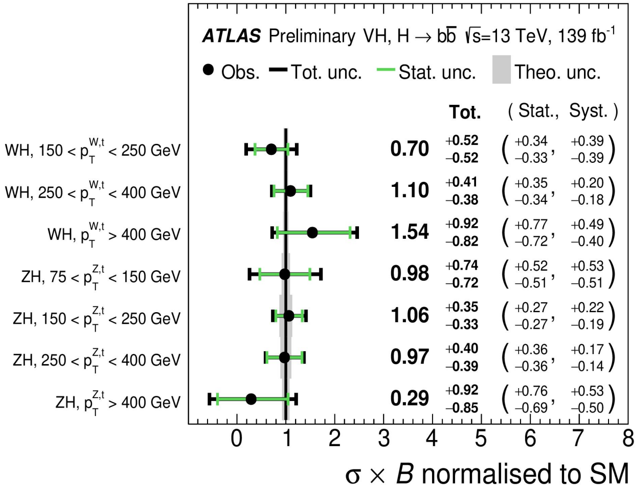

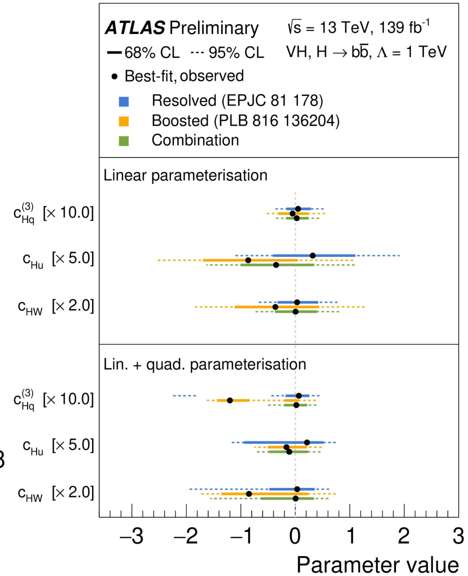

ATLAS

- **Resolved+Boosted combination, STXS meas.**

$$\mu_{WH}^{bb} = 1.03^{+0.28}_{-0.27} = 1.03 \pm 0.19\,(\text{stat.})^{+0.21}_{-0.19}\,(\text{syst.})$$
$$\mu_{ZH}^{bb} = 0.97^{+0.25}_{-0.23} = 0.97 \pm 0.17\,(\text{stat.})^{+0.18}_{-0.15}\,(\text{syst.}).$$

- **Effective field theory (EFT) interpretation**

  c_i = Wilson coefficient: $c_i = 0 \Leftrightarrow$ SM-like

$$\mathcal{L}_{\text{SMEFT}} = \mathcal{L}_{\text{SM}} + \sum_{D \geq 5} \sum_{i \in \mathcal{W}_D} \frac{c_i^{(D)}}{\Lambda^{D-4}} \mathcal{O}_i^{(D)}$$

CMS-PAS-HIG-20-001 (2023)

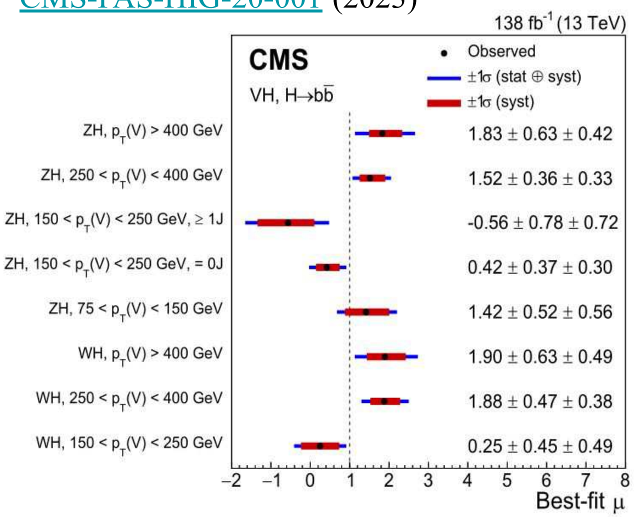

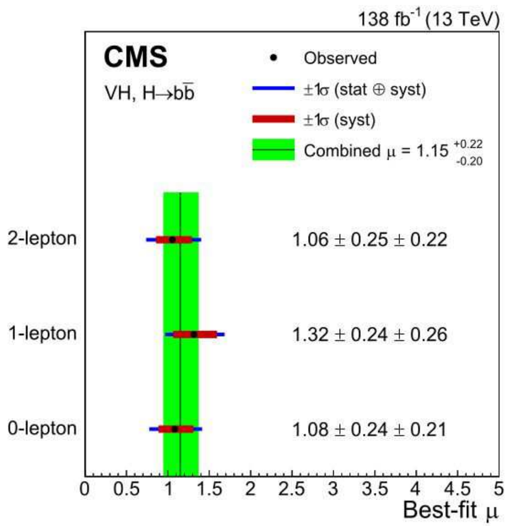

CMS

- **Resolved+Boosted combination, STXS meas.**

$$\mu_{WH}^{bb} = 1.31^{+0.35}_{-0.35} = 1.31 \pm 0.24\,(\text{stat.}) \pm 0.26\,(\text{syst.}),$$
$$\mu_{ZH}^{bb} = 1.07^{+0.24}_{-0.24} = 1.07 \pm 0.17\,(\text{stat.}) \pm 0.17\,(\text{syst.}).$$

→ STXS measurement & EFT interpretation compatible with SM predictions

Higgs-to-charm coupling measurement with the $H \to c\bar{c}$ decay

Eur. Phys. J. C 82 (2022) 717

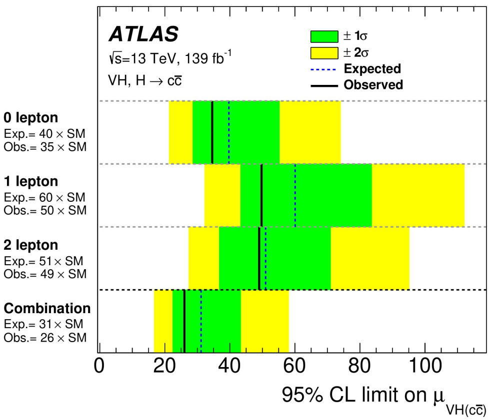

Phys. Rev. Lett. 131 (2023) 061801

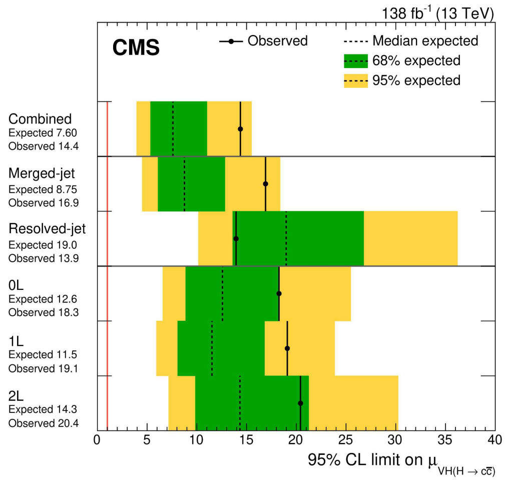

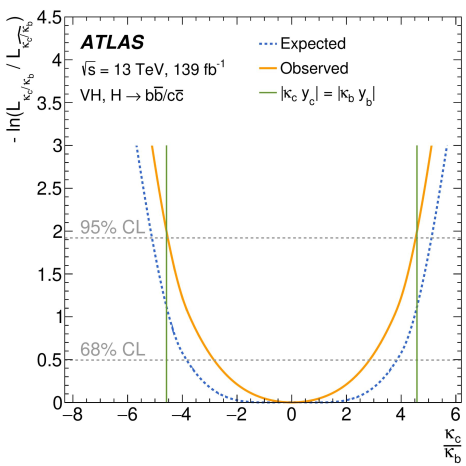

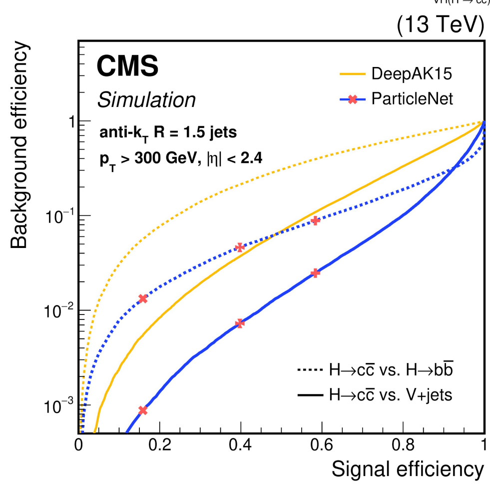

***VH, $H \to c\bar{c}$, $V \to$ leptons* is the most sensitive process**

ATLAS

- Only resolved topology
- **Observed (expected) 95% CL VH, $H \to c\bar{c}$ signal strength upper limit: 26 (31)**
- **Observed (expected) 95% CL interval:**

  $|\kappa_c| < 8.5$ ($|\kappa_c| < 12.4$)

  → **Found that $|\kappa_c|/|\kappa_b| < m_b/m_c = 4.5$ i.e. Higgs-to-charm coupling weaker than Higgs-to-bottom**

CMS

- Resolved+Boosted combination
- **Sensitivity driven by the boosted topology**
  GNN $H \to c\bar{c}$ boosted tagger (ParticleNet)
- **Observed (expected) 95% CL VH, $H \to c\bar{c}$ signal strength upper limit: 14.4 (7.60)**
- **Observed (expected) 95% CL interval:**

  $1.1 < |\kappa_c| < 5.5$ ($|\kappa_c| < 3.4$)

→ **CMS = most stringent constraints to date**
Reached sensitivity foreseen for the end of HL-LHC!

Determination of the relative sign of the Higgs-to-*W* & *Z* couplings with VBF *WH* process

$\lambda_{WZ} := \kappa_W / \kappa_Z$ ⇒ SM predicts that $\lambda_{WZ} = 1$ *since* $\kappa_W = \kappa_Z = 1$

Previously ATLAS & CMS have both measured $|\lambda_{WZ}| = 1$ with a precision of ~6%

However the λ_{WZ} sign was largely unconstrained
→ Probe the EW symmetry breaking
→ Negative sign would imply new physics !

Some LO VBF *WH* processes

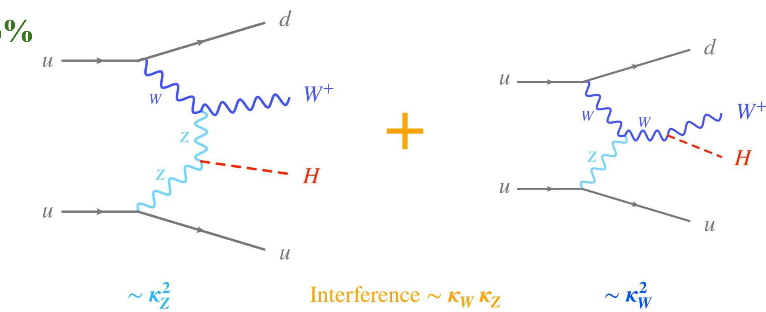

$$\sigma_{\mathrm{VBF},WH} \propto \kappa_Z^2 |\mathcal{M}_Z|^2 + \kappa_W^2 |\mathcal{M}_W|^2 - 2\kappa_Z \kappa_W \Re[\mathcal{M}_Z^\dagger \mathcal{M}_W]$$
$$= \kappa_Z^2 |\mathcal{M}_Z|^2 + \kappa_W^2 |\mathcal{M}_W|^2 - 2\kappa_Z^2 \lambda_{WZ} \Re[\mathcal{M}_Z^\dagger \mathcal{M}_W]$$

In VBF *WH* process, the Higgs boson interacts with either a *W* or *Z* boson.

- **Destructive** interferences between those processes if $\lambda_{WZ} > 0$
- **Constructive** interferences if $\lambda_{WZ} < 0$

→ Through VBF *WH* process probe λ_{WZ} sign

ATLAS & CMS are selecting VBF $WH \to l\nu b\bar{b}jj$ events

Both collaboration are excluding $\lambda_{WZ} = -1$ with a significance greater than 5σ

HIGG-2021-21 (2024)

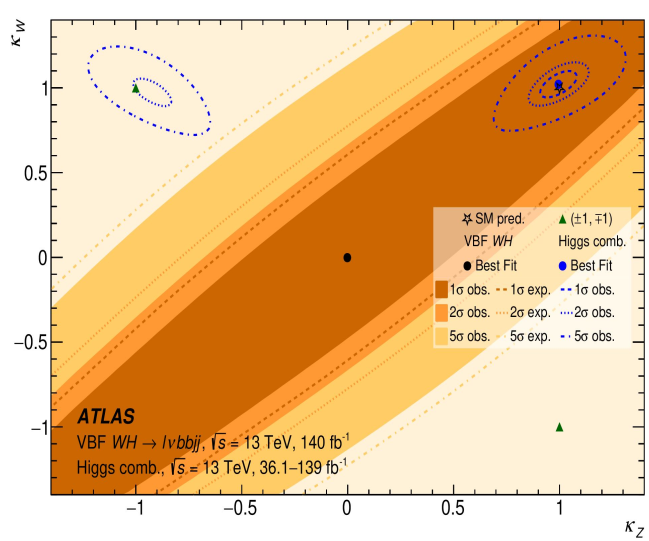

CMS-PAS-HIG-23-007 (2023)

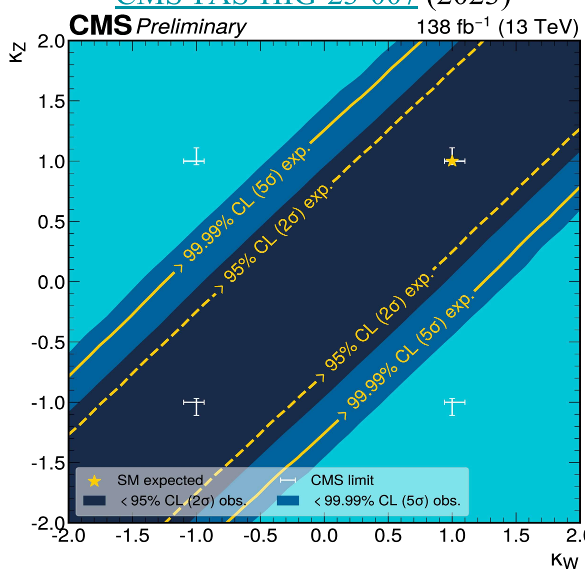

CMS, Nature **607**, 60–68 (2022)

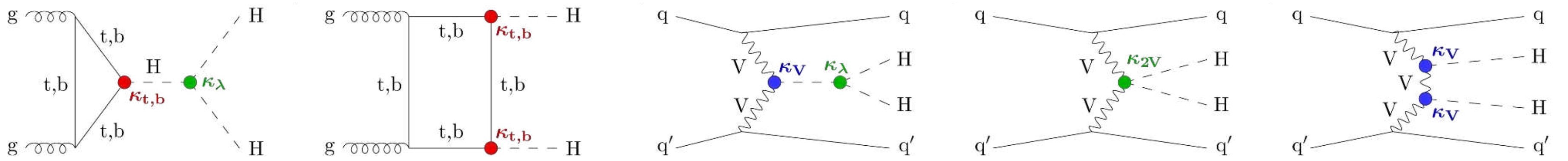

Allows probing $\kappa_\lambda = \lambda/\lambda_{SM}$ & $\kappa_{2V} = \lambda_{2V}/\lambda_{2V,SM}$ ***modifiers***

- The Higgs self-coupling & Higgs potential shape remain largely unconstrained
  → Different shape would imply new Physics (Phys. Rev. D 101, 075023)
- Challenging di-Higgs searches as $\sigma_{HH} / \sigma_H \sim 10^{-3}$
- Three most sensitive analyses (BR): *$HH \to b\bar{b}b\bar{b}$ (34%), $b\bar{b}\tau\tau$ (7.3%) & $b\bar{b}\gamma\gamma$ (0.3%)*
  → Combination to improve sensitivity to couplings
- Single Higgs analyses are indirectly sensitive to the Higgs self-coupling
  (due to higher order corrections, 2 examples below)

ATLAS, Phys. Lett. B 843 (2023) 137745

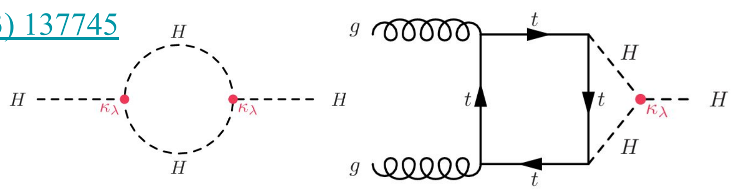

Higgs potential

$$V(\phi) = \mu^2 |\phi|^2 + \lambda |\phi|^4$$

Spontaneous symmetry breaking for
$\mu^2 < 0$ & $\lambda > 0$

λ = Higgs self coupling constant

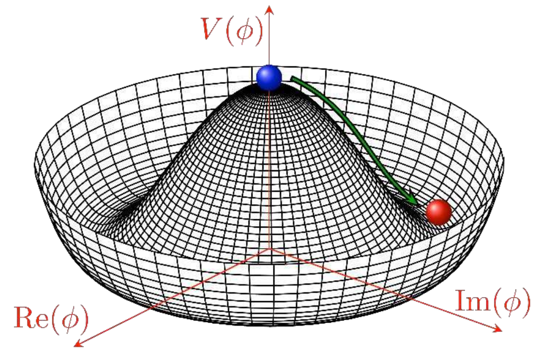

λ_{2V} = Higgs quartic VVHH coupling

For some BSM theories $\kappa_{2V} \neq 1$

Phys. Lett. B 843 (2023) 137745

Nature 607, 60–68 (2022)

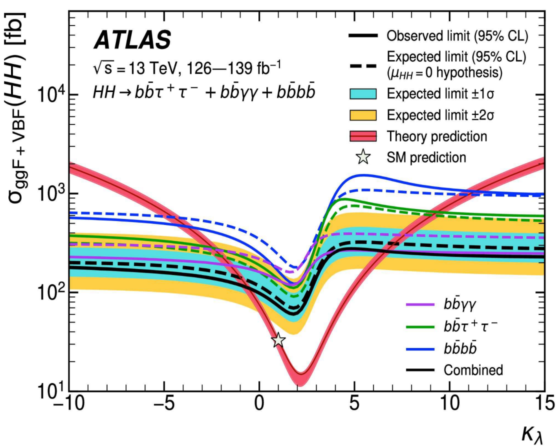

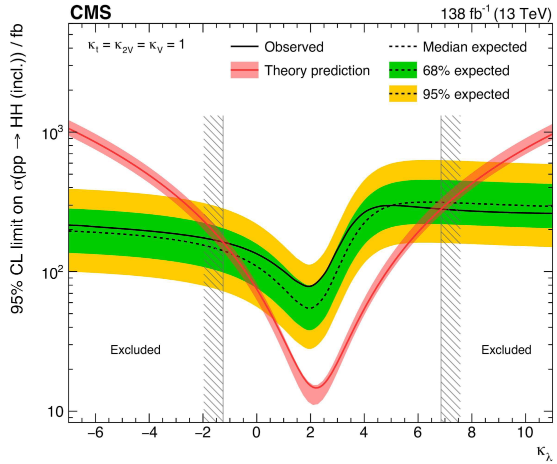

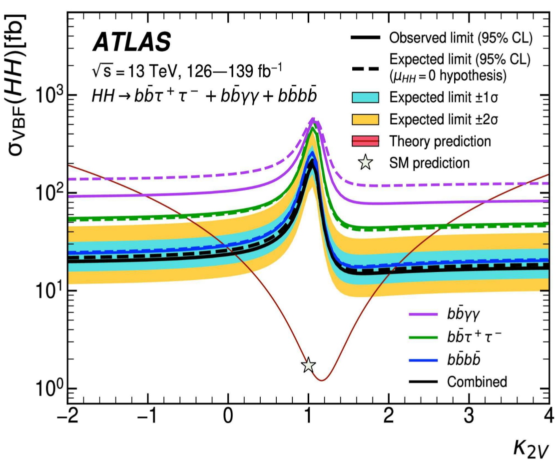

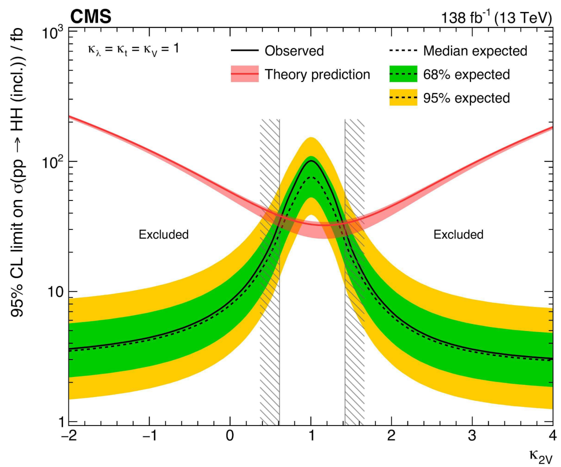

ATLAS: *$HH \to b\bar{b}b\bar{b}$, $b\bar{b}\gamma\gamma$ & $b\bar{b}\tau\tau$*
(assuming that the other Higgs boson interactions are as predicted by the SM)

obs: $-0.6 < \kappa_\lambda < 6.6$ (exp: $-2.1 < \kappa_\lambda < 7.8$)

obs: $0.1 < \kappa_{2V} < 2.0$ (exp: $0.0 < \kappa_{2V} < 2.1$)

CMS: *$HH \to b\bar{b}b\bar{b}$, $b\bar{b}\gamma\gamma$, $b\bar{b}\tau\tau$, $b\bar{b}ZZ$ & Multilepton*
(same assumption about other interactions)

obs: $-1.24 < \kappa_\lambda < 6.49$ (exp*: $-1 < \kappa_\lambda < 7$)

obs: $0.67 < \kappa_{2V} < 1.38$ (exp*: $0.6 < \kappa_\lambda < 1.4$)

CMS: $\kappa_{2V} = 0$ excluded with 6.6σ

*CMS expected limits estimated from plots (missing info in publication)
NB: the observed values are obtained from
a LLR test statistic and NOT from the plots in this slide

[Phys. Lett. B 843 (2023) 137745]

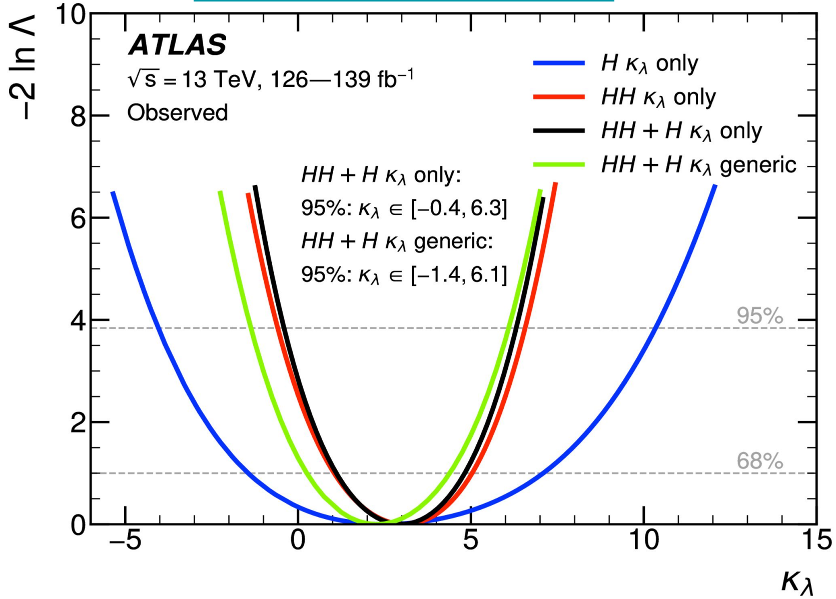

[CMS-PAS-HIG-23-006]

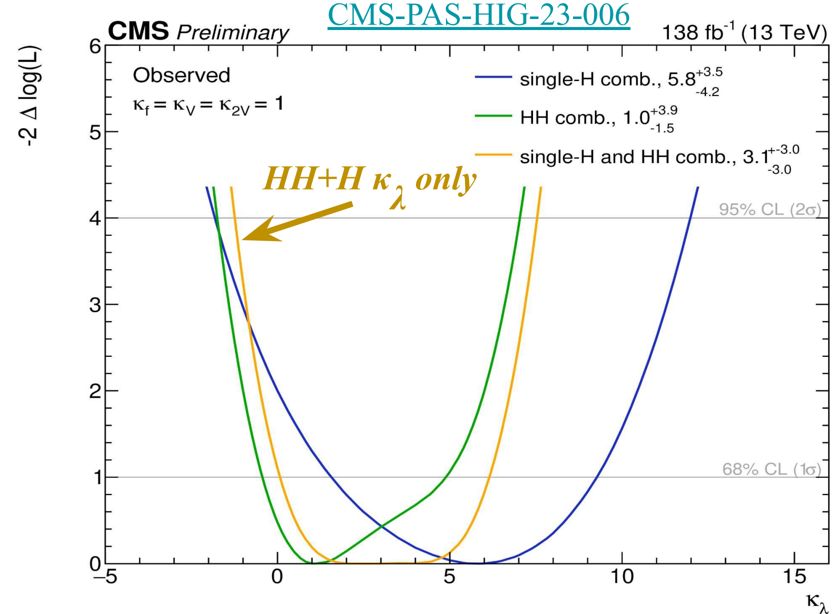

- *HH+H κ_λ only* = *κ_λ is the only floating parameter*
  - ATLAS *obs: $-0.4 < \kappa_\lambda < 6.3$ (exp: $-1.9 < \kappa_\lambda < 7.6$)*
  - CMS *obs: $-1.2 < \kappa_\lambda < 7.5$ (exp: $-2.0 < \kappa_\lambda < 7.7$)*

→ ATLAS & CMS have very similar sensitivities to κ_λ

- *HH+H κ_λ generic* = κ_λ, κ_t, κ_b, κ_V & κ_τ **free parameters**
  - ATLAS *obs: $-1.4 < \kappa_\lambda < 6.1$ (exp: $-2.2 < \kappa_\lambda < 7.7$)*
  - CMS *obs: $-1.4 < \kappa_\lambda < 7.8$ (exp: $-2.3 < \kappa_\lambda < 7.7$)*

→ Less assumptions required on the other couplings for *H+HH* combination

Higgs CP properties

Test of Higgs CP invariance with $H \to VV^* \to 4l$ processes ($l=e,\mu$)

CP violation in SM could explain the matter-antimatter asymmetry in the universe

→ Search for CP-odd BSM couplings* in $H \to VV^* \to 4l$ events with EFT interpretation

$$|\mathcal{M}|^2 = \left|\mathcal{M}_{\mathrm{SM}} + \sum_i \frac{c_i}{\Lambda^2}\mathcal{M}_{\mathrm{BSM},i}\right|^2$$
$$= |\mathcal{M}_{\mathrm{SM}}|^2 + 2\sum_i \frac{c_i}{\Lambda^2}\Re\left(\mathcal{M}^*_{\mathrm{SM}}\mathcal{M}_{\mathrm{BSM},i}\right) + \sum_i\sum_j \frac{c_i c_j}{\Lambda^4}\Re\left(\mathcal{M}^*_{\mathrm{BSM},i}\mathcal{M}_{\mathrm{BSM},j}\right)$$

→ Define (CP-odd) optimal observables:

$$OO = \frac{2\Re\left(\mathcal{M}^*_{\mathrm{SM}}\mathcal{M}_{\mathrm{BSM}}\right)}{|\mathcal{M}_{\mathrm{SM}}|^2}$$

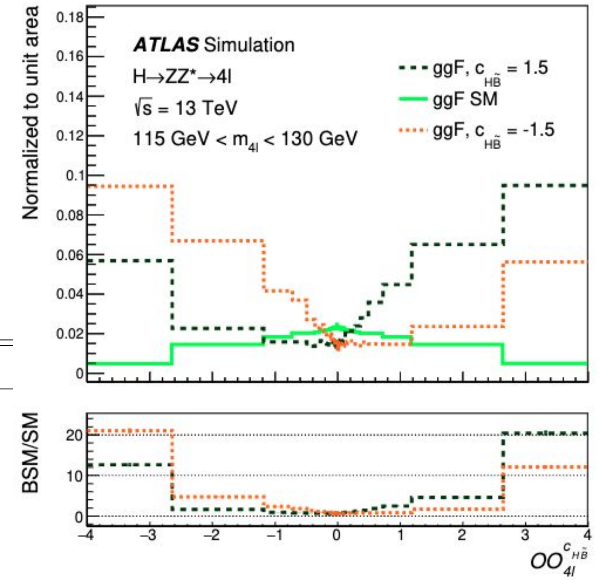

→ No anomalous CP couplings observed by ATLAS & CMS

HIGG-2018-30 (2023)

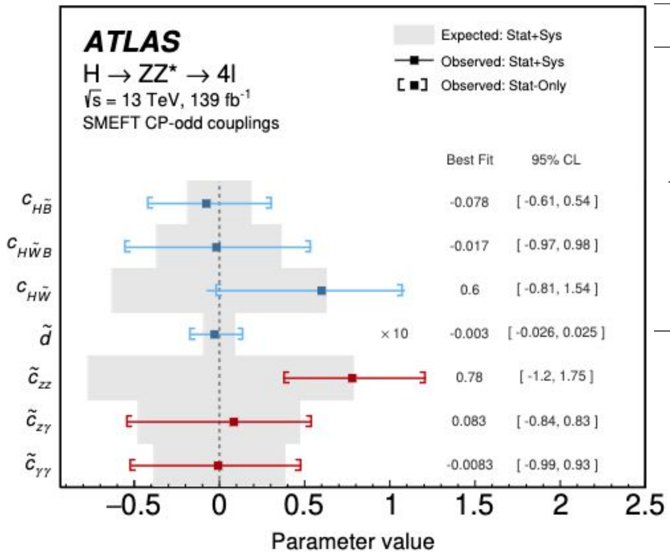

CMS, Phys. Rev. D 104, 052004 (2021)

Channels	Coupling	Observed	Expected
VBF & VH & $H \to 4\ell$	$c_{H\Box}$	$0.04^{+0.43}_{-0.45}$	$0.00^{+0.75}_{-0.93}$
	c_{HD}	$-0.73^{+0.97}_{-4.21}$	$0.00^{+1.06}_{-4.60}$
	c_{HW}	$0.01^{+0.18}_{-0.17}$	$0.00^{+0.39}_{-0.28}$
	c_{HWB}	$0.01^{+0.20}_{-0.18}$	$0.00^{+0.42}_{-0.31}$
	c_{HB}	$0.00^{+0.05}_{-0.05}$	$0.00^{+0.03}_{-0.08}$
	$c_{H\tilde{W}}$	$-0.23^{+0.51}_{-0.52}$	$0.00^{+1.11}_{-1.11}$
	$c_{H\tilde{W}B}$	$-0.25^{+0.56}_{-0.57}$	$0.00^{+1.21}_{-1.21}$
	$c_{H\tilde{B}}$	$-0.06^{+0.15}_{-0.16}$	$0.00^{+0.33}_{-0.33}$

*The spin-parity (J^P) of the Higgs is 0^+ in the SM.
The observation of the $H \to \gamma\gamma$, ZZ, WW decays by ATLAS & CMS excluded pure states 0^-, $1^\pm$, $2^\pm$ at more than 99% confidence level (CL)
(quote from HIGG-2018-30)

- **Higgs mass measurement: ATLAS & CMS are reaching the per mil precision for the Run 2!**
  → $\delta m_H \sim 0.1$ GeV
  → The Higgs mass is one of the most crucial SM parameters to measure
  as many Higgs properties are m_H-dependent

- **Higgs widths Γ_H measured by ATLAS & CMS are compatible with the SM predictions**

- **Higgs couplings measured up-to-date are SM-like, no significant deviation from SM predictions are observed**
  → Crucial constraining Higgs-to-fermion & Higgs-to-boson couplings
  to extensively probe the Yukawa, BEH mechanisms & thus the EW symmetry breaking

  → STXS and EFT interpretations to extensively test the validity of the SM in different region of phase space
  e.g. high energy domain + testing CP properties of the Higgs

  → Di-Higgs searches to constrain the Higgs potential shape, Higgs-self (κ_λ) and quartic *HHVV* (κ_{2V}) couplings

  → Single & di-Higgs measurements combination to constrain κ_λ & κ_{2V} with looser SM assumptions

- **I could unfortunately NOT cover all measurements from ATLAS & CMS in this presentation**
  Many more interesting results out there!

Thanks for your attention!

Backup

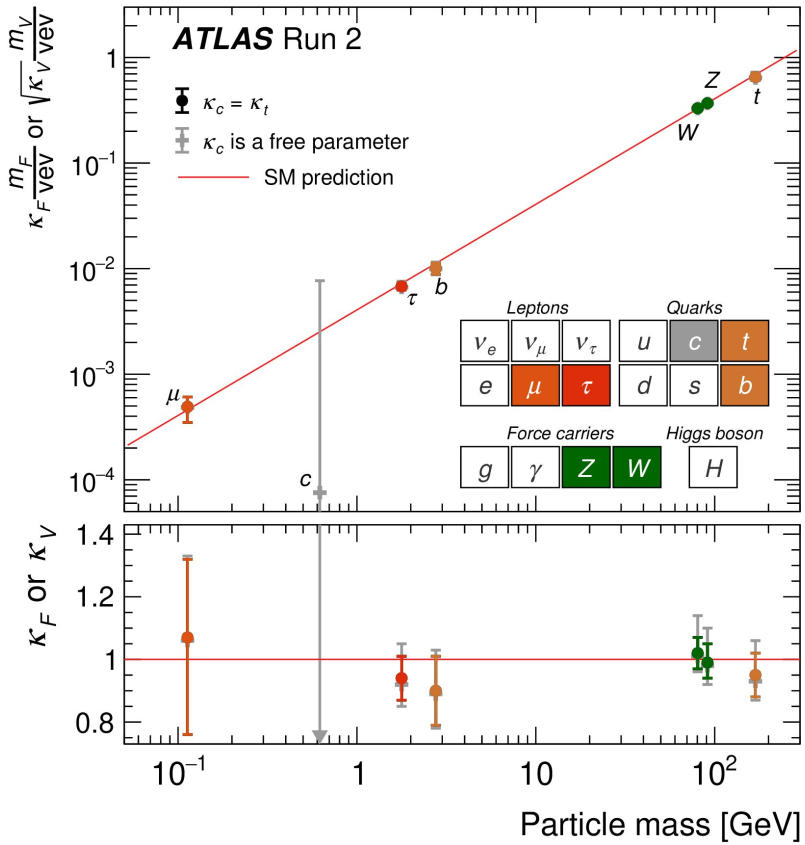

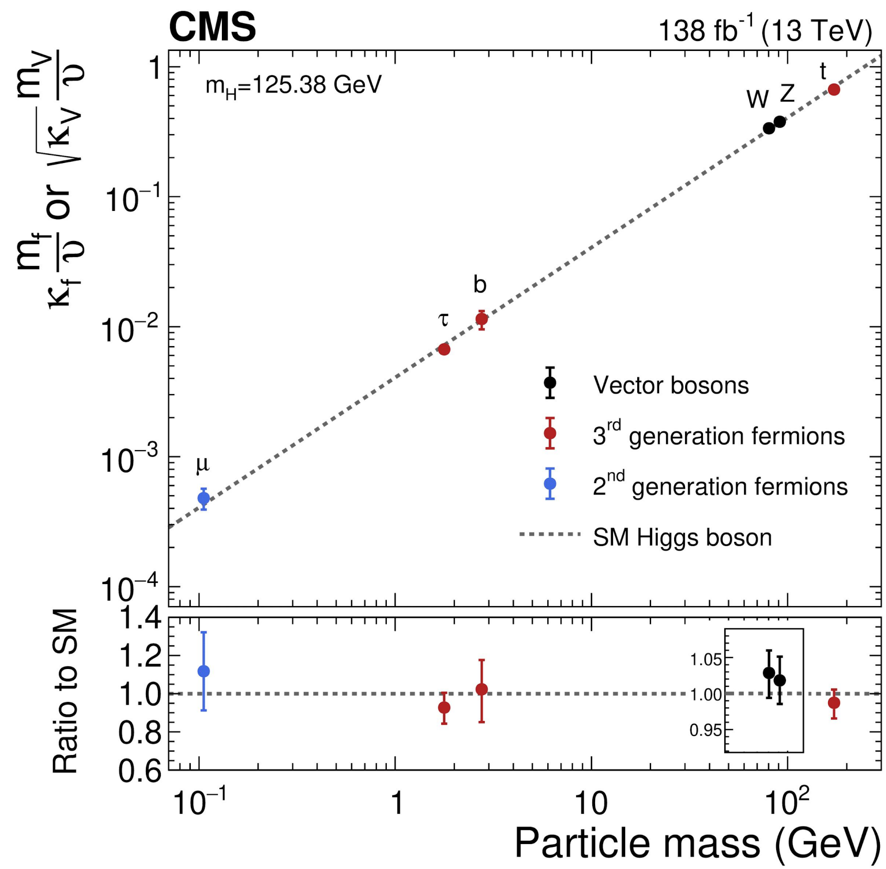

→ Good agreement with the SM predictions

Higgs couplings verified over 3 order of magnitude m_μ ~ 105 MeV vs m_t ~ 172.5 GeV

ATLAS (Nature 607, 52–59 (2022)) & CMS (Nature 607, 60–68 (2022))
Publications for the 10th year of the discovery of the Higgs

Higgs production mode measurements

μ = *signal strength* = $\dfrac{\sigma \cdot \mathcal{B}}{\sigma_{SM} \cdot \mathcal{B}_{SM}}$ $\Rightarrow$ $\mu = 1 \Leftrightarrow$ *Measurement compatible with the SM*

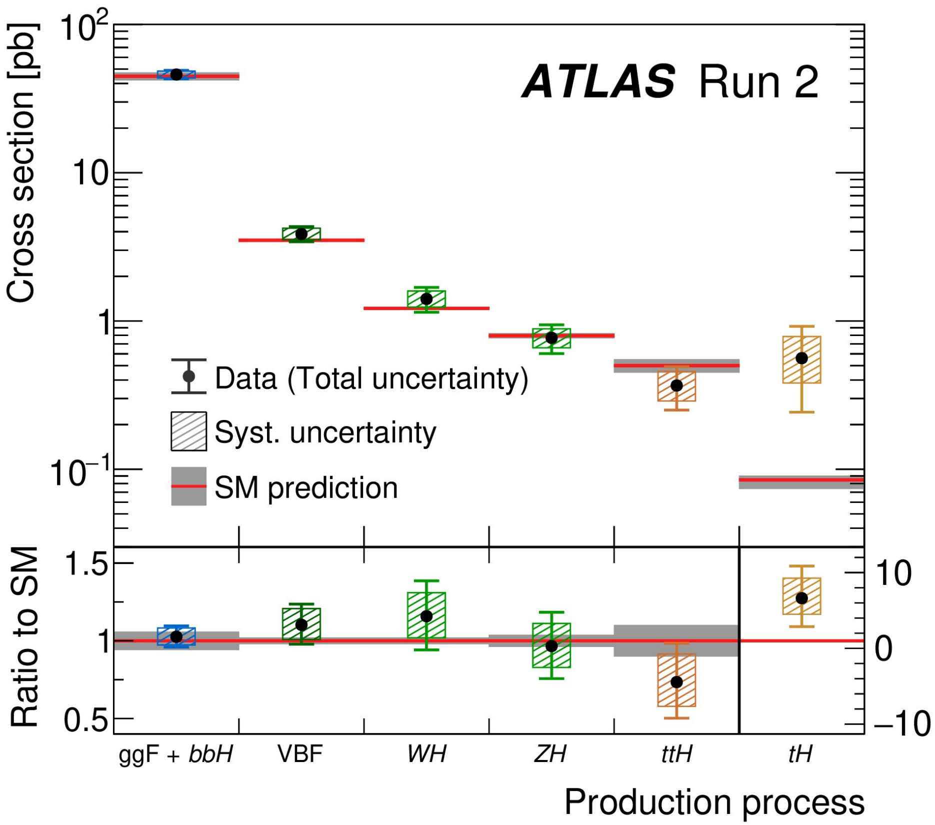

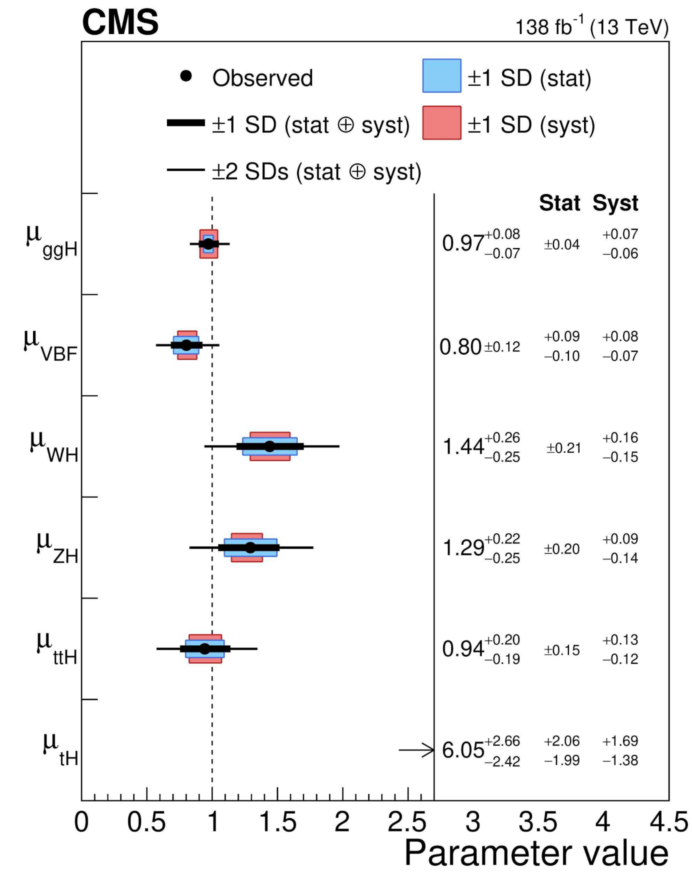

→ Good agreement with the SM predictions except for the very rare tH process

ATLAS (Nature 607, 52–59 (2022)) & CMS (Nature 607, 60–68 (2022))
Publications for the 10th year of the discovery of the Higgs

Nature 607, 52–59 (2022)

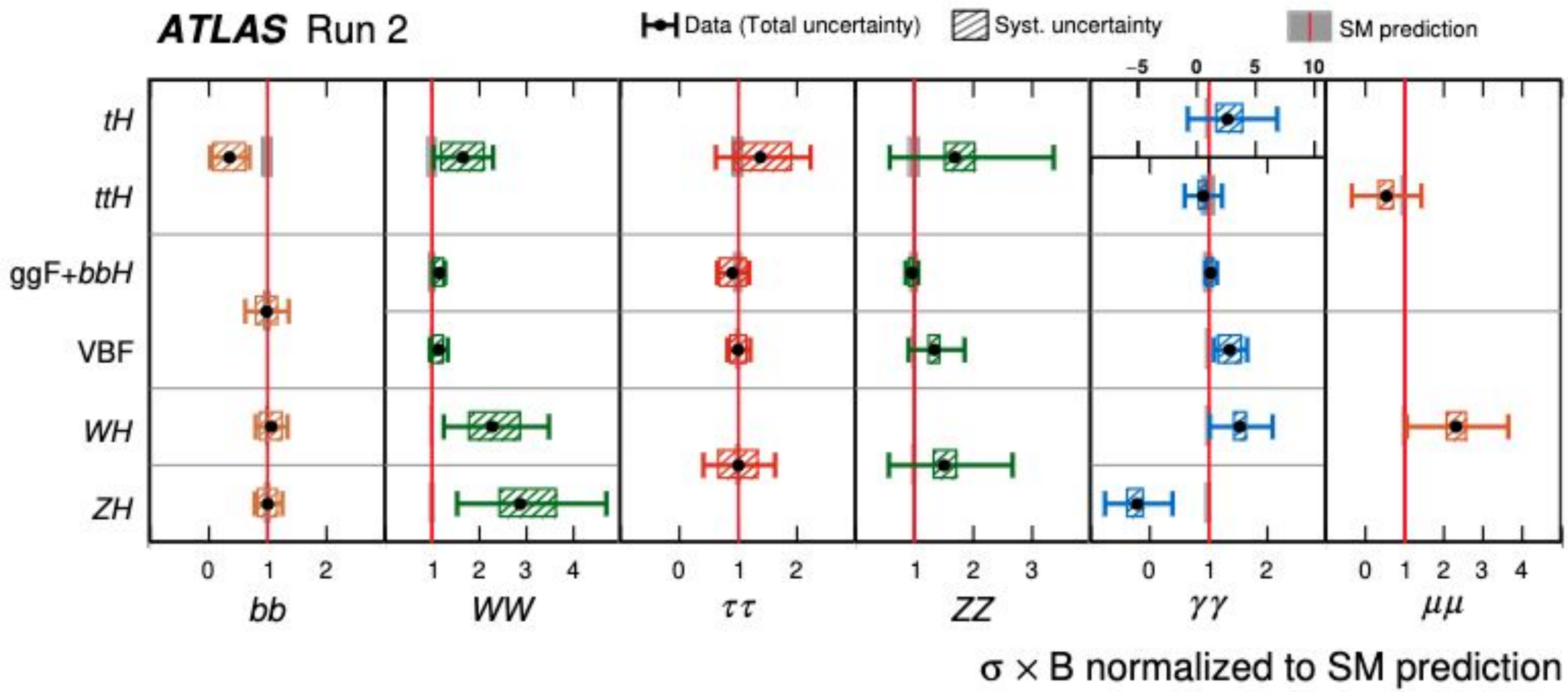

[Nature **607**, 60–68 (2022)](#)

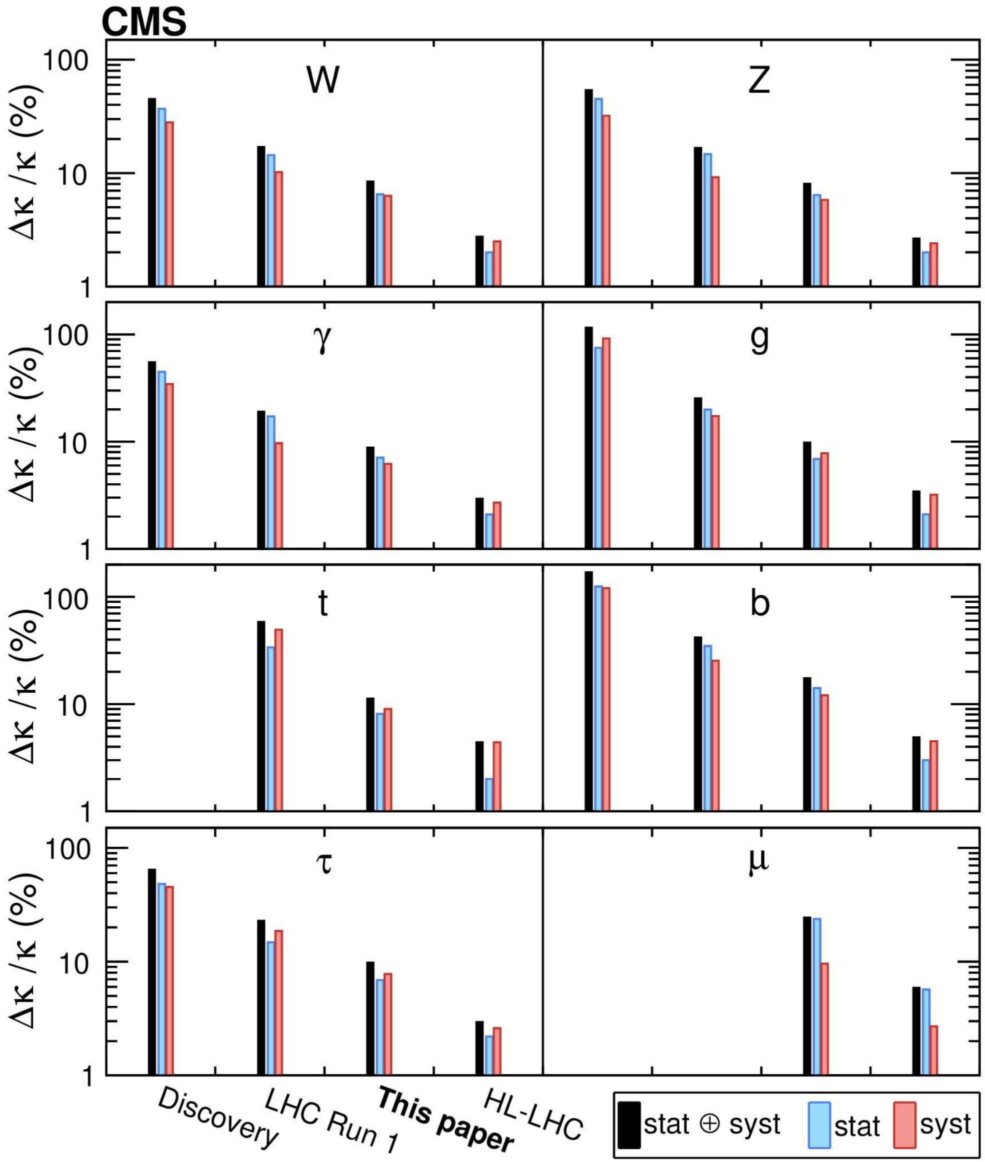

ATLAS Higgs mass measurement with the $H \to ZZ^* \to 4l$ decay

Phys. Lett. B 843 (2023) 137880

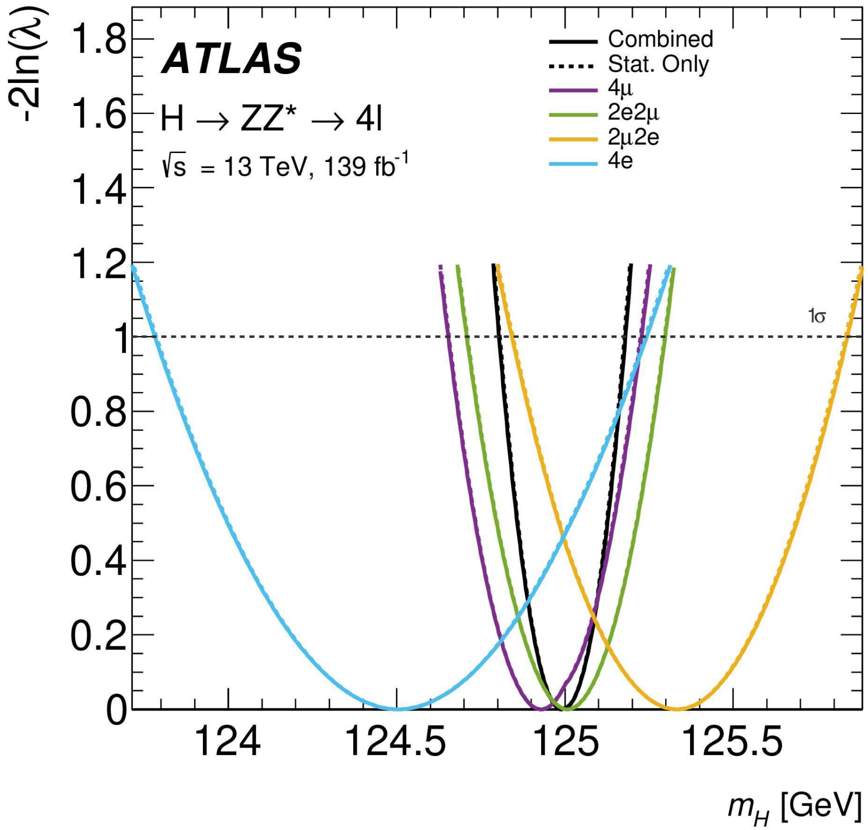

Systematic Uncertainty	Contribution [MeV]
Muon momentum scale	±28
Electron energy scale	±19
Signal-process theory	±14

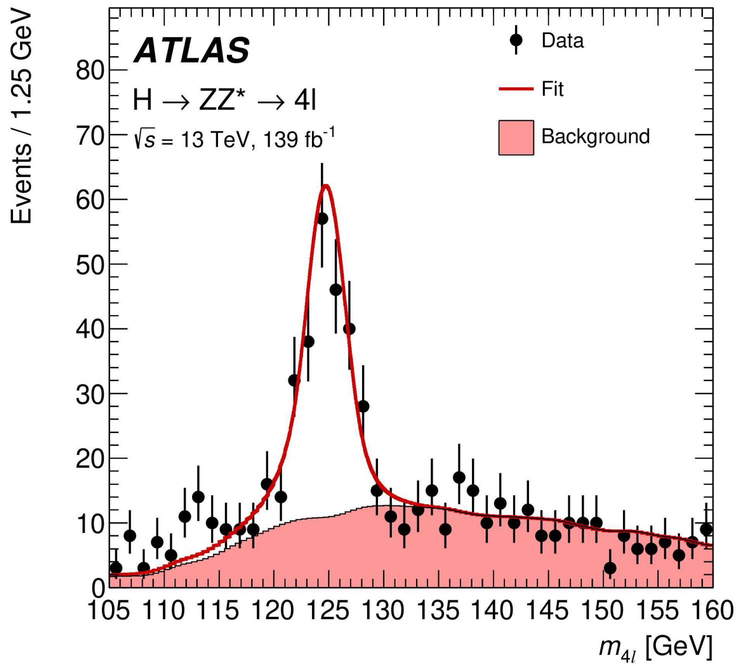

ATLAS Higgs mass measurement with the $H \to ZZ^* \to 4l$ decay

Phys. Lett. B 843 (2023) 137880

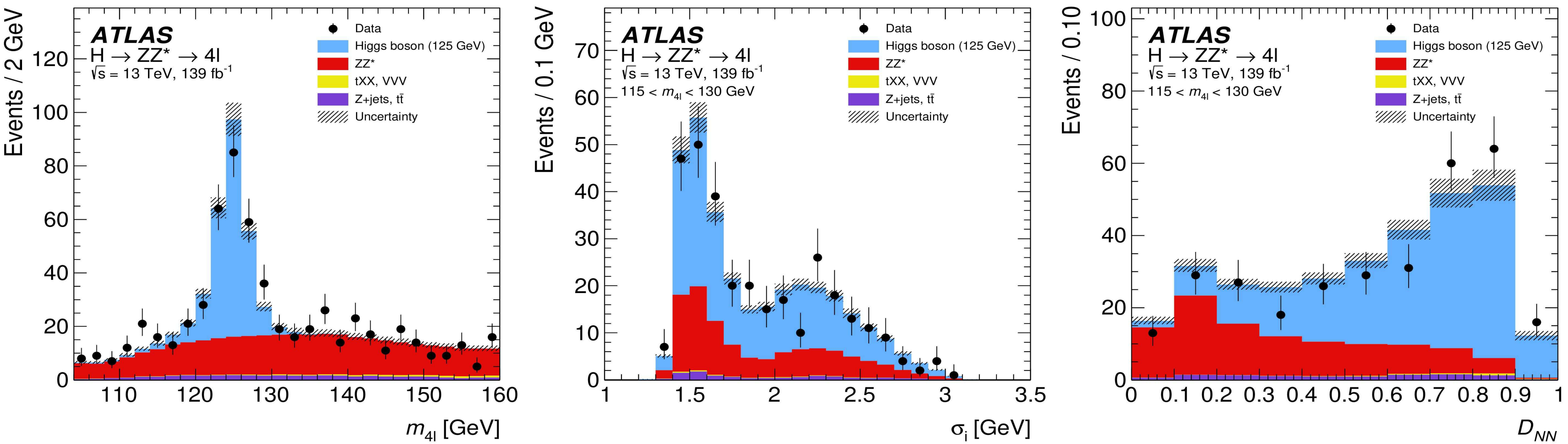

CMS-PAS-HIG-21-019 (2023)

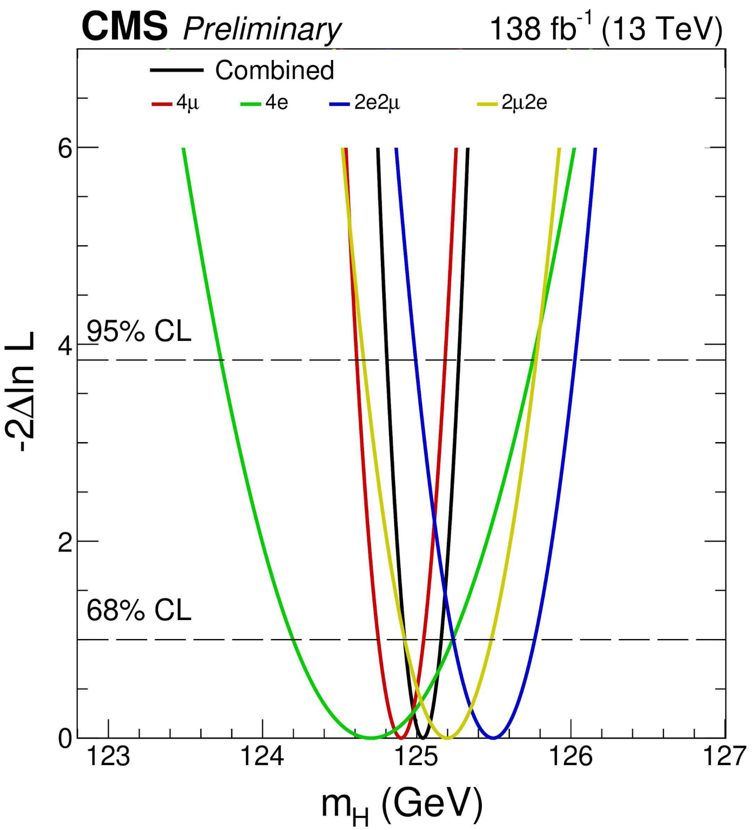

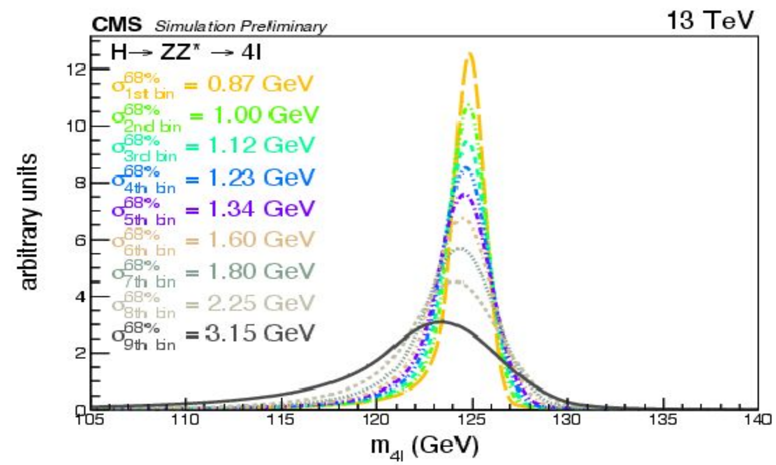

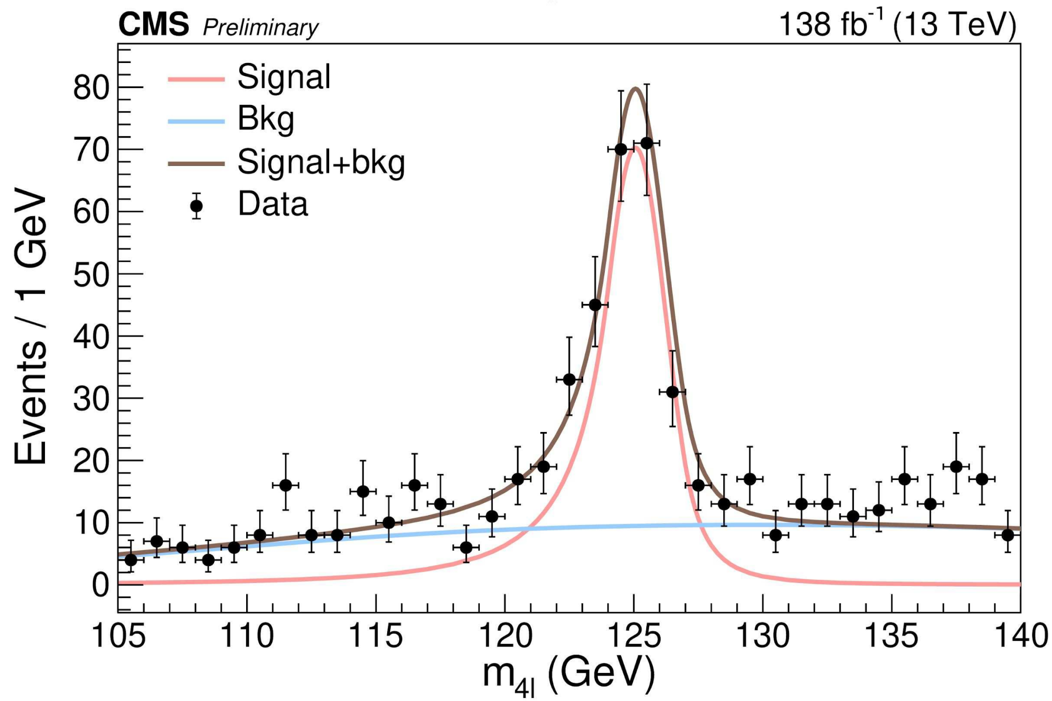

CMS-PAS-HIG-21-019 (2023)

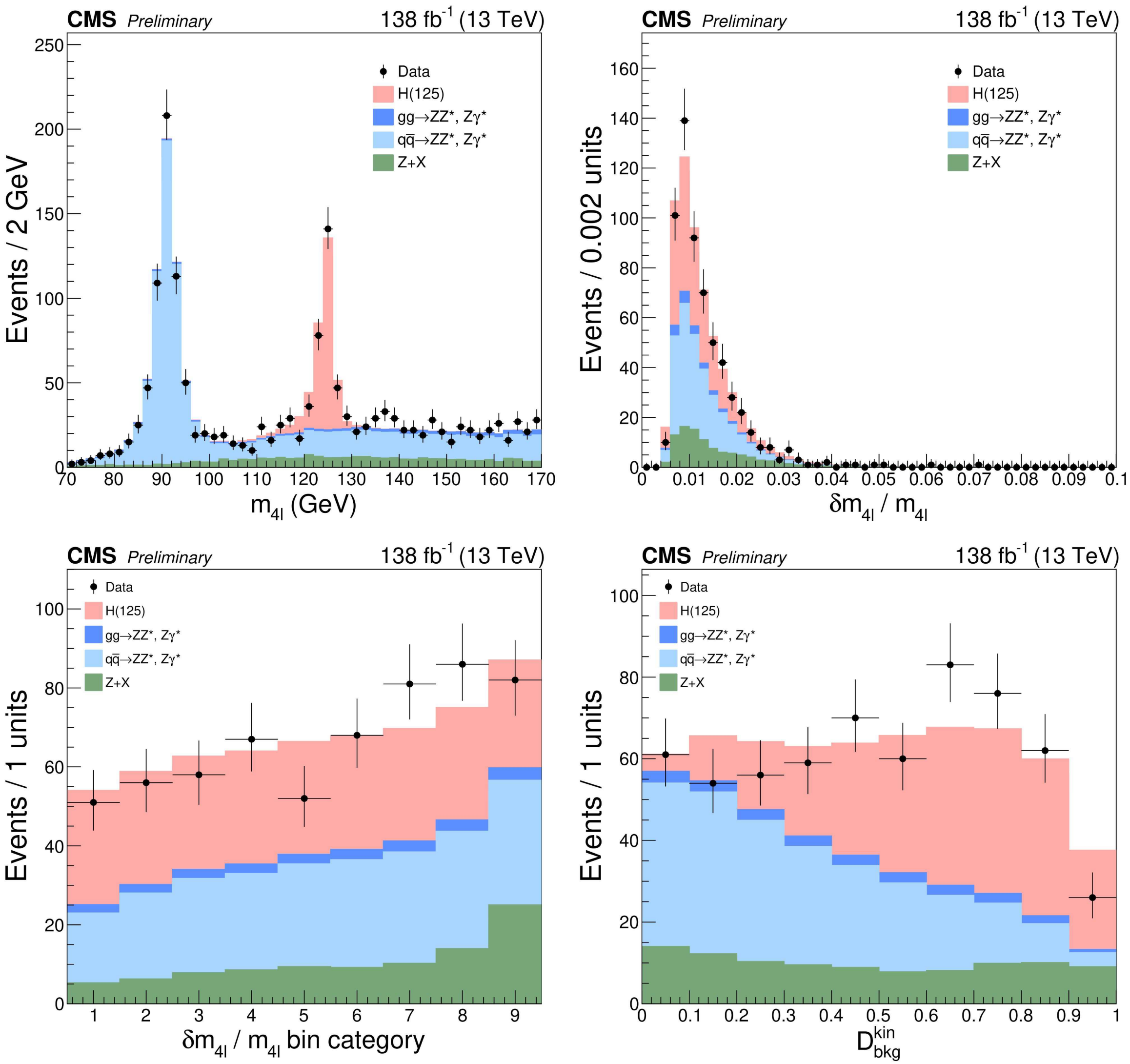

Romain Bouquet
University of Genova – INFN
romain.bouquet@cern.ch

ATLAS Run 2 Higgs mass measurement with the $H \rightarrow \gamma\gamma$ decay

Phys. Lett. B 847 (2023) 138315

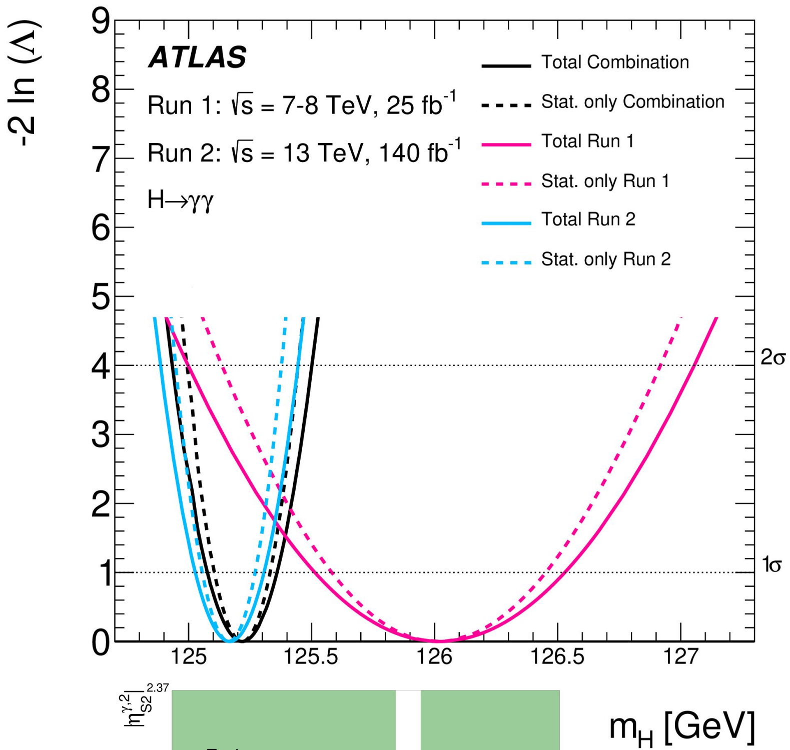

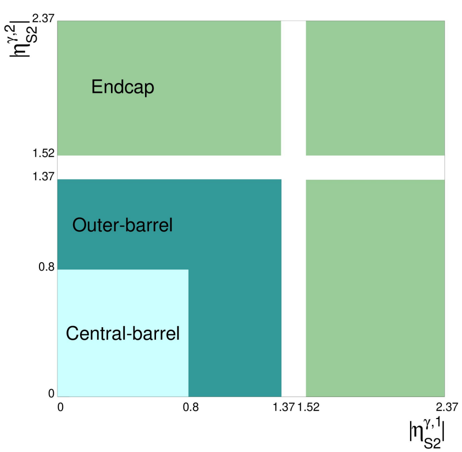

Source	Impact [MeV]
Photon energy scale	83
$Z \rightarrow e^+e^-$ calibration	59
E_T-dependent electron energy scale	44
$e^{\pm} \rightarrow \gamma$ extrapolation	30
Conversion modelling	24
Signal–background interference	26
Resolution	15
Background model	14
Selection of the diphoton production vertex	5
Signal model	1
Total	90

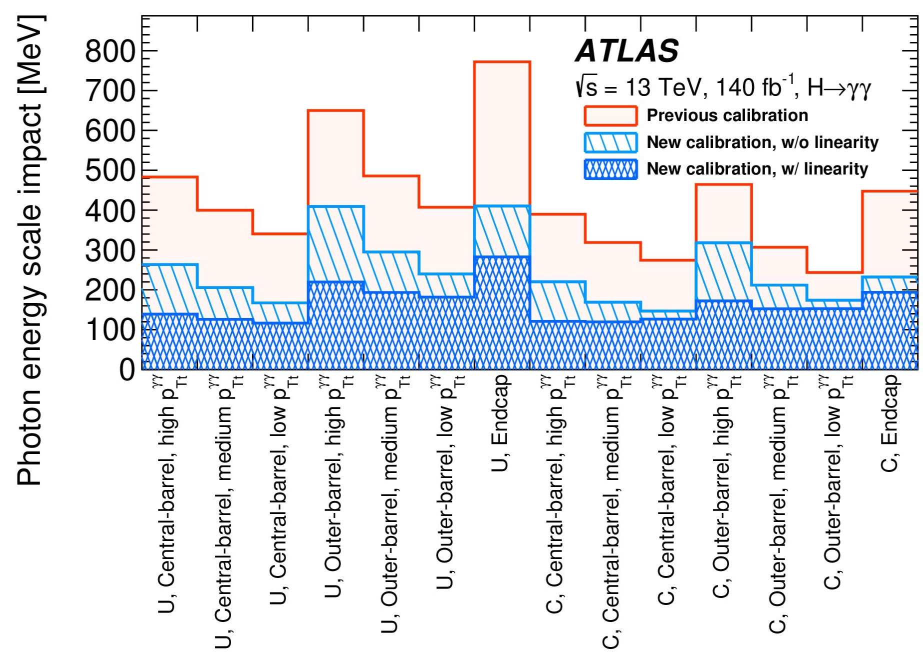

Romain Bouquet | University of Genova – INFN | romain.bouquet@cern.ch

CMS partial Run 2 Higgs mass measurement with the $H \to \gamma\gamma$ decay

Phys. Lett. B 805 (2020) 135425

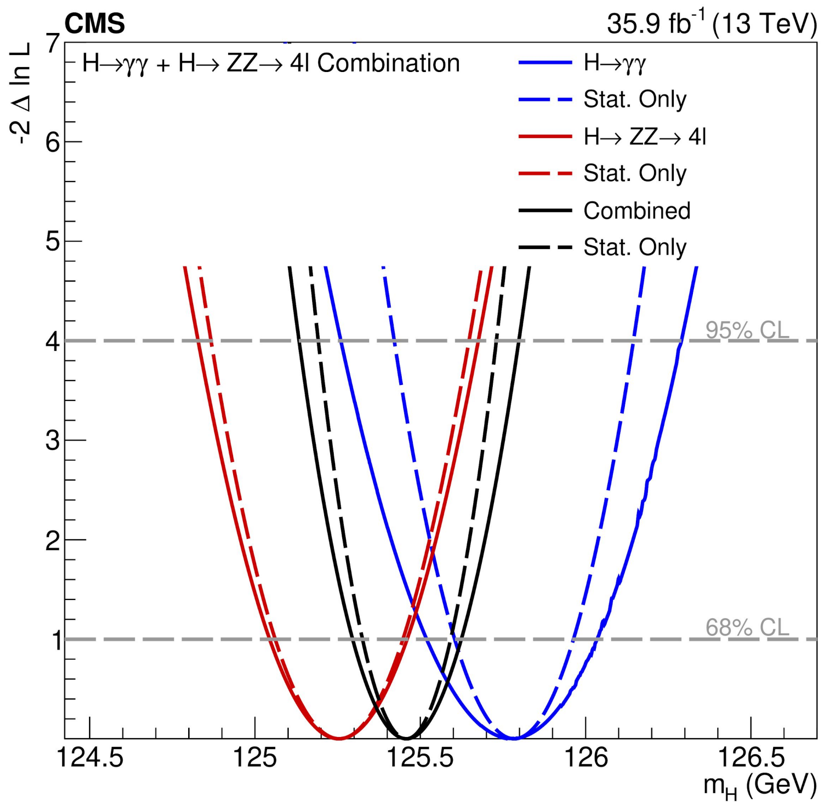

Source	Contribution (GeV)
Electron energy scale and resolution corrections	0.10
Residual p_T dependence of the photon energy scale	0.11
Modelling of the material budget	0.03
Nonuniformity of the light collection	0.11
Total systematic uncertainty	0.18
Statistical uncertainty	0.18
Total uncertainty	0.26

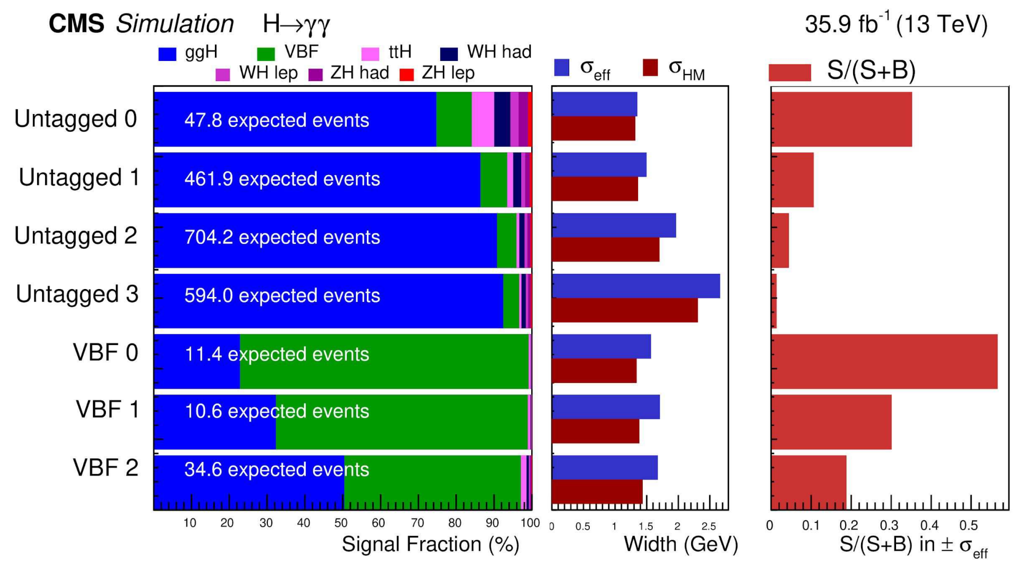

ATLAS combination of $H\to\gamma\gamma$ & $H\to ZZ^*\to 4l$ for Higgs mass measurement

Phys. Rev. Lett. 131, 251802

Source	Systematic uncertainty on m_H [MeV]
e/γ E_T-independent $Z\to ee$ calibration	44
e/γ E_T-dependent electron energy scale	28
$H\to\gamma\gamma$ interference bias	17
e/γ photon lateral shower shape	16
e/γ photon conversion reconstruction	15
e/γ energy resolution	11
$H\to\gamma\gamma$ background modelling	10
Muon momentum scale	8
All other systematic uncertainties	7

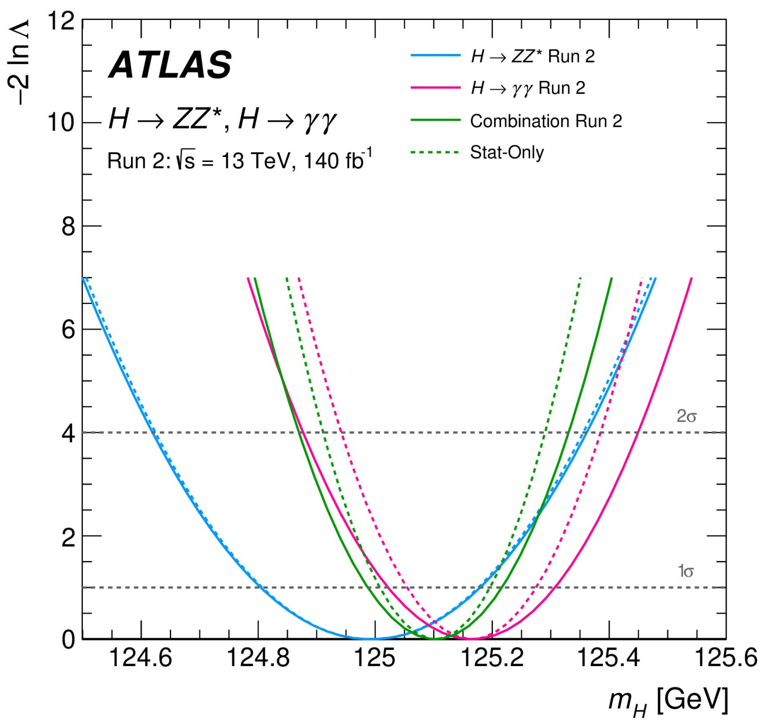

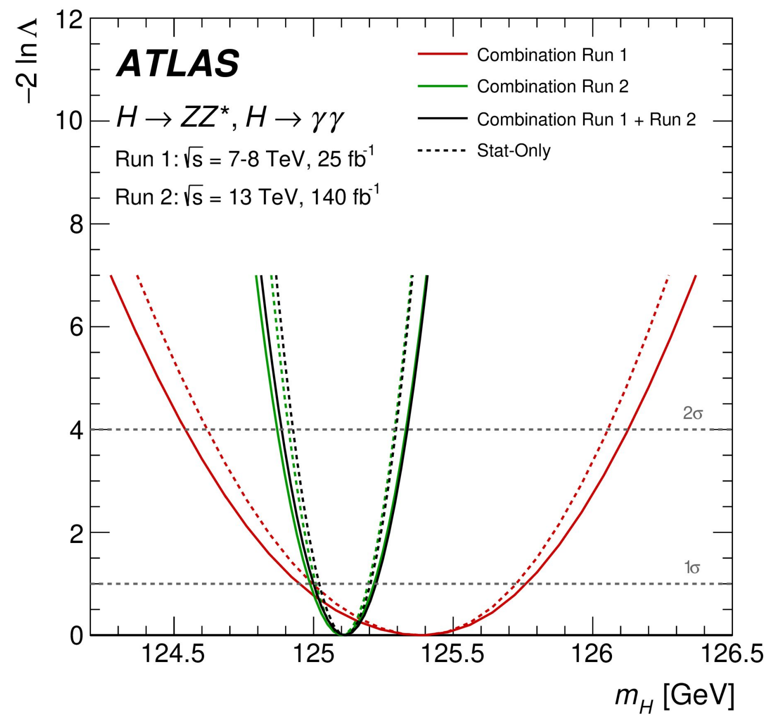

CMS, Nature Phys. 18, 1329–1334 (2022)*

Particles are understood to be *on the mass shell* (on-shell) if their mass is close to the nominal mass value, and *off-shell* if their mass takes a value far away from it. By the aforementioned property of the Breit–Wigner line shape, particles are generally more likely to be produced on-shell than off-shell when energy and momentum conservation allows it. Scattering amplitudes (A) for off-shell particle production, followed by a specific decay final state, may be modified further by interference with other processes, which is large and destructive in the case of the H boson. In this specific case, writing $A = H + C$, with H standing for the H boson contribution and C for other interfering contributions, we will use the term "off-shell production" as a shorthand for the $|H|^2$ term in $|A|^2$.

For broad resonances, the width can be obtained by directly measuring the Breit–Wigner line shape, e.g., as was done in the case of the Z boson, measured to have a mass of $m_Z = 91.188 \pm 0.002$ GeV and a width of $\Gamma_Z = 2.495 \pm 0.002$ GeV at the CERN Large Electron Positron collider [9]. The H boson is expected to live three orders of magnitude longer, with a theoretically predicted width of $\Gamma_H = 4.1$ MeV (0.0041 GeV) [10], and a deviation from the SM prediction would indicate the existence of new physics. This width is too small to be measured directly from the line shape because of the limited mass resolution of order 1 GeV achievable with the present LHC detectors. Another direct way of measuring the H boson width would be to measure its lifetime by means of its decay length and use the relationship $\Gamma_H = h/(2\pi\tau_H)$, but its lifetime is still too short ($\tau_H = 1.6 \times 10^{-22}$ s) to be detectable directly. The present experimental limit on this quantity is $\tau_H < 1.9 \times 10^{-13}$ s at 95% confidence level (CL) [11], nine orders of magnitude above the SM lifetime.

The value of Γ_H can be extracted with much better precision through a combined measurement of on-shell and off-shell H boson production. In the decay of an H boson with $m_H \approx 125$ GeV to a pair of massive gauge bosons V (V = W or Z, with masses around 80.4 or 91.2 GeV, respectively), we have $m_V < m_H < 2m_V$. Therefore, when the H boson is produced on-shell (with the VV invariant mass $m_{VV} \sim m_H$), one of the V bosons must be off-shell to satisfy four-momentum conservation. Once the H boson is produced off-shell with large enough invariant mass $m_{VV} > 2m_V$ (off-shell H boson production region), the V bosons themselves are produced on-shell. Since the Breit–Wigner mass distribution of either the H or V boson maximizes at their respective nominal masses, the rate of off-shell H boson production above the V boson pair production threshold is enhanced with respect to what one would expect from the Breit–Wigner line shape of the H boson alone.

*the most recent CMS publication is not this one but CMS-PAS-HIG-21-019

CMS, Nature Phys. 18, 1329–1334 (2022)*

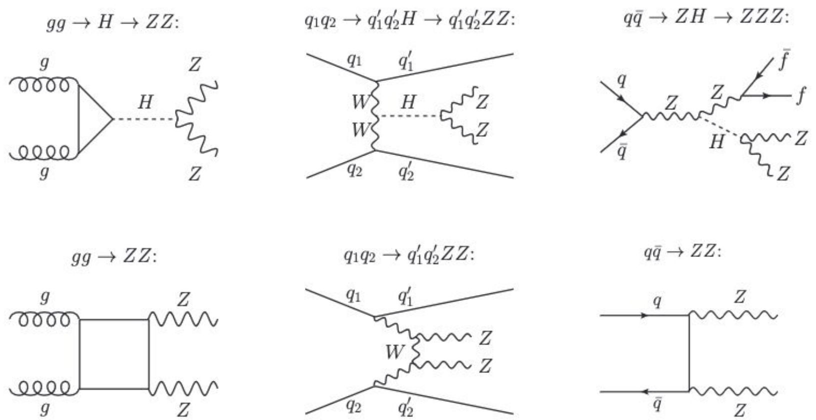

Figure 1: **Feynman diagrams for important contributions to ZZ production.** Diagrams can be distinguished as those involving the H boson (top), and those that give rise to continuum ZZ production (bottom). The interaction displayed at tree level in each diagram is meant to progress from left to right. Each straight, curvy, or curly line refers to the different set of particles denoted. Straight, solid lines with no arrows indicate the line could refer to either a particle or an antiparticle, whereas those with forward (backward) arrows refer to a particle (an antiparticle).

It is important to distinguish between two types of H boson production modes: the gluon fusion gg → H → ZZ process, where the H boson is produced via its couplings to fermions, and the EW processes, which involve HVV (i.e., HWW or HZZ) couplings. The top row of Fig. 1 shows the Feynman diagrams for the most dominant contributions to the gg (top left) process, and the EW processes of vector boson fusion (VBF, top center) and VH (top right). A more complete set of diagrams for the EW process are shown in Extended Data Figs. 1 and 2. Because different H boson couplings are involved in the gg and EW processes, we extract two off-shell signal strength parameters $\mu_F^{\text{off-shell}}$ for the gg mode and $\mu_V^{\text{off-shell}}$ for the EW mode. We also consider an overall off-shell signal strength parameter $\mu^{\text{off-shell}}$ with different assumptions on the ratio $R_{V,F}^{\text{off-shell}} = \mu_V^{\text{off-shell}} / \mu_F^{\text{off-shell}}$.

A major challenge arises from the fact that there are other sources of ZZ pairs in the SM (continuum ZZ production), see for example the bottom row of Fig. 1. These contributions, particularly those from $q\bar{q}$ → ZZ, are typically much larger than the contribution from off-shell H → ZZ. In addition, some of the amplitudes from continuum ZZ processes interfere with the H boson amplitudes because they share the same initial and final states. For example, the amplitudes in the first column of Fig. 1, or those in the second column, interfere with each other; the amplitude shown in the lower right panel (shown more generically in Extended Data Fig. 3) does not interfere with any of the other diagrams as we omit the negligible contribution of $q\bar{q}$ → H → ZZ that would interfere with it.

The interference between the H boson and continuum ZZ amplitudes is destructive [16–21]. This destructive interference plays a key role in the SM as it is one of the contributions that unitarizes the scattering of massive gauge bosons, keeping the computation of the cross section for ZZ production in proton-proton (pp) collisions finite [16–19]. Figure 2 displays the interplay

between the H boson production modes and the interfering continuum amplitudes, illustrating the growing importance of their destructive interference as m_{ZZ} grows in the two final states included in the analysis, ZZ → $2\ell 2\nu$ and ZZ → 4ℓ. In the parametrization of the total cross section, contributions from this type of interference between the H boson and continuum ZZ amplitudes scale with $\sqrt{\mu_F^{\text{off-shell}}}$ and $\sqrt{\mu_V^{\text{off-shell}}}$ for the gg and EW modes, respectively.

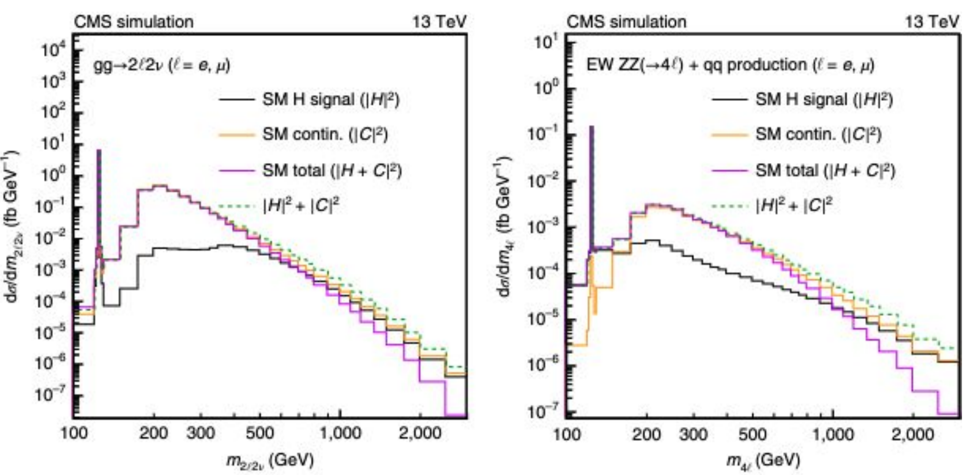

Fig. 2 | SM calculations of ZZ invariant mass in the gg and EW processes. Distributions for the $2\ell 2\nu$ invariant mass ($m_{2\ell 2\nu}$) from the gg → $2\ell 2\nu$ process (left) and for the 4ℓ invariant mass ($m_{4\ell}$) from the EW ZZ(→4ℓ) + qq processes (right). These processes involve the H boson ($|H|^2$) and interfering continuum ($|C|^2$) contributions to the scattering amplitude, as shown in black and gold, respectively. The dashed green curve represents their direct sum without interference ($|H|^2 + |C|^2$), and the solid magenta curve represents the sum with interference included ($|H + C|^2$). Note that the interference is destructive, and its importance grows as the mass increases. The integrated luminosity is taken to be 1 fb^{-1}, so these distributions are equivalent to the differential cross-section spectra $d\sigma/dm_{2\ell 2\nu}$ (left) and $d\sigma/dm_{4\ell}$ (right). The distributions are shown after requiring that all charged leptons satisfy $p_T > 7$ GeV and $|\eta| < 2.4$, and that the invariant mass of any charged lepton pair with the same flavour and opposite charge is greater than 4 GeV. Here, p_T denotes the magnitude of the momentum of these leptons transverse to the pp collision axis, and η denotes their pseudorapidity, defined as $-\ln[\tan(\theta/2)]$ using the angle θ between the momentum vector and the collision axis. Calculations for the gg → 4ℓ and EW ZZ(→$2\ell 2\nu$) + qq processes exhibit similar qualitative properties. The details of the Monte Carlo programs used for these calculations are provided in the Methods.

*the most recent CMS publication is not this one but CMS-PAS-HIG-21-019

Phys. Lett. B 846 (2023) 138223

Systematic Uncertainty Fixed	$\mu_{\text{off-shell}}$ value at which $-2\ln\lambda(\mu_{\text{off-shell}}) = 4$
Parton shower uncertainty for $gg \to ZZ$ (normalisation)	2.26
Parton shower uncertainty for $gg \to ZZ$ (shape)	2.29
NLO EW uncertainty for $qq \to ZZ$	2.27
NLO QCD uncertainty for $gg \to ZZ$	2.29
Parton shower uncertainty for $qq \to ZZ$ (shape)	2.29
Jet energy scale and resolution uncertainty	2.26
None	2.30

To maximize the signal sensitivity, a multi-class dense NN is employed in the SRs to enhance events with a Higgs boson candidate. The NN, implemented using Keras [77] with TensorFlow [78] as the backend, is designed to differentiate among the three event classes: the off-shell Higgs boson signal (S), the interfering background (B), and the non-interfering (NI) background. The interfering backgrounds to the ggF and EW signals are the $gg \to ZZ$ and EW $q\bar{q} \to ZZ + 2j$ processes, respectively. The non-interfering background is the $q\bar{q} \to ZZ$ process in both production modes.

The outputs of the NN use a normalized exponential function so that they can be interpreted as probabilities of an event belonging to a particular class (P_S, P_B and P_{NI}) and their ratio is used to define the final observable:

$$O_{NN} = \log_{10}\left(\frac{P_S}{P_B + P_{NI}}\right).$$

As the analysis attempts to constrain both the ggF- and EW-induced off-shell signals independently, two separate NNs are trained, one in the ggF SR and the other in the EW SR. The observable from the first NN (O_{NN}^{ggF}) is then used as the discriminating variable in both the ggF and mixed SRs, while that of the second NN (O_{NN}^{EW}) is used in the EW SR.

The first NN is trained to discriminate among the ggF-induced signal, the $gg \to ZZ$ background, and the $q\bar{q} \to ZZ$ process. The features used by this NN include the kinematic information of the four leptons

The second NN is used to separate the EW-induced off-shell signal process from the non-Higgs boson EW $q\bar{q} \to ZZjj$ background and the QCD-induced $q\bar{q} \to ZZjj$ process. In addition to the variables

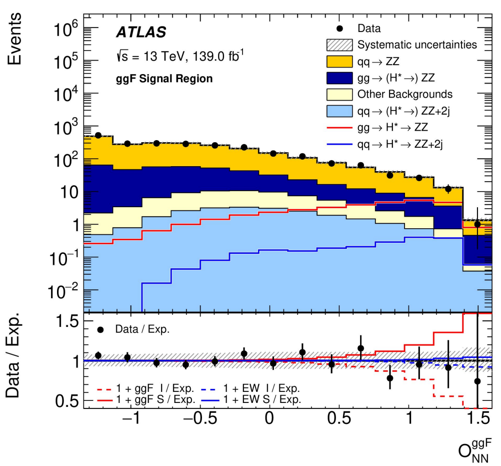

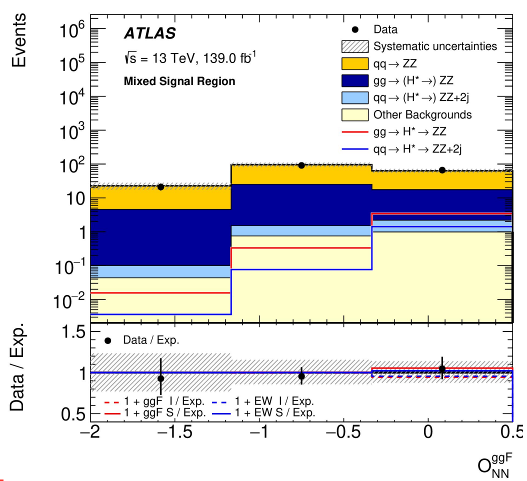

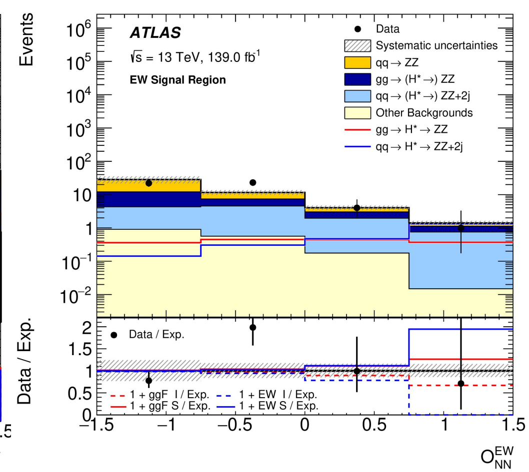

Phys. Lett. B 846 (2023) 138223

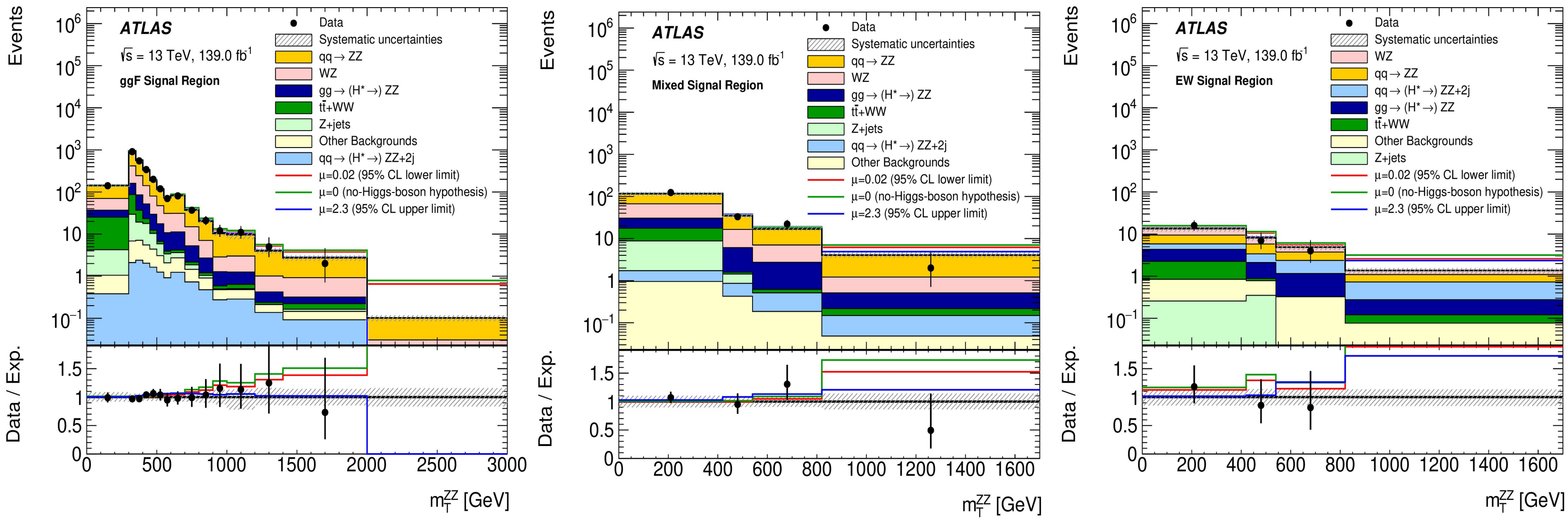

Due to the quadratic parameterisation of the yield as a function of the parameter of interest, the distribution of the test statistic $-2\ln\lambda$ is slightly different from the asymptotic χ^2 distribution predicted by Wilks' theorem [87]. Therefore confidence intervals on $\mu_{\text{off-shell}}$ are built based on the Neyman construction [88] using

CMS Higgs width measurement

CMS-PAS-HIG-21-019 (2023)

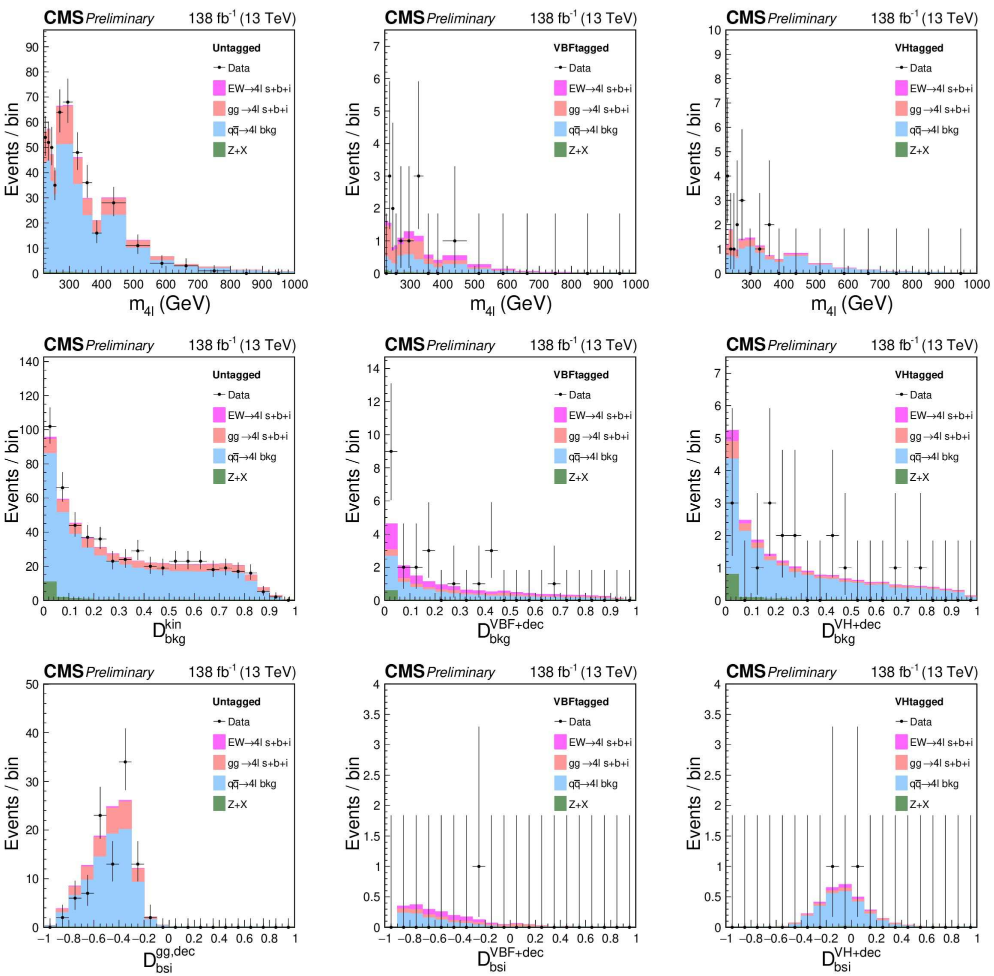

Figure 5: Observed data and pre-fit distributions of events in the off-shell region, in the Untagged (left column), VBF-tagged (middle column), and VH-tagged (right column) categories. The top row shows $m_{4\ell}$ where a requirement on $\mathcal{D}^{\text{kin}}_{\text{bkg}}$, $\mathcal{D}^{\text{VBF+dec}}_{\text{bkg}}$ or $\mathcal{D}^{\text{VH+dec}}_{\text{bkg}} > 0.6$ is applied in order to enhance signal over background contributions. The middle row shows $\mathcal{D}^{\text{kin}}_{\text{bkg}}$ (left), $\mathcal{D}^{\text{VBF+dec}}_{\text{bkg}}$ (middle), $\mathcal{D}^{\text{VH+dec}}_{\text{bkg}}$ (right). The requirement $m_{4\ell} > 340$ GeV is applied in order to enhance signal over background contributions. The bottom row shows $\mathcal{D}_{\text{bsi}}$ with both of the $m_{4\ell}$ and $\mathcal{D}^{\text{kin}}_{\text{bkg}}$ requirements enhancing the signal contribution.

Table 1: Summary of the three production categories in the off-shell $m_{4\ell}$ region. All discriminants are calculated with the JHUGEN signal and MCFM background matrix elements. The VH interference discriminant in the VH-tagged category is defined as the simple average of the ones corresponding to the ZH and WH processes.

Category	VBF-tagged	VH-tagged	Untagged
Selection	$\mathcal{D}^{\text{VBF}}_{\text{2jet}} > 0.5$	$\mathcal{D}^{\text{ZH}}_{\text{2jet}}$ or $\mathcal{D}^{\text{WH}}_{\text{2jet}} > 0.5$	Rest of events
Observables	$m_{4\ell}, \mathcal{D}^{\text{VBF+dec}}_{\text{bkg}}, \mathcal{D}^{\text{VBF+dec}}_{\text{bsi}}$	$m_{4\ell}, \mathcal{D}^{\text{VH+dec}}_{\text{bkg}}, \mathcal{D}^{\text{VH+dec}}_{\text{bsi}}$	$m_{4\ell}, \mathcal{D}^{\text{kin}}_{\text{bkg}}, \mathcal{D}^{\text{gg,dec}}_{\text{bsi}}$

- The VBF-2jet category requires exactly four leptons. In addition, there must be either two or three jets of which at most one is b-tagged, or at least four jets and no b-tagged jets. Finally, $\mathcal{D}^{\text{VBF}}_{\text{2jet}} > 0.5$ for the VBF production is required.
- The VH-hadronic category requires exactly four leptons. In addition, there must be either two or three jets, or at least four jets and no b-tagged jets. Finally, $\max\left(\mathcal{D}^{\text{WH}}_{\text{2jet}}, \mathcal{D}^{\text{ZH}}_{\text{2jet}}\right) > 0.5$ for the VH production is required.
- The Untagged category consists of the remaining events.

romain.bouquet@cern.ch

$VH,\ H \to b\bar{b}$ resolved and boosted topology (Jet radius values used by ATLAS)

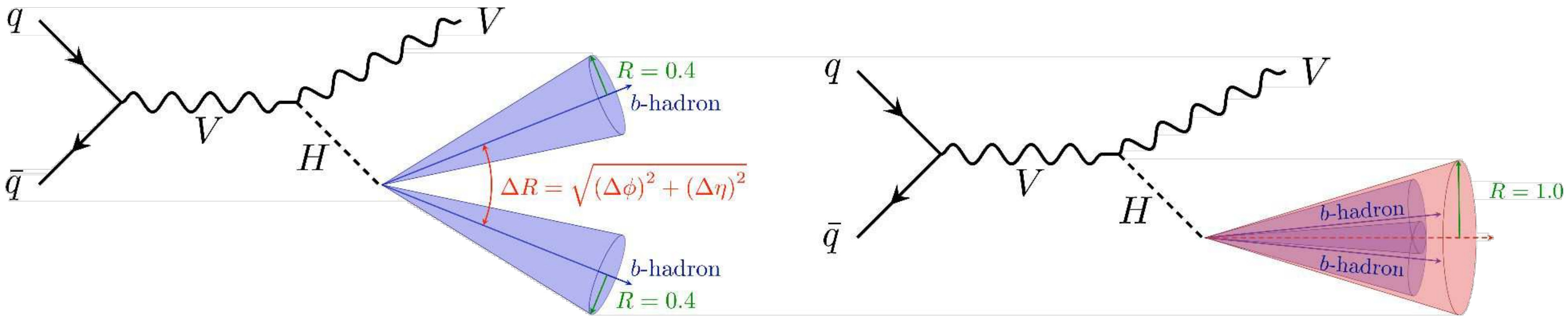

Angular distance between jets

$$\Delta R \approx \frac{2m_H}{p_T^H}$$

$$m_H = 125 \text{ GeV}$$

$\Rightarrow$ boosted for $p_T^H \approx$ few hundred of GeV

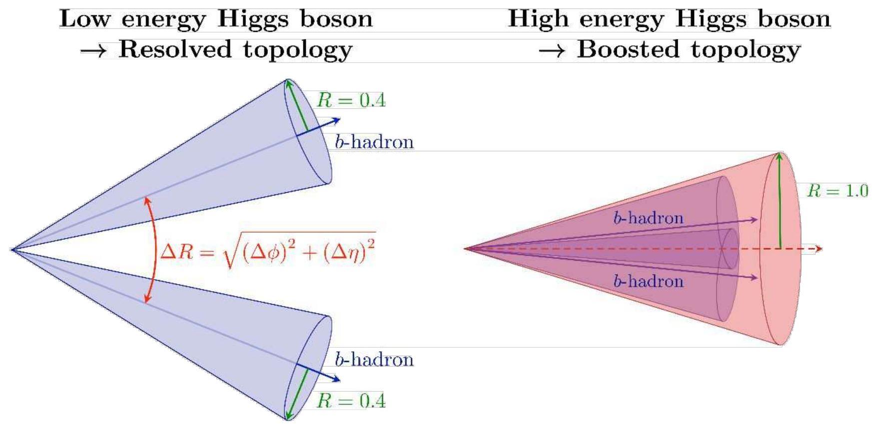

ATLAS-CONF-2021-051

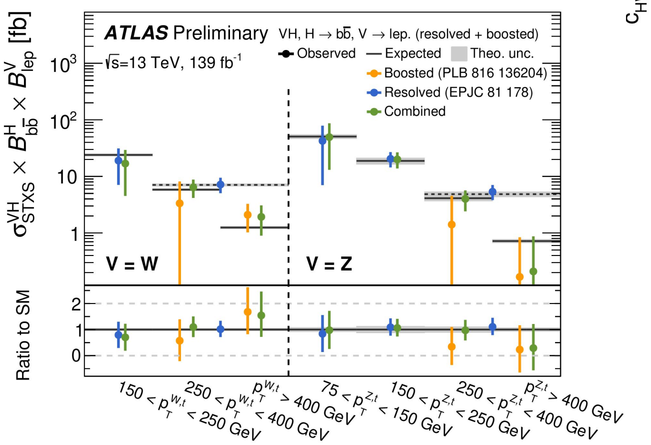

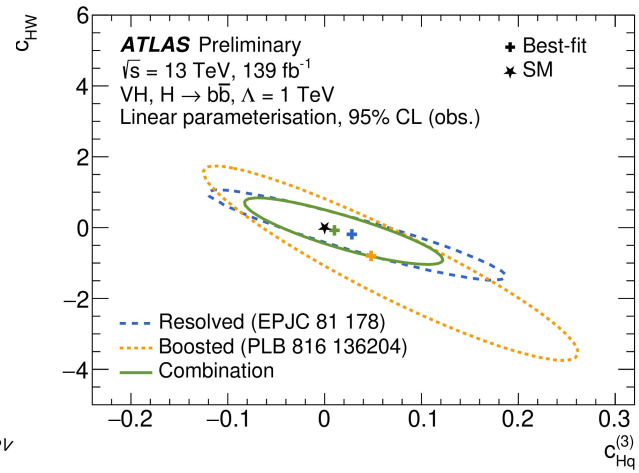

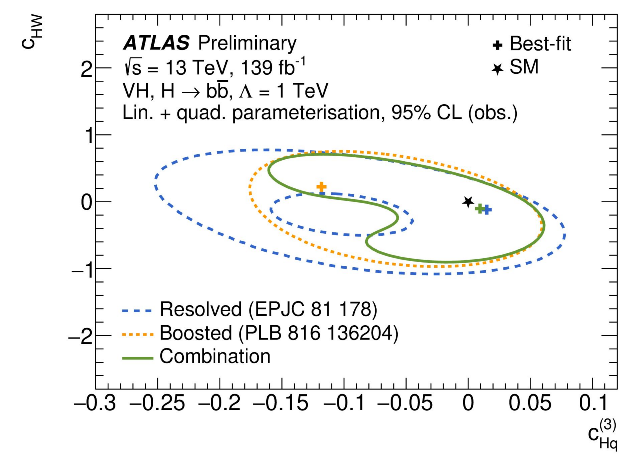

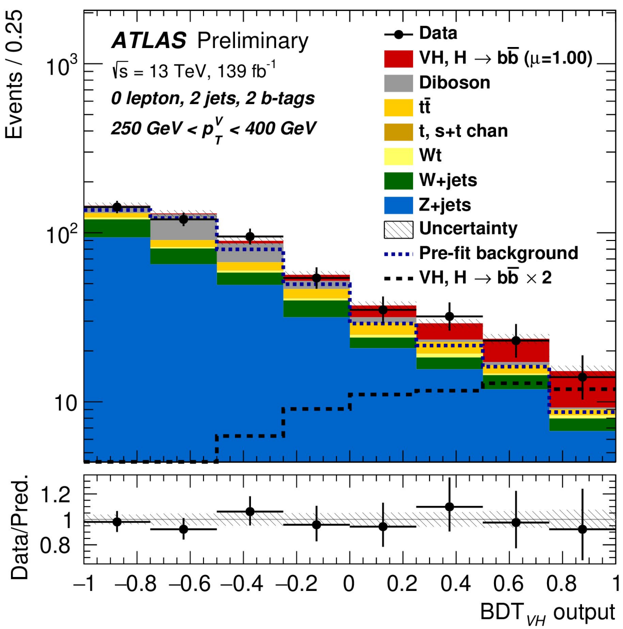

Category	WH, 150–250 GeV	WH, 250–400 GeV	WH, > 400 GeV	ZH, 75–150 GeV	ZH, 150–250 GeV	ZH, 250–400 GeV	ZH, > 400 GeV
Total	73%	36%	56%	75%	32%	40%	305%
Statistical	48%	32%	48%	52%	26%	37%	248%
Systematic	56%	17%	29%	53%	19%	16%	177%
Statistical uncertainties							
Data stat only	44%	29%	45%	44%	23%	34%	242%
Floating normalisations	26%	9%	14%	21%	11%	10%	57%
$t\bar{t}$ $e\mu$ control region	4%	≤1%	≤1%	23%	4%	8%	3%
Experimental uncertainties							
Total experimental	34%	9%	14%	42%	11%	7%	95%
↪ lepton	4%	2%	3%	3%	≤1%	≤1%	4%
↪ $E_{\mathrm{T}}^{\mathrm{miss}}$	24%	≤1%	≤1%	25%	3%	≤1%	9%
↪ Small-R jets	17%	6%	6%	28%	7%	4%	19%
↪ Large-R jets	≤1%	≤1%	9%	≤1%	≤1%	≤1%	89%
↪ Calo b-tagging (b-jets)	8%	2%	≤1%	18%	8%	5%	6%
↪ Calo b-tagging (c-jets)	14%	6%	≤1%	2%	2%	≤1%	3%
↪ Calo b-tagging (light-flavour jets)	≤1%	≤1%	≤1%	≤1%	≤1%	2%	2%
↪ Calo b-tagging (extrap. from charm)	≤1%	≤1%	≤1%	≤1%	≤1%	≤1%	≤1%
↪ VR b-tagging (b-jets)	≤1%	≤1%	7%	≤1%	≤1%	≤1%	15%
↪ VR b-tagging (c-jets)	≤1%	≤1%	2%	≤1%	≤1%	≤1%	8%
↪ VR b-tagging (light-flavour jets)	≤1%	≤1%	≤1%	≤1%	≤1%	≤1%	21%
↪ VR b-tagging (extrap. from charm)	≤1%	≤1%	≤1%	≤1%	≤1%	≤1%	3%
↪ Pile-up	2%	≤1%	≤1%	5%	≤1%	≤1%	≤1%
↪ Luminosity	2%	2%	2%	≤1%	≤1%	≤1%	5%
Theoretical and modelling uncertainties							
Signal	5%	5%	9%	13%	9%	9%	23%
Backgrounds	43%	13%	23%	37%	12%	11%	145%
↪ single top	17%	8%	8%	5%	≤1%	2%	4%
↪ $t\bar{t}$	22%	3%	9%	10%	4%	3%	13%
↪ W+jets	25%	6%	8%	2%	≤1%	≤1%	14%
↪ Z+jets	7%	2%	5%	29%	9%	6%	115%
↪ Diboson	6%	3%	3%	9%	4%	4%	27%
↪ Multi-jet	≤1%	≤1%	3%	≤1%	≤1%	≤1%	3%
↪ MC statistical	17%	8%	13%	17%	6%	7%	77%

CMS $VH, H\to b\bar{b}$ Run 2 analysis

CMS-PAS-HIG-20-001 (2023)

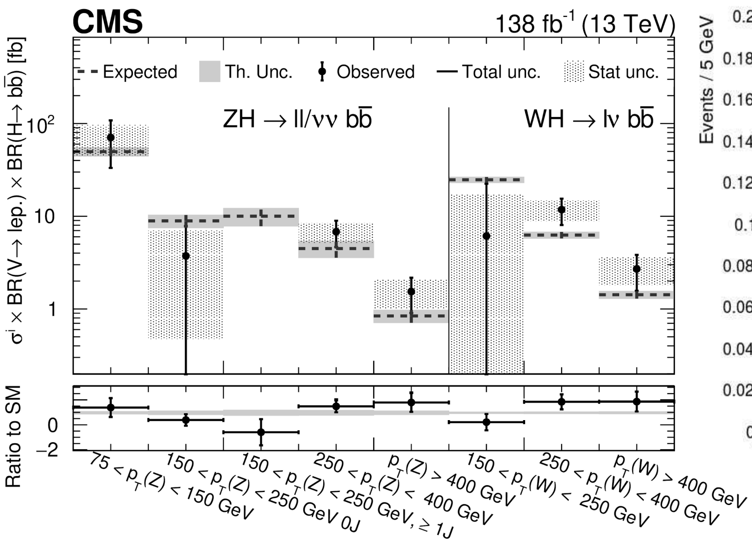

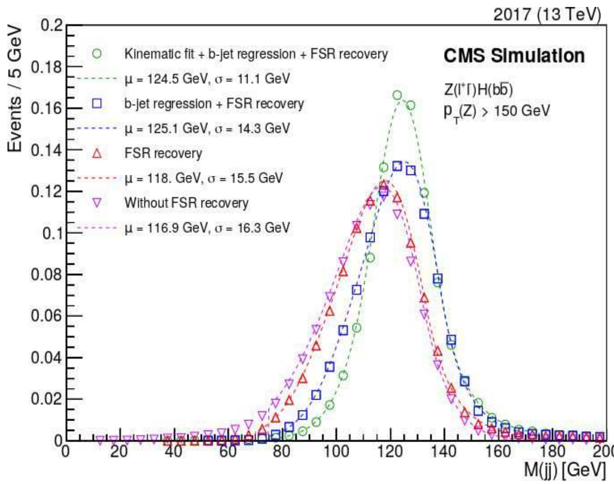

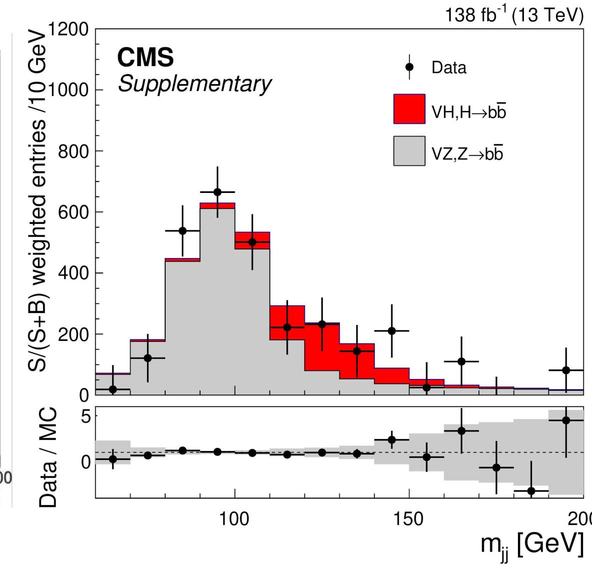

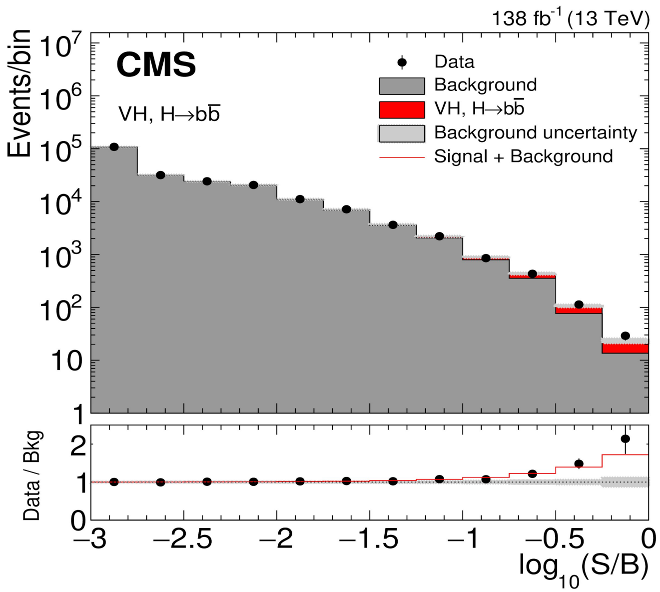

	$\Delta\mu$
Background (theory)	+0.043 −0.043
Signal (theory)	+0.088 −0.059
MC sample size	+0.078 −0.078
Simulation modeling	+0.059 −0.059
b tagging	+0.050 −0.046
Jet energy resolution	+0.036 −0.028
Int. luminosity	+0.032 −0.027
Jet energy scale	+0.025 −0.025
Lepton ident.	+0.008 −0.007
Trigger ($\vec{p}_T^{\,miss}$)	+0.002 −0.001

Eur. Phys. J. C 82 (2022) 717

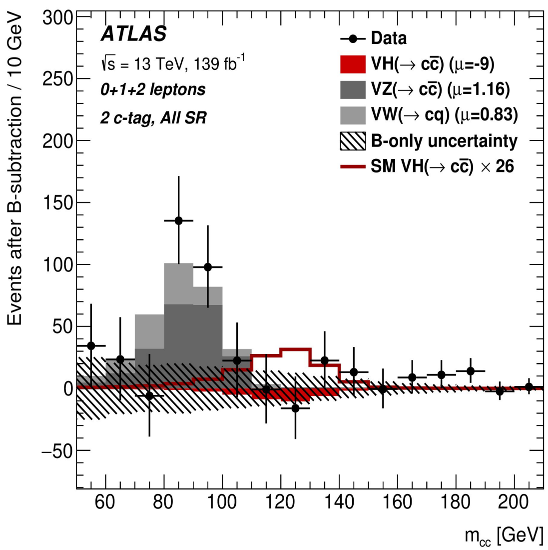

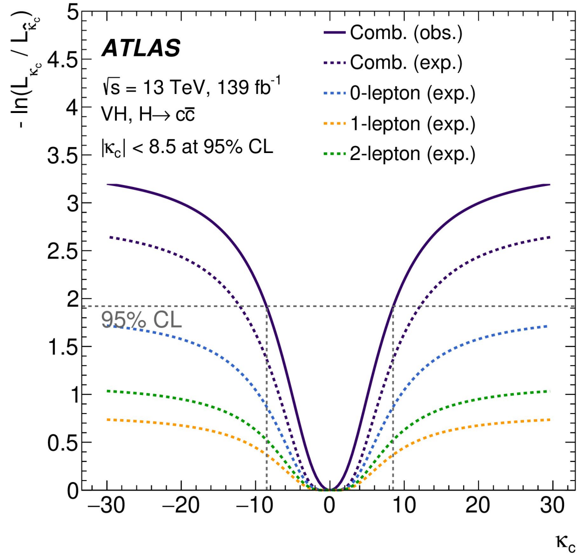

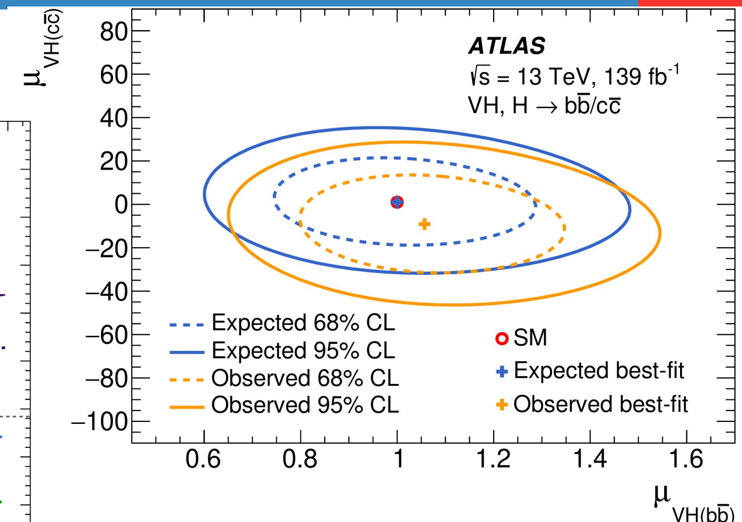

Source of uncertainty		$\mu_{VH(c\bar{c})}$	$\mu_{VW(cq)}$	$\mu_{VZ(c\bar{c})}$
Total		13.4	0.23	0.43
Statistical		8.9	0.10	0.29
Systematics		9.8	0.20	0.31
Statistical uncertainties				
Data statistics only		7.1	0.05	0.21
Floating normalisations		4.4	0.08	0.19
Theoretical and modelling uncertainties				
$VH(\to c\bar{c})$		1.2	< 0.01	0.01
Z+jets		5.8	0.04	0.15
Top-quark		3.5	0.12	0.08
W+jets		2.3	0.04	0.08
Diboson		0.8	0.101	0.10
$VH(\to b\bar{b})$		0.7	< 0.01	0.01
Multi-Jet		0.9	0.03	0.02
Simulation statistics		3.5	0.08	0.11
Experimental uncertainties				
Jets		2.0	0.06	0.11
Leptons		0.5	< 0.01	0.01
E_T^{miss}		0.3	0.01	0.01
Pile-up and luminosity		0.2	< 0.01	0.01
Flavour tagging	c-jets	1.6	0.05	0.14
	b-jets	0.8	0.01	0.03
	light-jets	0.6	0.01	0.04
	τ-jets	0.4	0.01	0.03
Truth-flavour tagging	ΔR correction	2.8	0.02	0.07
	Residual non-closure	0.2	0.03	0.08

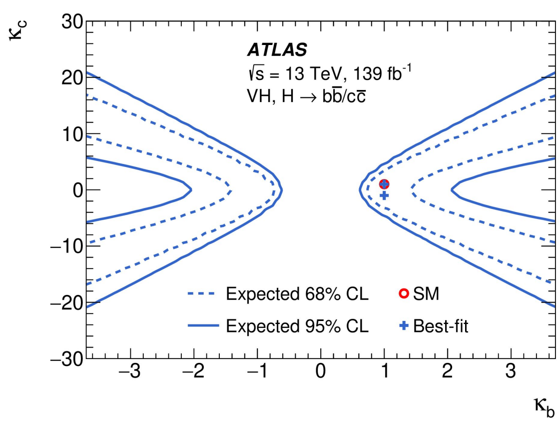

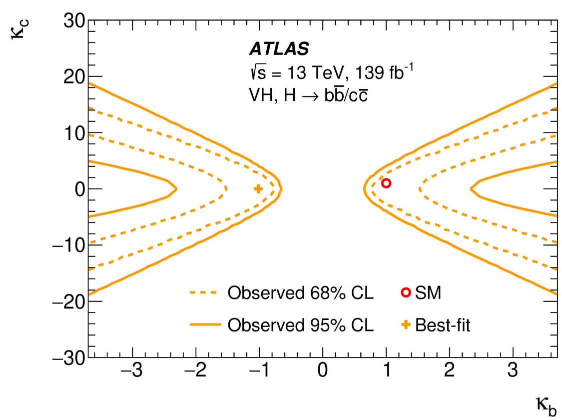

Phys. Rev. Lett. 131 (2023) 061801

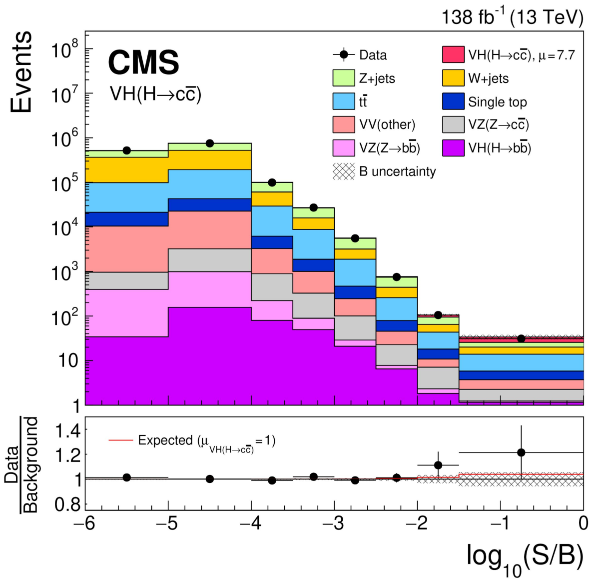

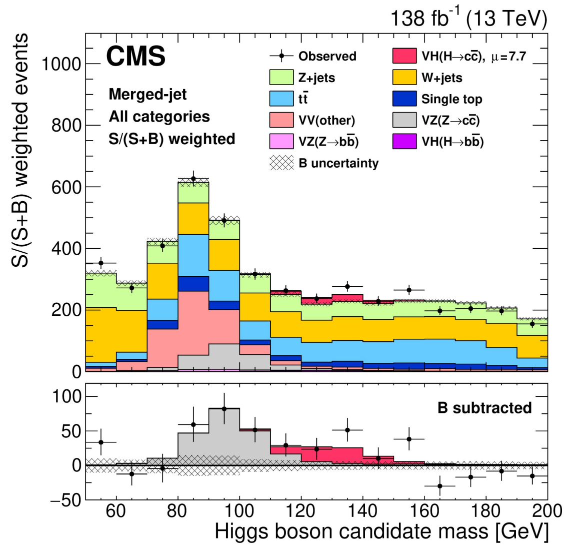

Boosted $H \to c\bar{c}$ tagger (ParticleNet)

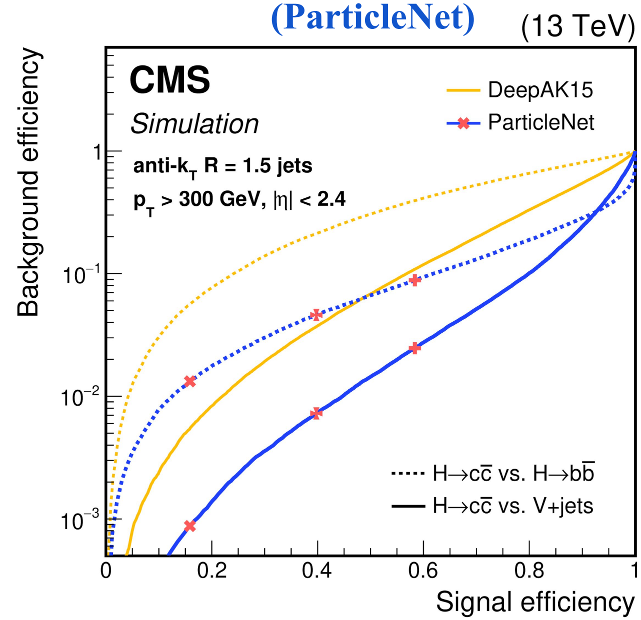

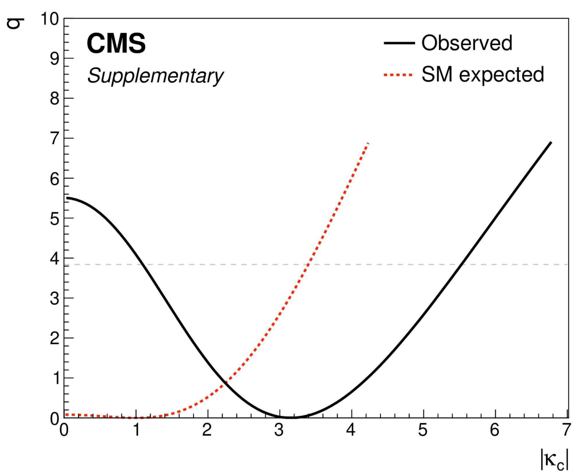

Uncertainty source	$\Delta\mu / (\Delta\mu)_{tot}$
Statistical	85%
Background normalizations	37%
Experimental	48%
Sizes of the simulated samples	37%
c jet identification efficiencies	23%
Jet energy scale and resolution	15%
Simulation modeling	11%
Integrated luminosity	6%
Lepton identification efficiencies	4%
Theory	22%
Backgrounds	17%
Signal	15%

VZ, $Z \to c\bar{c}$ cross-check

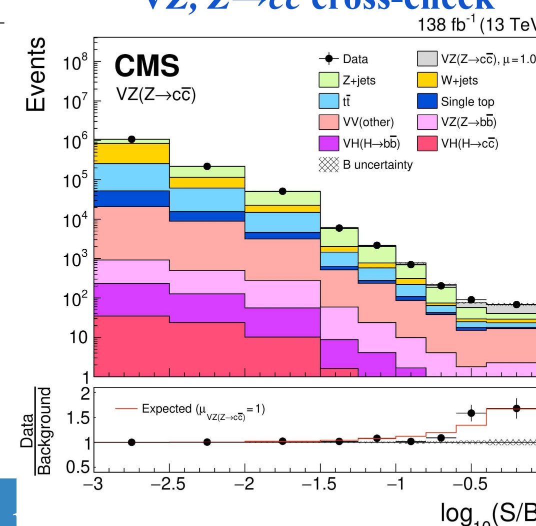

CMS, VH, $H\rightarrow c\bar{c}$ analysis extrapolation of sensitivity for HL-LHC

Phys. Rev. Lett. 131 (2023) 061801

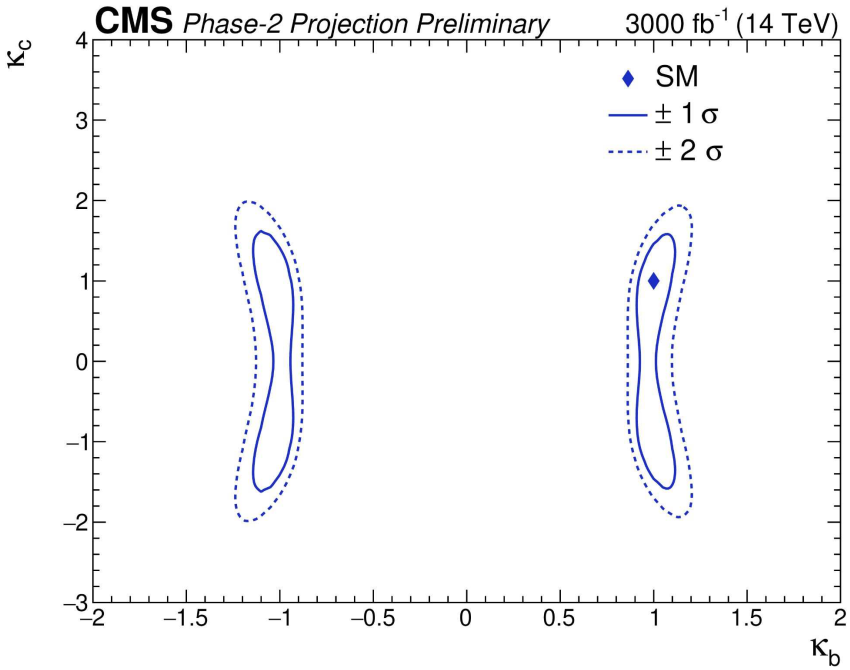

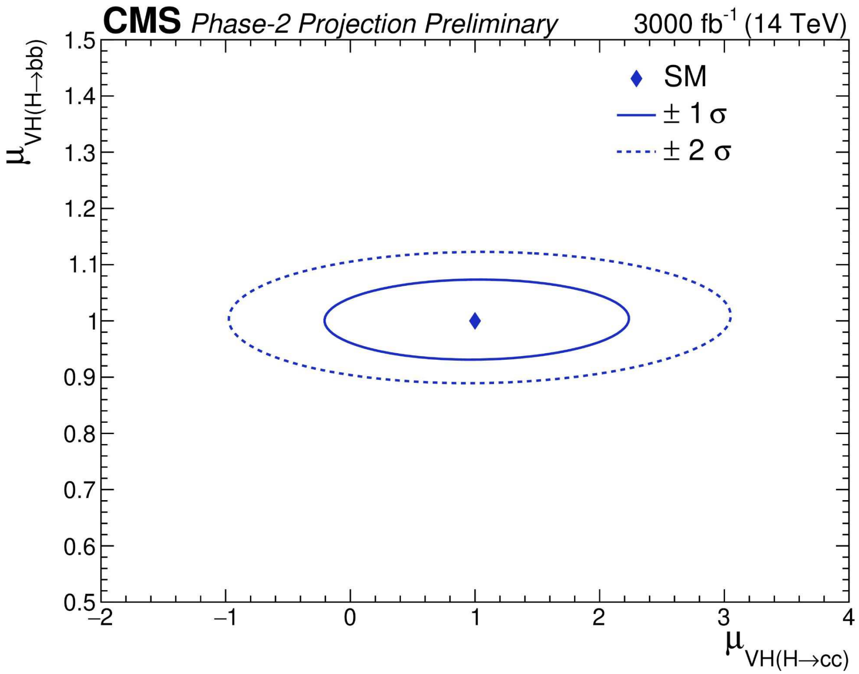

Phys. Lett. B 843 (2023) 137745

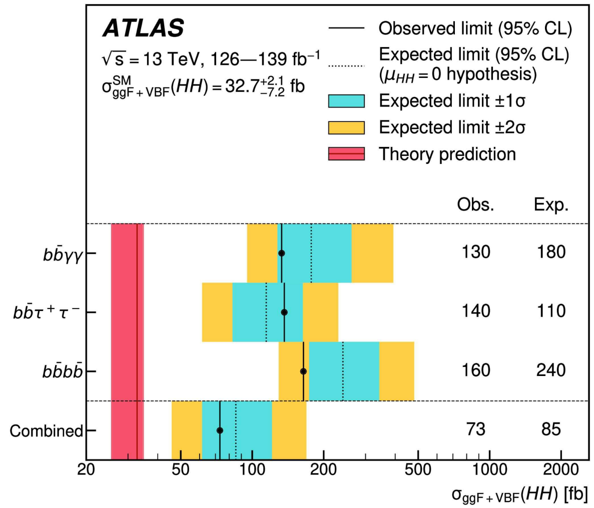

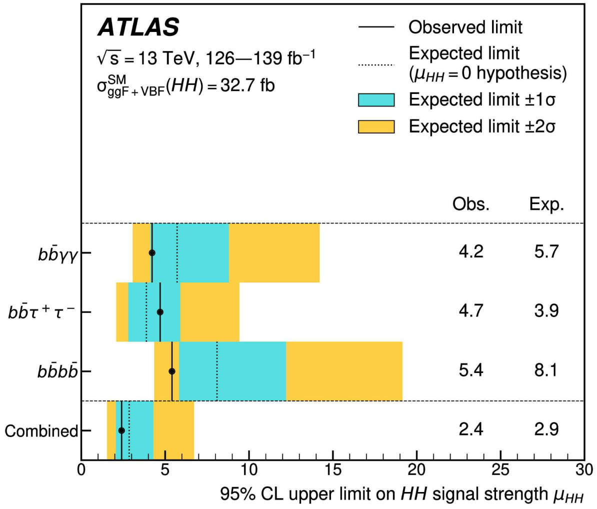

Final state	Obs. 95% CL	Exp. 95% CL	Obs. value$^{+1\sigma}_{-1\sigma}$
$HH \to b\bar{b}\gamma\gamma$	$-1.4 < \kappa_\lambda < 6.5$	$-3.2 < \kappa_\lambda < 8.1$	$\kappa_\lambda = 2.8^{+2.0}_{-2.2}$
$HH \to b\bar{b}\tau^+\tau^-$	$-2.7 < \kappa_\lambda < 9.5$	$-3.1 < \kappa_\lambda < 10.2$	$\kappa_\lambda = 1.5^{+5.9}_{-2.5}$
$HH \to b\bar{b}b\bar{b}$	$-3.3 < \kappa_\lambda < 11.4$	$-5.2 < \kappa_\lambda < 11.6$	$\kappa_\lambda = 6.2^{+3.0}_{-5.2}$
HH combination	$-0.6 < \kappa_\lambda < 6.6$	$-2.1 < \kappa_\lambda < 7.8$	$\kappa_\lambda = 3.1^{+1.9}_{-2.0}$

Final state	Obs. 95% CL	Exp. 95% CL	Obs. value$^{+1\sigma}_{-1\sigma}$
$HH \to b\bar{b}\gamma\gamma$	$-0.8 < \kappa_{2V} < 3.0$	$-1.6 < \kappa_{2V} < 3.7$	$\kappa_{2V} = 1.1^{+1.0}_{-1.0}$
$HH \to b\bar{b}\tau^+\tau^-$	$-0.6 < \kappa_{2V} < 2.7$	$-0.5 < \kappa_{2V} < 2.7$	$\kappa_{2V} = 1.5^{+0.7}_{-1.7}$
$HH \to b\bar{b}b\bar{b}$	$0.0 < \kappa_{2V} < 2.1$	$0.0 < \kappa_{2V} < 2.1$	$\kappa_{2V} = 1.0^{+0.7}_{-0.6}$
HH combination	$0.1 < \kappa_{2V} < 2.0$	$0.0 < \kappa_{2V} < 2.1$	$\kappa_{2V} = 1.1^{+0.6}_{-0.6}$

Nature **607**, 60–68 (2022)

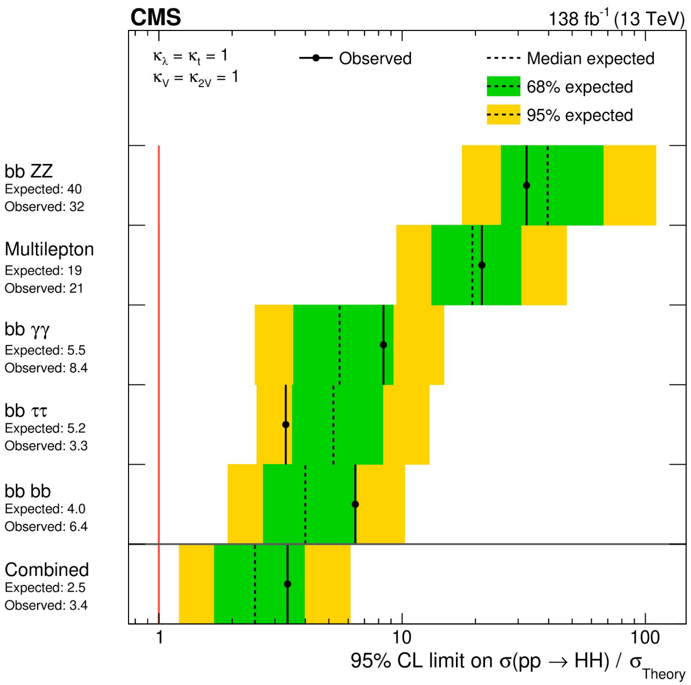

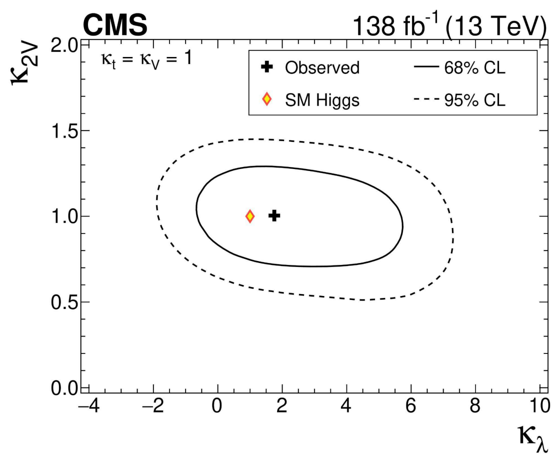

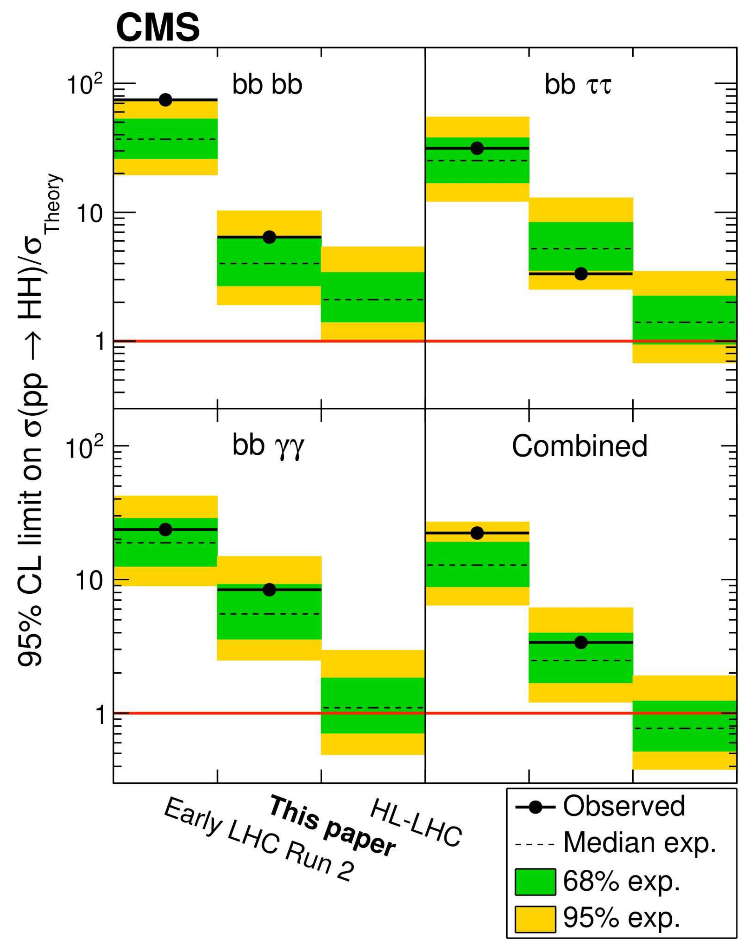

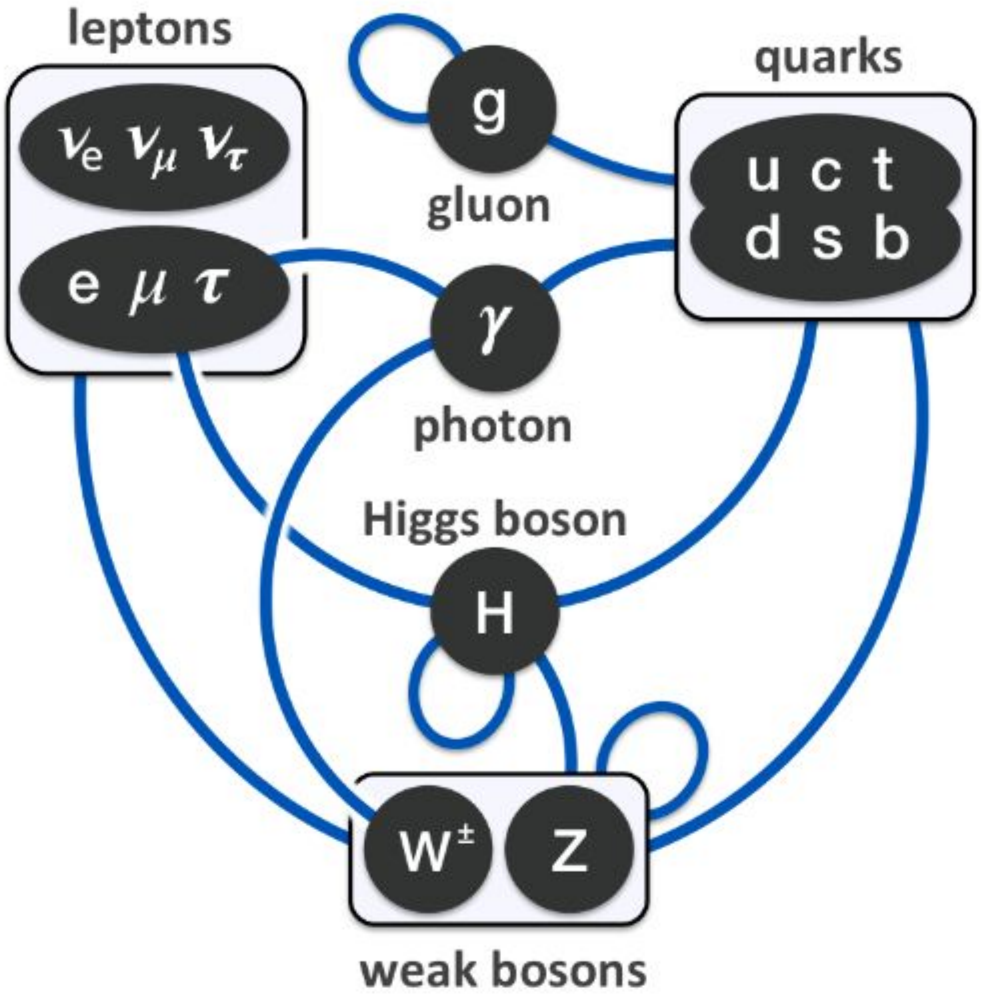
leptons
ν_e ν_μ ν_τ
e μ τ
g
gluon
quarks
u c t
d s b
γ
photon
Higgs boson
H
W±
Z
weak bosons

ATLAS, ATL-PHYS-PUB-2023-039

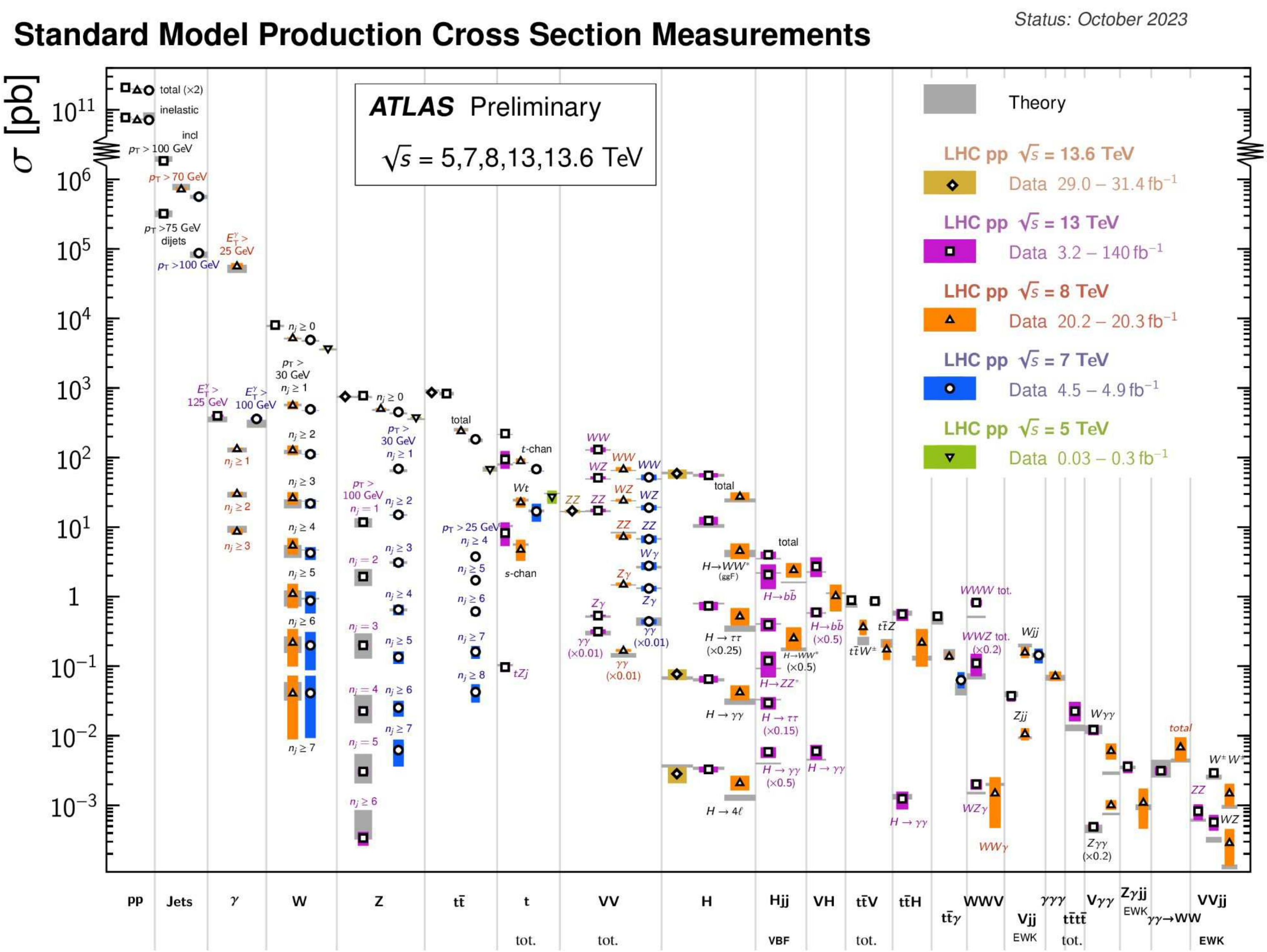

Romain Bouquet
University of Genova – INFN
romain.bouquet@cern.ch

$$\mathcal{L}_{\text{SM}} = \mathcal{L}_{\text{EW}} + \mathcal{L}_{\text{QCD}} + \underbrace{\mathcal{L}_{\text{Higgs}} + \mathcal{L}_{\text{Yukawa}}}_{\text{Higgs mechanism terms}}$$

$$\mathcal{L}_{\text{Higgs}} = (D^{\mu}\phi)^{\dagger}(D_{\mu}\phi) - V(\phi) \quad (\phi = \text{2D complex scalar field})$$

$$V(\phi) = \mu^2 |\phi|^2 + \lambda |\phi|^4 \quad (V(\phi) = \text{Higgs potential})$$

- Spontaneous symmetry breaking for $\mu^2 < 0$ & $\lambda > 0$

$\mu^2 \geq 0$

$\phi_{\text{min}} = 0$

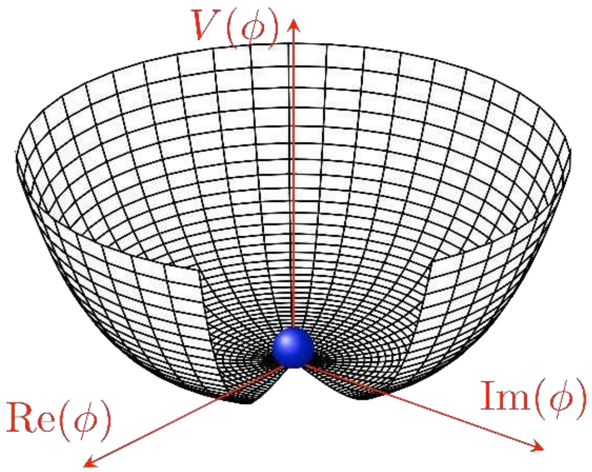

$\mu^2 < 0$

$|\phi_{\text{min}}|^2 = -\frac{\mu^2}{2\lambda} = \frac{v^2}{2}$

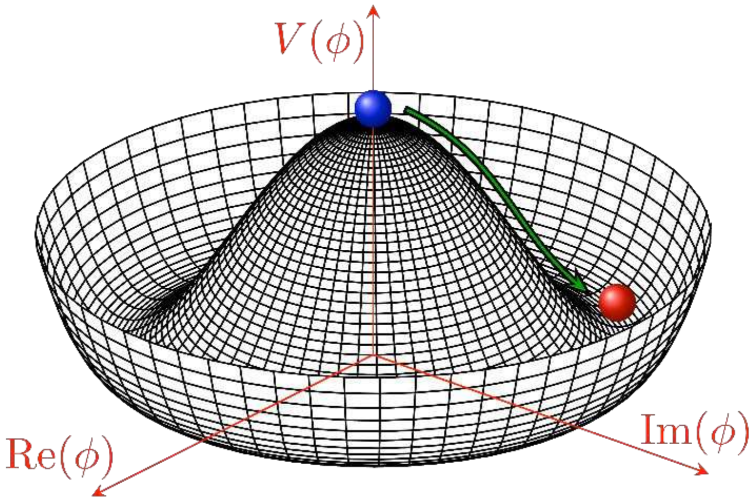

$$\mathcal{L}_{\text{SM}} = \mathcal{L}_{\text{EW}} + \mathcal{L}_{\text{QCD}} + \underbrace{\mathcal{L}_{\text{Higgs}} + \mathcal{L}_{\text{Yukawa}}}_{\text{Higgs mechanism terms}}$$

The BEH mechanism does not explain the mass of fermions

→ Need for another mechanism

$$\mathcal{L}_{\text{Yukawa}} = -y_f(\bar{\psi}_L \phi \psi_R + \bar{\psi}_R \phi^\dagger \psi_L)$$

y_f = Yukawa coupling for the fermion f

After spontaneous symmetry breaking & expansion around the ground state:

$$m_f = -\frac{y_f v}{\sqrt{2}}$$

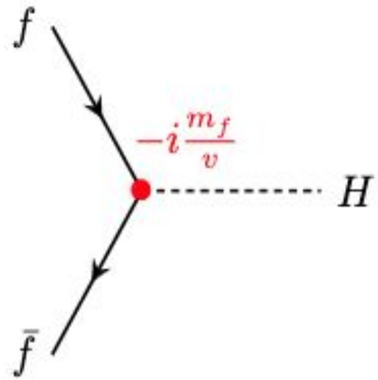

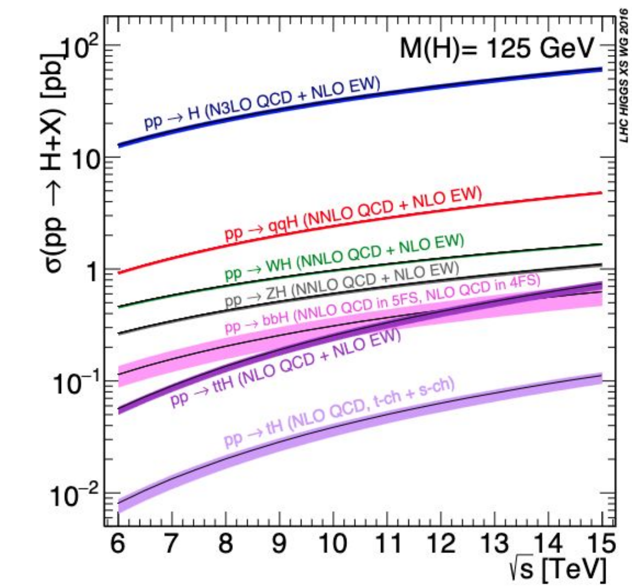

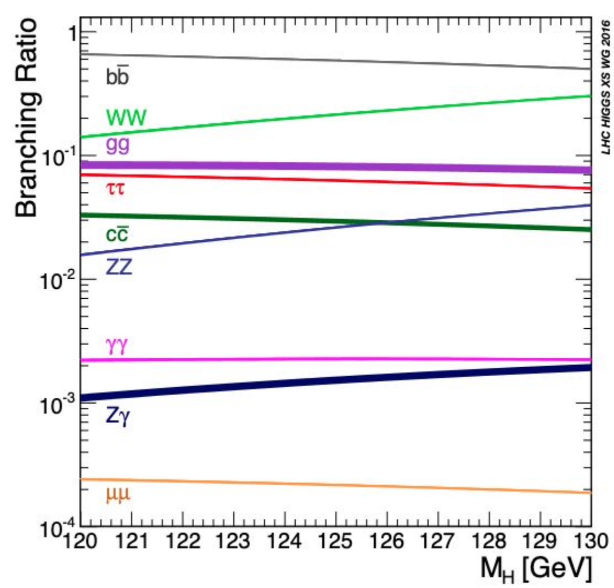

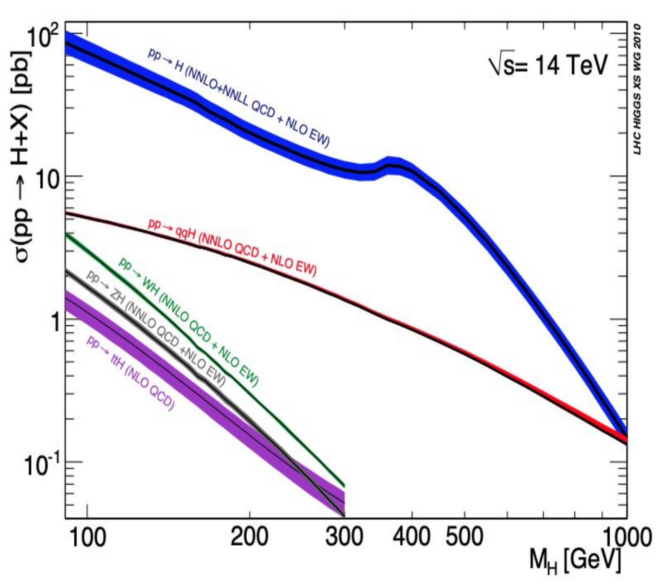

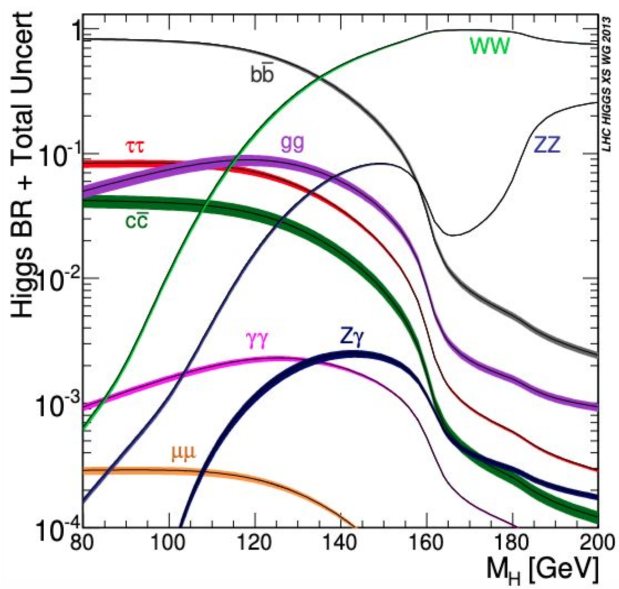

LHC Higgs Cross Section Working Group, arXiv:1610.07922

Particle Data Group, Status of Higgs Boson Physics (2023) **Cross-sections in pb**

$\sqrt{s}$ (TeV)	Production cross section (in pb) for $m_H = 125\,\text{GeV}$					
	ggF	VBF	WH	ZH	$t\bar{t}H$	total
1.96	$0.95^{+17\%}_{-17\%}$	$0.065^{+8\%}_{-7\%}$	$0.13^{+8\%}_{-8\%}$	$0.079^{+8\%}_{-8\%}$	$0.004^{+10\%}_{-10\%}$	$1.23^{+15\%}_{-15\%}$
7	$16.9^{+5.5\%}_{-7.6\%}$	$1.24^{+2.2\%}_{-2.2\%}$	$0.58^{+2.2\%}_{-2.3\%}$	$0.34^{+3.1\%}_{-3.0\%}$	$0.09^{+5.6\%}_{-10.2\%}$	$19.1^{+5\%}_{-7\%}$
8	$21.4^{+5.4\%}_{-7.6\%}$	$1.60^{+2.1\%}_{-2.1\%}$	$0.70^{+2.1\%}_{-2.2\%}$	$0.42^{+3.4\%}_{-2.9\%}$	$0.13^{+5.9\%}_{-10.1\%}$	$24.2^{+5\%}_{-7\%}$
13	$48.6^{+5.6\%}_{-7.4\%}$	$3.78^{+2.1\%}_{-2.1\%}$	$1.37^{+2.0\%}_{-2.0\%}$	$0.88^{+4.1\%}_{-3.5\%}$	$0.50^{+6.8\%}_{-9.9\%}$	$55.1^{+5\%}_{-7\%}$
13.6	$52.2^{+5.6\%}_{-7.4\%}$	$4.1^{+2.1\%}_{-1.5\%}$	$1.46^{+1.8\%}_{-1.9\%}$	$0.95^{+4.0\%}_{-3.6\%}$	$0.57^{+6.9\%}_{-9.9\%}$	$59.2^{+5\%}_{-7\%}$
14	$54.7^{+5.6\%}_{-7.4\%}$	$4.28^{+2.1\%}_{-2.1\%}$	$1.51^{+1.8\%}_{-1.9\%}$	$0.99^{+4.1\%}_{-3.7\%}$	$0.61^{+6.9\%}_{-9.8\%}$	$62.1^{+5\%}_{-7\%}$

Di-Higgs production cross sections

Rev. in Phys., Vol 5 (2020), 100045

Cross-sections in fb

ggF ~ 90 % & VBF ~ 5% for the total di-Higgs production cross-section

$\sqrt{s}$	13 TeV	14 TeV	27 TeV	100 TeV
ggF HH	$31.05^{+2.2\%}_{-5.0\%} \pm 3.0\%$	$36.69^{+2.1\%}_{-4.9\%} \pm 3.0\%$	$139.9^{+1.3\%}_{-3.9\%} \pm 2.5\%$	$1224^{+0.9\%}_{-3.2\%} \pm 2.4\%$
VBF HH	$1.73^{+0.03\%}_{-0.04\%} \pm 2.1\%$	$2.05^{+0.03\%}_{-0.04\%} \pm 2.1\%$	$8.40^{+0.11\%}_{-0.04\%} \pm 2.1\%$	$82.8^{+0.13\%}_{-0.04\%} \pm 2.1\%$
ZHH	$0.363^{+3.4\%}_{-2.7\%} \pm 1.9\%$	$0.415^{+3.5\%}_{-2.7\%} \pm 1.8\%$	$1.23^{+4.1\%}_{-3.3\%} \pm 1.5\%$	$8.23^{+5.9\%}_{-4.6\%} \pm 1.7\%$
W^+HH	$0.329^{+0.32\%}_{-0.41\%} \pm 2.2\%$	$0.369^{+0.33\%}_{-0.39\%} \pm 2.1\%$	$0.941^{+0.52\%}_{-0.53\%} \pm 1.8\%$	$4.70^{+0.90\%}_{-0.96\%} \pm 1.8\%$
W^-HH	$0.173^{+1.2\%}_{-1.3\%} \pm 2.8\%$	$0.198^{+1.2\%}_{-1.3\%} \pm 2.7\%$	$0.568^{+1.9\%}_{-2.0\%} \pm 2.1\%$	$3.30^{+3.5\%}_{-4.3\%} \pm 1.9\%$
$t\bar{t}HH$	$0.775^{+1.5\%}_{-4.3\%} \pm 3.2\%$	$0.949^{+1.7\%}_{-4.5\%} \pm 3.1\%$	$5.24^{+2.9\%}_{-6.4\%} \pm 2.5\%$	$82.1^{+7.9\%}_{-7.4\%} \pm 1.6\%$
$tjHH$	$0.0289^{+5.5\%}_{-3.6\%} \pm 4.7\%$	$0.0367^{+4.2\%}_{-1.8\%} \pm 4.6\%$	$0.254^{+3.8\%}_{-2.8\%} \pm 3.6\%$	$4.44^{+2.2\%}_{-2.8\%} \pm 2.4\%$

Rev. in Phys., Vol 5 (2020), 100045

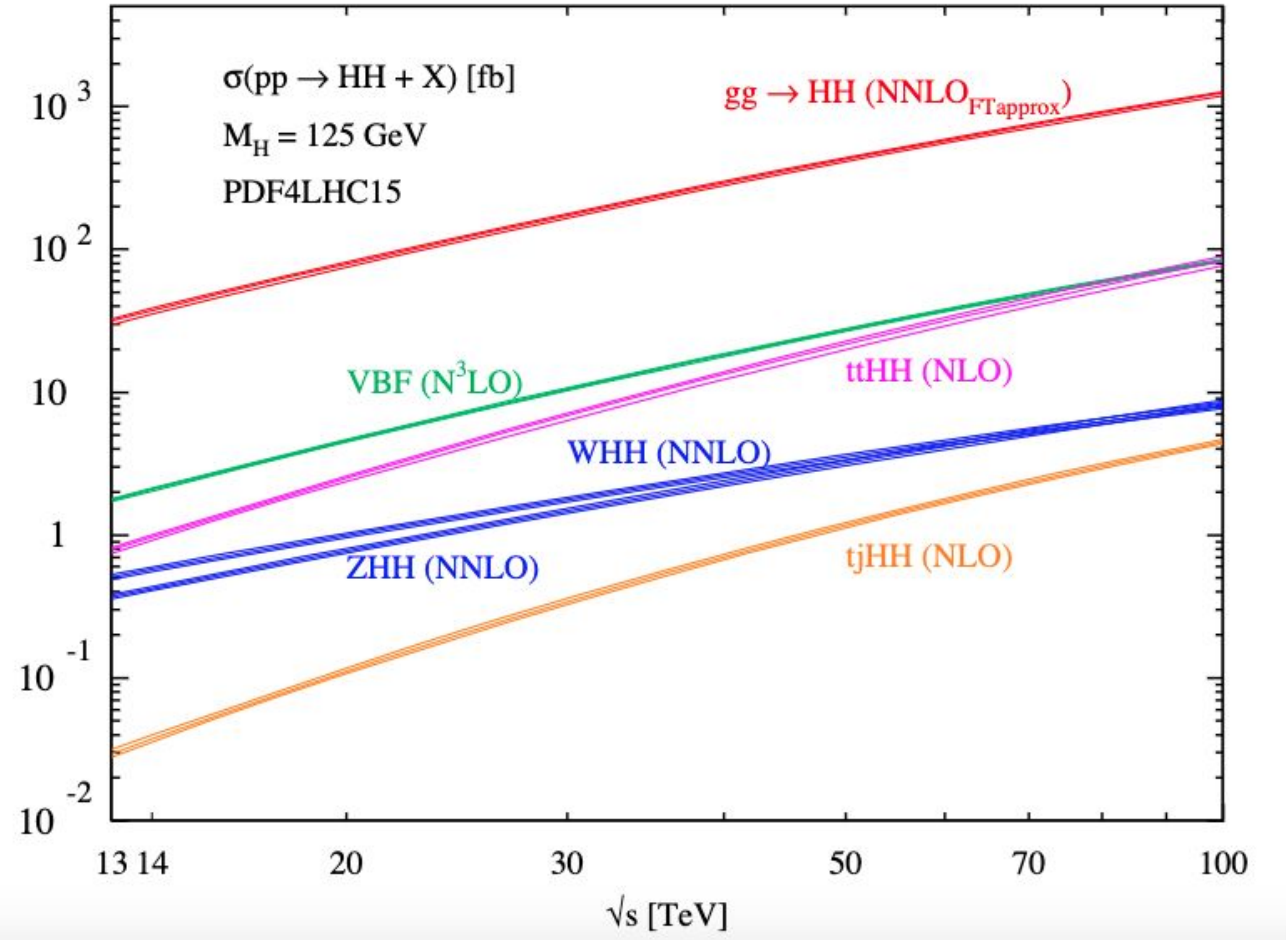

Leading order Feynman diagrams of the 2 main di-Higgs production modes: ggF & VBF

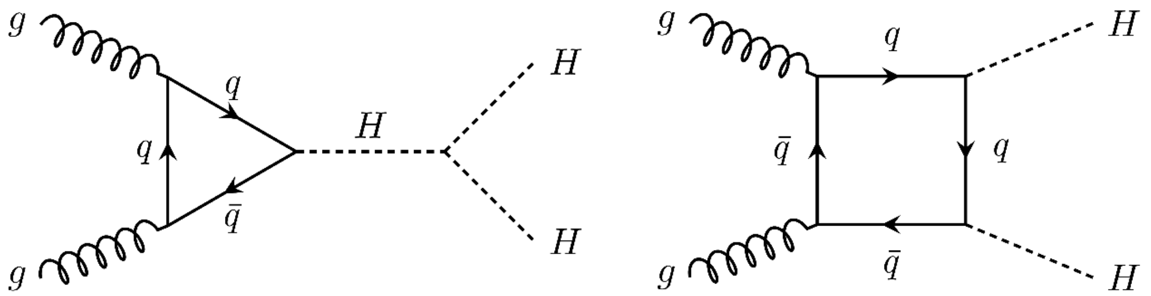

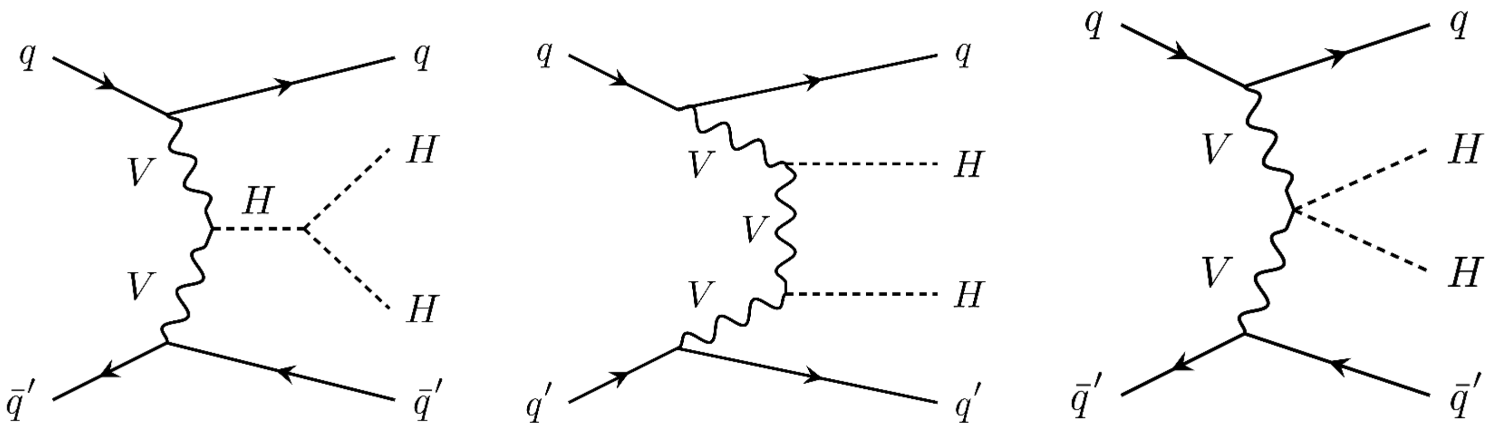

Di-Higgs production modes
all leading order Feynman diagrams

Rev. in Phys., Vol 5 (2020), 100045

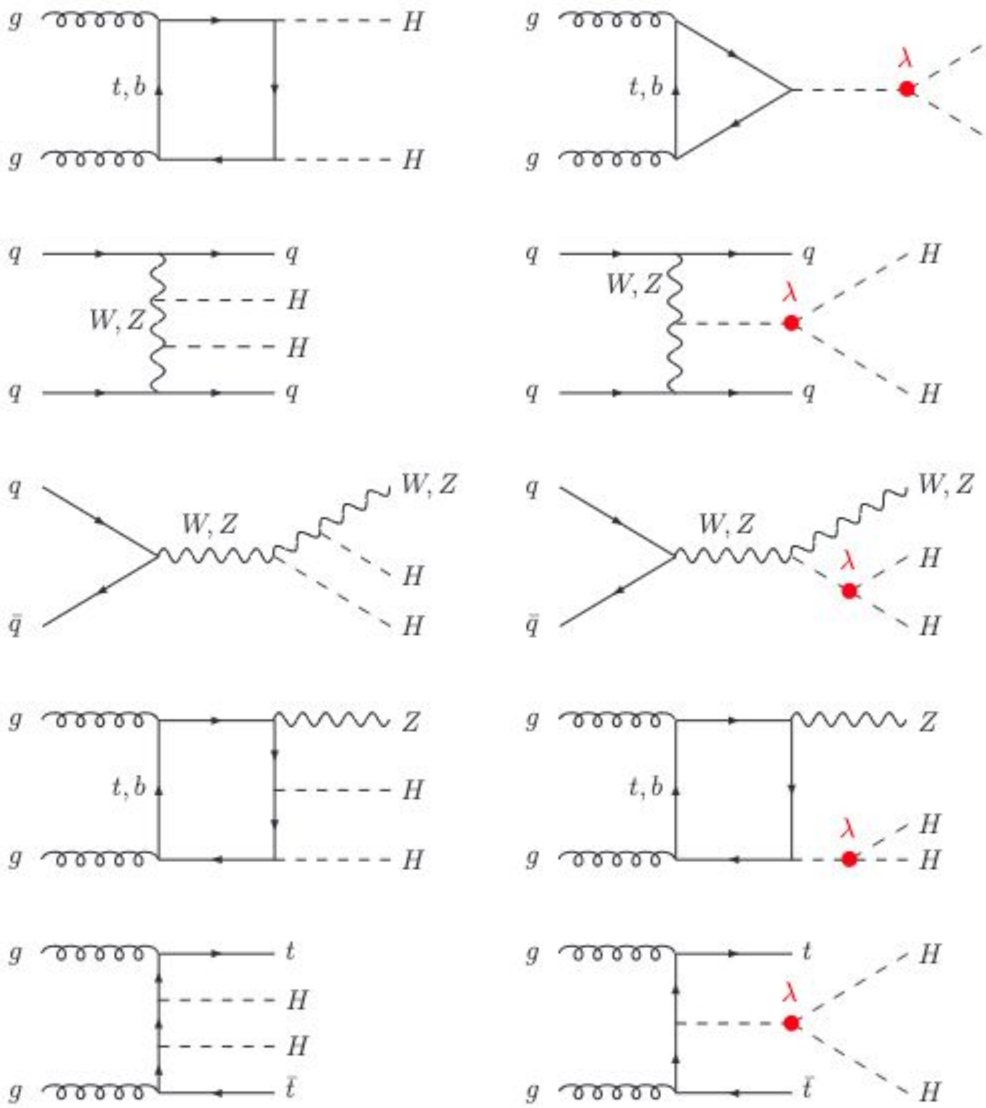

Romain Bouquet | University of Genova – INFN | romain.bouquet@cern.ch

Rev. in Phys., Vol 5 (2020), 100045

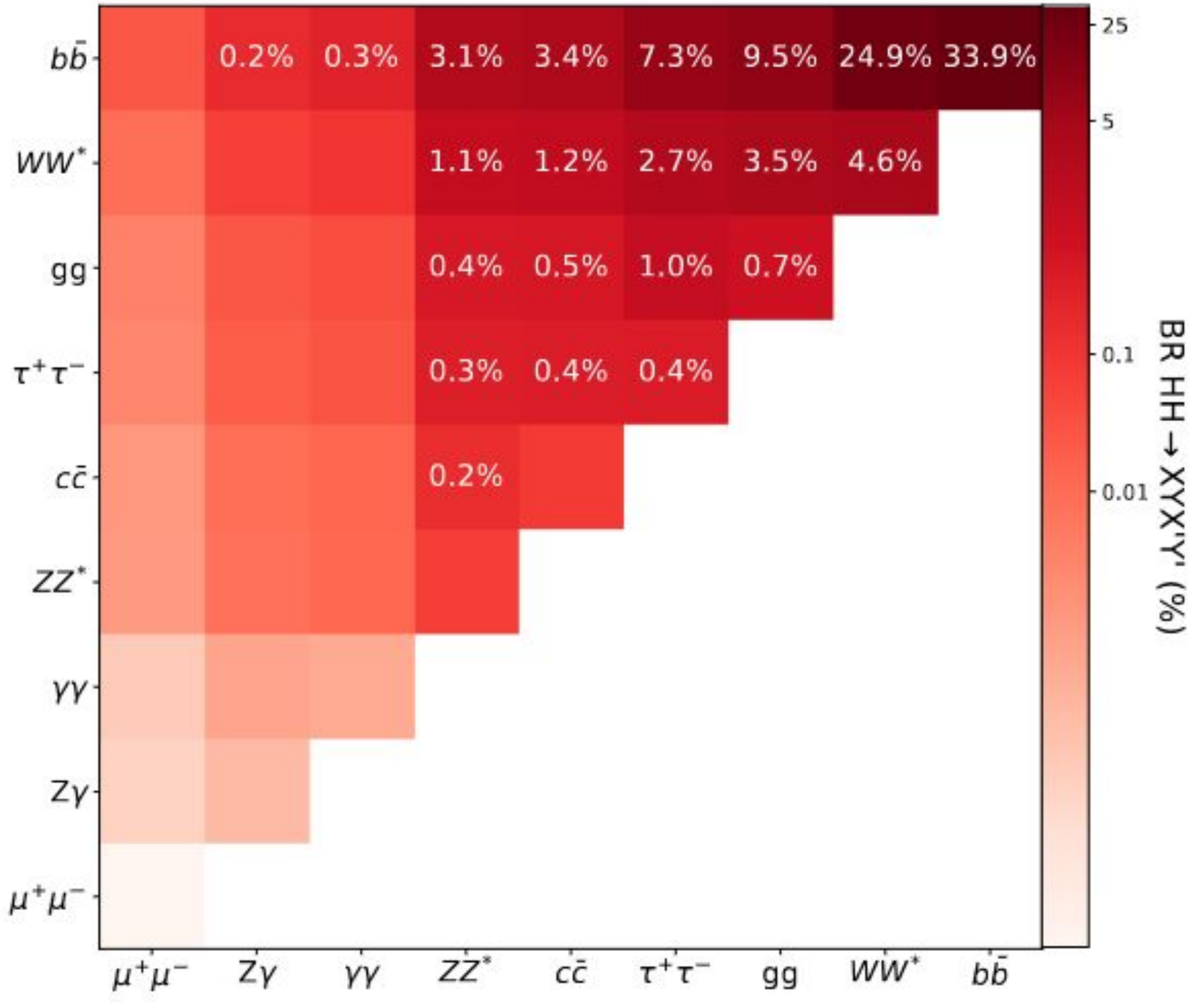

Rev. in Phys., Vol 5 (2020), 100045

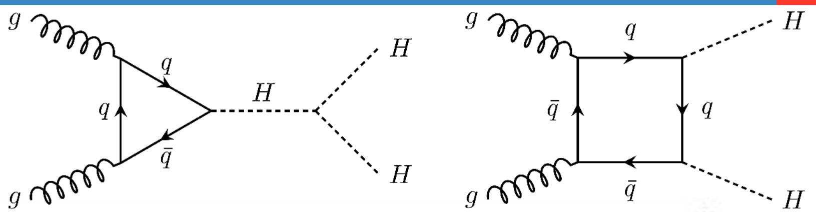

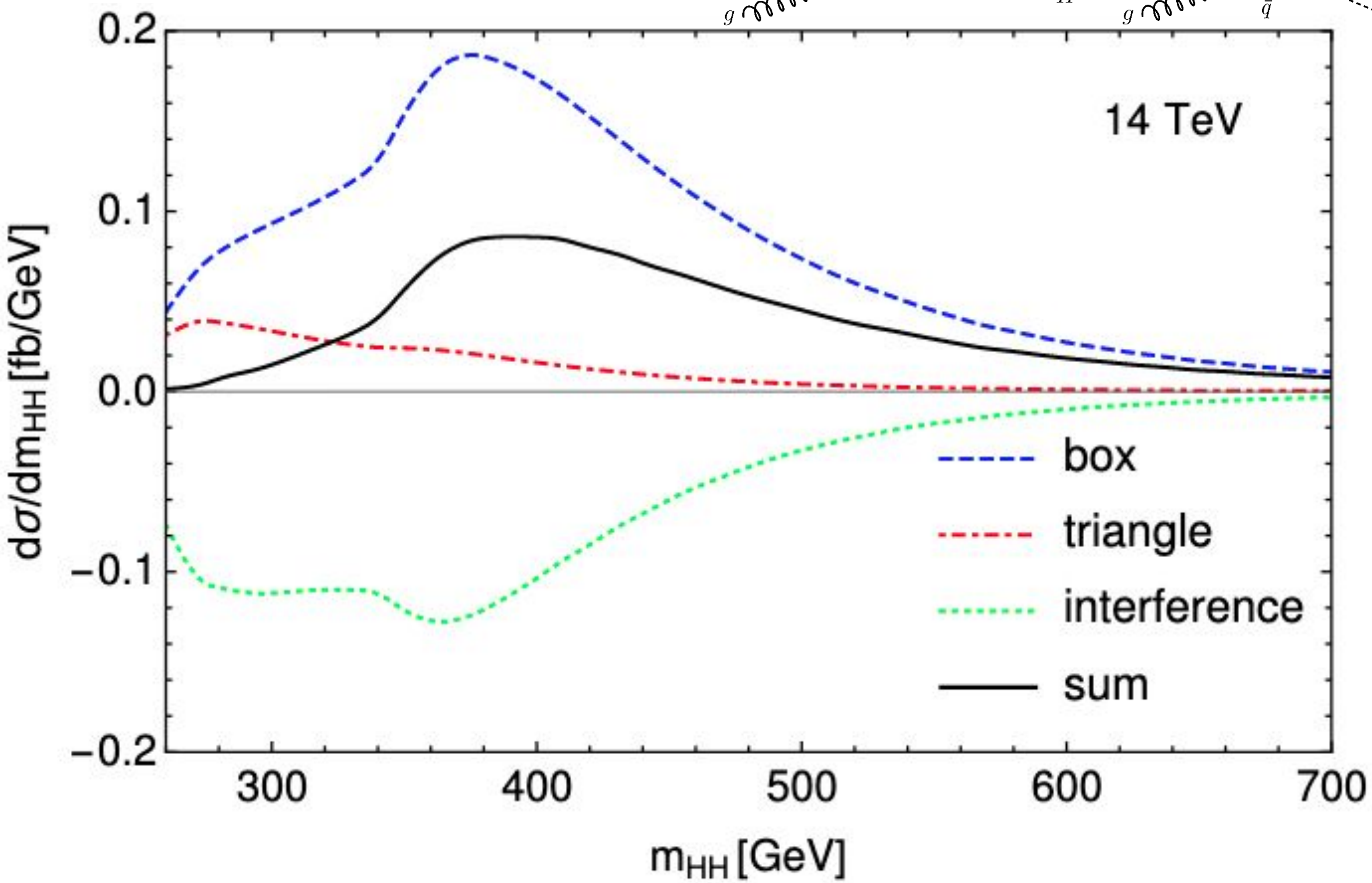

Romain Bouquet
University of Genova – INFN
romain.bouquet@cern.ch

Di-Higgs invariant mass and transverse momenta distribution w.r.t. κ_λ for $\sqrt{s}$ = 14 TeV

Rev. in Phys., Vol 5 (2020), 100045

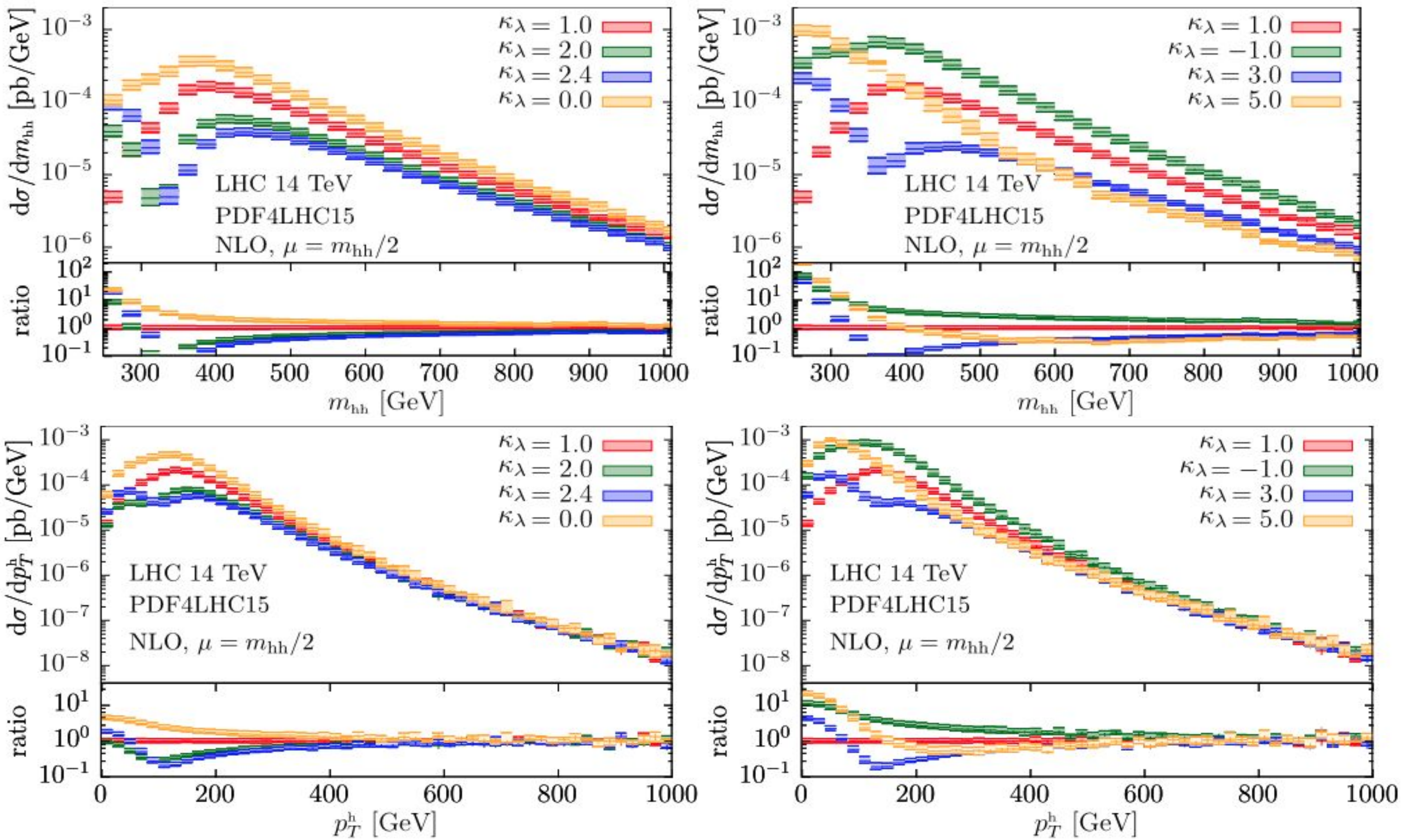

Simplified template cross-section (STXS) Stage 1.2 scheme

LHC Higgs Working Group, Fiducial And STXS

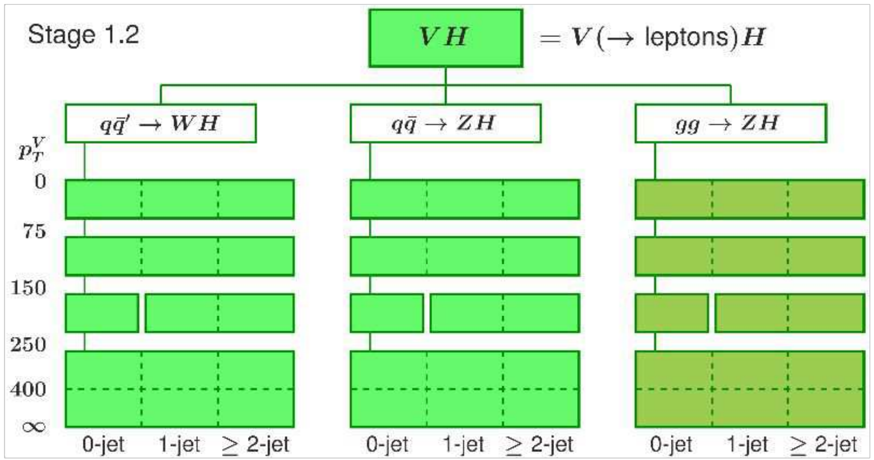

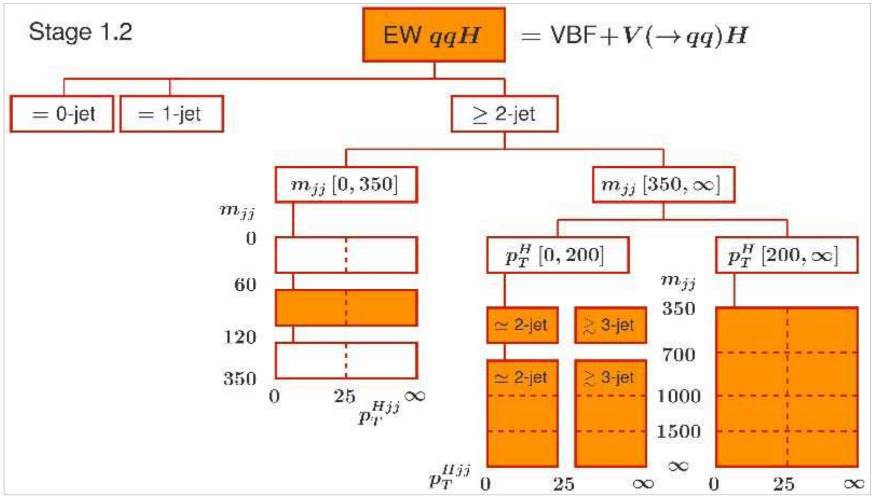

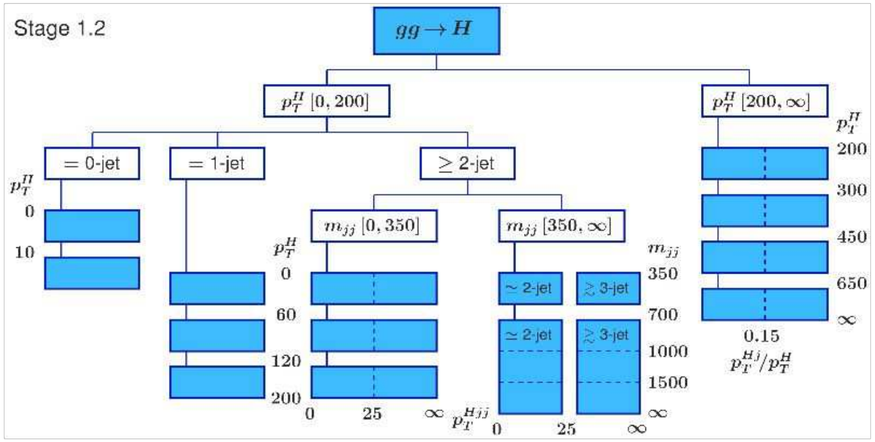

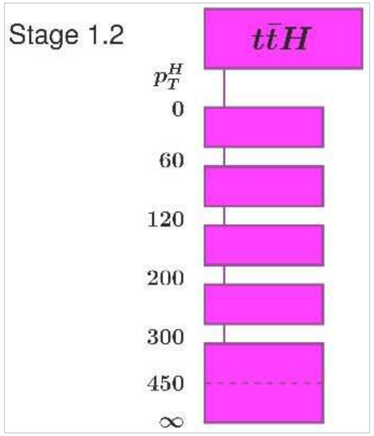

$$\mathcal{L}_{\text{SMEFT}} = \mathcal{L}_{\text{SM}} + \sum_{D\geq 5} \sum_{i\in\mathcal{W}_D} \frac{c_i^{(D)}}{\Lambda^{D-4}} \mathcal{O}_i^{(D)},$$

- $D \geq 5$ is the dimension of the EFT operators,
- $\mathcal{O}_i^{(D)}$ operators expressed in the Warsaw basis,
- $c_i^{(D)}$ are the Wilson coefficients associated to the operators and $\mathcal{W}_D$ is the ensemble of allowed type of operators for a given dimension.

$$\sigma^i_{\text{SMEFT}} = \sigma^i_{\text{SM}} + \sigma^i_{\text{int}} + \sigma^i_{\text{BSM}},$$

- σ^i_{SM} is the cross-section computed with the SM predictions for the initial state i,
- σ^i_{int} accounts for potential interferences between the SM and the hypothetical BSM processes,
- σ^i_{BSM} is exclusively related to the hypothetical BSM processes.

The possible cross-section deviations from the SM predictions can then be re-expressed thanks to the Wilson coefficients:

$$\frac{\sigma^i_{\text{SMEFT}}}{\sigma^i_{\text{SM}}} = 1 + \sum_j A_j^{\sigma_i} c_j + \sum_{j,k} B_{jk}^{\sigma_i} c_j c_k,$$

$A_j^{\sigma_i}$ and $B_{j,k}^{\sigma_i}$ respectively referred to as the linear and the quadratic terms (associated to the initial state i) which are computed from the SMEFT operators and which define σ^i_{int} and σ^i_{BSM}:

$$\frac{\sigma^i_{\text{int}}}{\sigma^i_{\text{SM}}} := \sum_j A_j^{\sigma_i} c_j, \qquad \frac{\sigma^i_{\text{BSM}}}{\sigma^i_{\text{SM}}} := \sum_{j,k} B_{jk}^{\sigma_i} c_j c_k,$$

those linear and quadratic terms being respectively of the order of $1/\Lambda^2$ and $1/\Lambda^4$.

JHEP 2208 (2022) 104

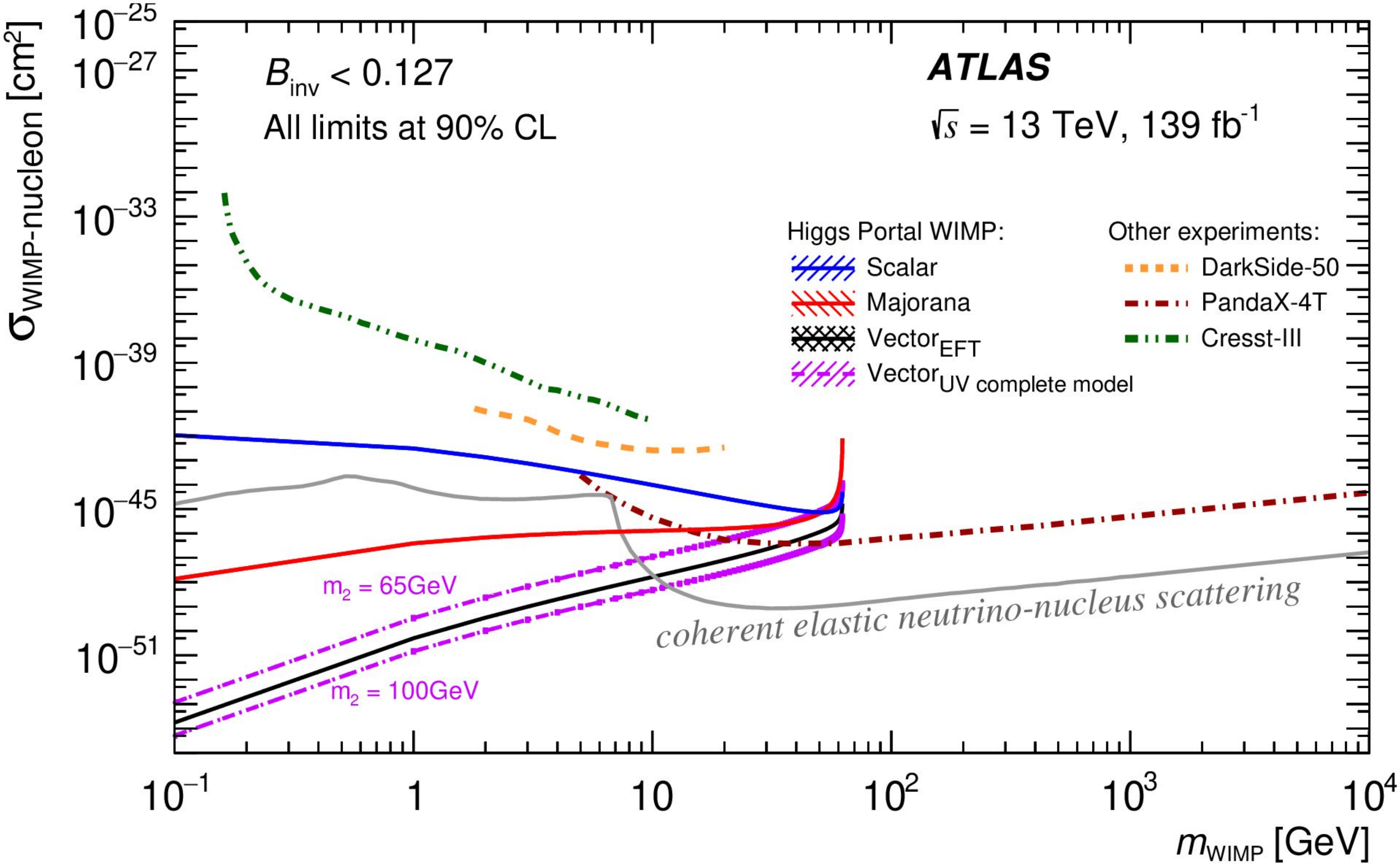

STDM-2019-24

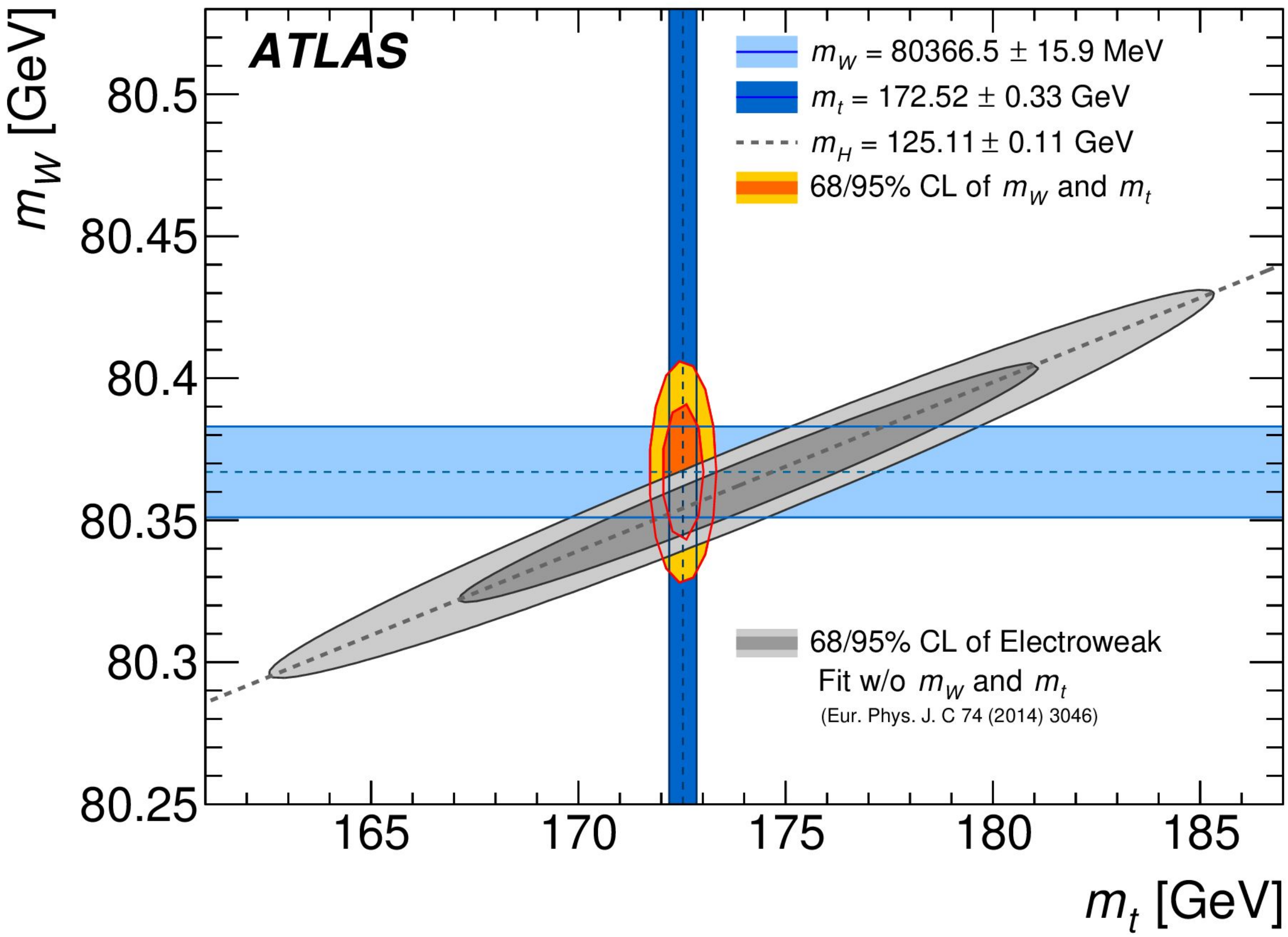

ATLAS
m_W = 80366.5 ± 15.9 MeV
m_t = 172.52 ± 0.33 GeV
m_H = 125.11 ± 0.11 GeV
68/95% CL of m_W and m_t
68/95% CL of Electroweak Fit w/o m_W and m_t
(Eur. Phys. J. C 74 (2014) 3046)
m_W [GeV]
80.25
80.3
80.35
80.4
80.45
80.5
165
170
175
180
185
m_t [GeV]